Assembly and activation of DNA damage sensing kinase Mec1-Ddc2

Inauguraldissertation

zur

Erlangung der Würde eines Doktors der Philosophie

vorgelegt der

Philosophisch-Naturwissenschaftlichen Fakultät

der Universität Basel

von

Ishan Deshpande

von Indien

Basel, 2017

Genehmigt von der Philosophisch-Naturwissenschaftlichen Fakultät

auf Antrag von

Prof. Dr. Susan M. Gasser

Prof. Dr. Laurence Harris Pearl

Basel, den 19. September 2017

Prof. Dr. Martin Spiess

Dekan

Table of Contents

Thesis overview

This thesis is based on the following publications:

Deshpande I, Seeber A, Shimada K, Keusch JJ, Gut H, Gasser SM. (2017). Structural basis of Mec1-Ddc2-RPA assembly and activation on single-stranded DNA at sites of damage. *Mol Cell.* 68(2):431-445.

Seeber A, Hegnauer AM, Hustedt N, Deshpande I, Poli J, Eglinger J, Pasero P, Gut H, Shinohara M, Hopfner KP, Shimada K, Gasser SM. (2016). RPA mediates recruitment of MRX to forks and double-strand breaks to hold sister chromatids together. *Mol Cell.* 64(5):951-966.

This thesis comprises five chapters.

Chapter 1 presents the introduction. It summarizes the role of checkpoint kinase Mec1-Ddc2 in the DNA damage response. In chapter 1, an extensive account of the literature on Mec1-Ddc2 recruitment and activation at DNA damage sites is provided which sets the foundation for chapter 2.

Chapter 2 presents results that contribute the major finding of my thesis. This chapter focuses on how homodimers of Ddc2 are recruited to DNA damage sites via interaction with RPA. Based on structural, biochemical and *in vivo* data, the chapter presents a to-scale model of Mec1-Ddc2 bound to ssDNA-RPA complexes at DNA damage sites and shows that cell survival after UV-damage is dependent on Ddc2 homodimerization and recruitment to RPA. These results are published in Deshpande et al., *Molecular Cell* 2017.

Chapter 3 presents experimental results which show that an N-terminal region within the coiled-coil domain of human ATRIP is important for coiled-coil homodimerization.

Chapter 4 presents results on the role of the MRX protein complex as a structural linchpin that holds sister chromatids together at DNA double-strand breaks. This function of MRX is apparently dependent on its interaction with a domain in RPA that also binds Ddc2. The results are published in Seeber et al., *Molecular Cell* 2016.

Chapter 5 summarizes the major conclusions of this thesis and discusses the future directions.

Chapter 1:

Introduction

Our genomes carry the information that is necessary to maintain proper functioning of the cells in our body. It is imperative that this genetic information is protected in the face of genomic insults and transmitted faithfully across generations. Genomic insults alter the chemical structure of DNA by causing breaks in the phosphate backbone of DNA strands, either single strand breaks (SSB) or double strand breaks (DSB); or by introducing base modifications such as alkylation, oxidation and thymine dimerization among others (Figure 1). Failure to repair such DNA lesions can cause local mutations, while highly toxic lesions such as DSBs can generate gross chromosomal rearrangements such as deletions, translocations and fusions of chromosomes, ultimately leading to cell death.

DNA damage occurs at a constant rate of ~100,000 events per cell per day, and can arise from exogenous as well as endogenous sources. One of the most common sources of DNA damage is ultraviolet (UV) light and ionizing radiation (IR) from sunlight. Indeed, exposure to sunlight is sufficient to generate 100,000 lesions per cell per day (Hoeijmakers, 2009). Other exogenous sources of DNA insults include, for example, cigarette smoke, medical treatments that employ X-rays, ionizing radiation and chemotherapeutic agents. Endogenous sources, most of which are by-products of cell metabolism, include DNA depurination which can generate abasic sites, DNA deamination which can interconvert bases, replication errors and reactive oxygen species.

To counter these toxic genomic insults, cells have evolved DNA repair mechanisms specific for the different types of DNA damage. Nucleotide excision repair (NER) is the most versatile repair pathway since it processes structurally unrelated DNA lesions such as thymine dimers, bulky adducts and intra-strand crosslinks and repairs them using a cut and patch type reaction (Marteijn et al., 2014). Less complicated lesions resulting from base modifications are repaired by base excision repair (BER) (Lindahl and Barnes, 2000). DSBs are prominently repaired by either error-free homologous recombination (HR) or error-prone nonhomologous end-joining (NHEJ) (Chapman et al., 2012), whereas SSBs are processed by the single-strand break repair pathway (Caldecott, 2008). The mismatch repair (MMR) pathway resolves mispaired bases (Jiricny, 2006), whereas interstrand crosslinks are largely repaired by the proteins involved in the Fanconi anemia pathway, making use of enzymes and reactions implicated in the other types of repair (Deans and West, 2011).

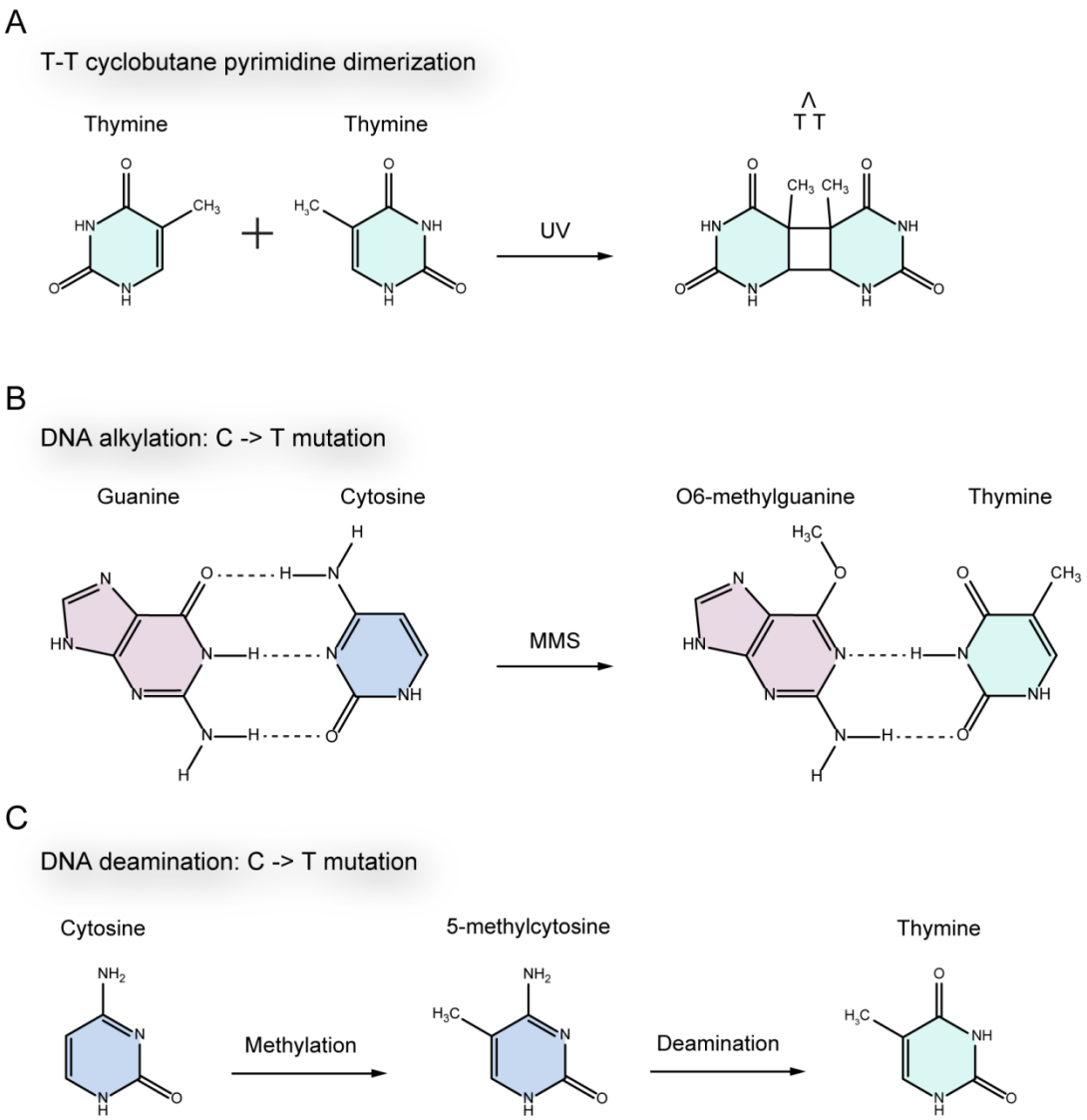

Figure 1: Alteration of DNA structure by DNA damage. **(A)** UV-light causes thymine-thymine (T-T) dimerization of two consecutive thymines on the same strand of DNA, resulting in the disruption of normal base-pairing. **(B)** Guanine is alkylated by methyl methanesulfonate (MMS) to form O6-methylguanine which base pairs with a thymine instead of a cytosine, resulting in a C -> T point mutation. **(C)** Cytosine can undergo methylation and deamination to form a thymine, resulting in a C -> T point mutation.

Indeed, our cells have evolved exhaustive pathways involving at least 450 proteins that repair the constant barrage of DNA insults. Owing to the high frequency of DNA damage events, specificity of repair pathways for lesions and the dangerous consequences of improper repair, eukaryotic cells have developed stringent mechanisms to regulate the assembly and activation of the right repair proteins at the right place and at the right time. These regulatory mechanisms, in addition to the cell cycle checkpoints,

collectively constitute a network of conserved and coordinated pathways called the DNA damage response (DDR). Efficient DDR is critical for protection of the genome and hence cell survival.

At the core of the DDR are two conserved kinases called Mec1 (Mitosis entry checkpoint 1, ATR in human and Rad3 in fission yeast *Schizosaccharomyces pombe*) and Tel1 (Telomere maintenance 1, ATM in human and fission yeast). Mec1 functions as an enzyme complex with its regulatory subunit Ddc2 (ATRIP, ATR Interacting Protein, in human, and Rad26 in *S. pombe*) and the function and stability of the two proteins are inter-dependent on each other (Cortez et al., 2001; Edwards et al., 1999; Paciotti et al., 2000; Wakayama et al., 2001). Therefore, Ddc2 is considered to be an obligate partner of Mec1. Unless noted otherwise, I will refer to the budding yeast *Saccharomyces cerevisiae* protein nomenclature (see Table 1 for an overview of DDR protein names in several model organisms). Upon DNA damage, either of the kinases can get recruited to damage sites and induce the DDR by phosphorylating hundreds of targets that set in motion a signaling cascade which coordinates DNA repair and cell cycle progression (Friedel et al., 2009). Since these apical kinases play a role in the early recognition of DNA damage and the subsequent induction of the DDR signaling cascade, they are referred to as “DNA damage sensing kinases” or “Signal transducing kinases” (Figure 2).

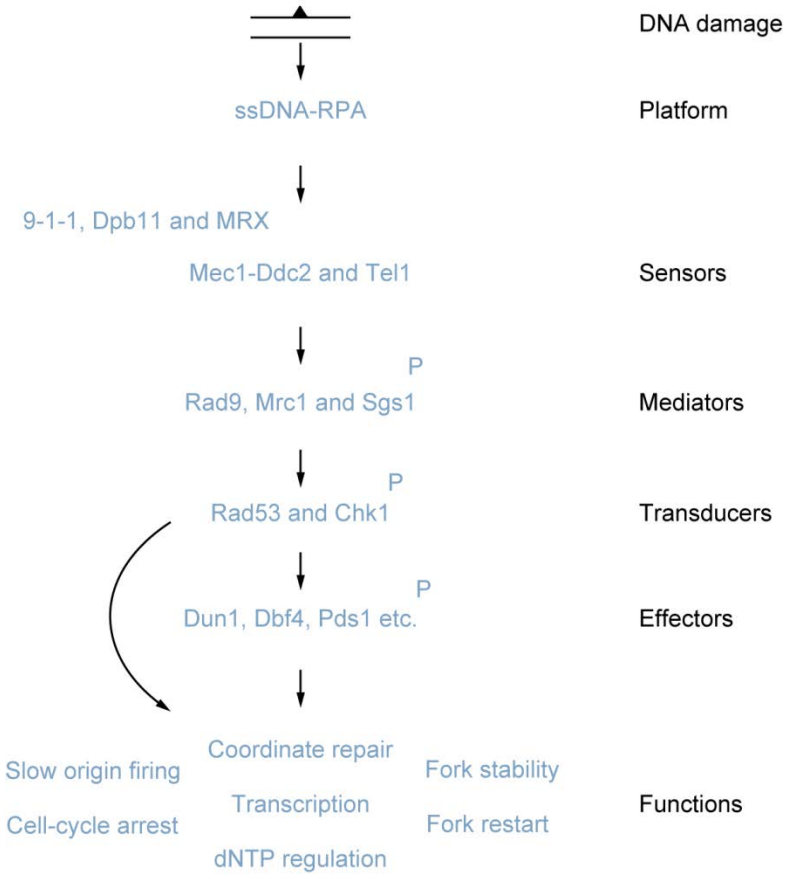

Figure 2: DNA damage response pathway. Upon DNA damage (represented by a black triangle), long stretches of ssDNA are generated which rapidly get coated by RPA to form an ssDNA-RPA platform. This platform recruits sensor kinase Mec1-Ddc2 through co-sensor and co-activator proteins such as 9-1-1 and Dpb11. Activated Mec1 phosphorylates several targets including Rad9, Mrc1 and Sgs1 which act as adaptors for the key signaling kinase Rad53. Activated Rad53 further phosphorylates several effector kinases to control cell cycle progression, origin firing, DNA repair and replication fork stability.

Mec1 and Tel1 belong to the phosphoinositide 3-kinase related protein kinases (PIKK) family which shares similar domain organization and a conserved kinase domain (details on PIKKs are presented in section 4). There are, however, key differences between Mec1 and Tel1. In budding yeast, Mec1 responds to a gamut of genomic insults such as replication stress, UV-induced lesions, base adducts and DSBs (Figure 3) (Cimprich and Cortez, 2008), whereas Tel1 responds primarily to DSBs.

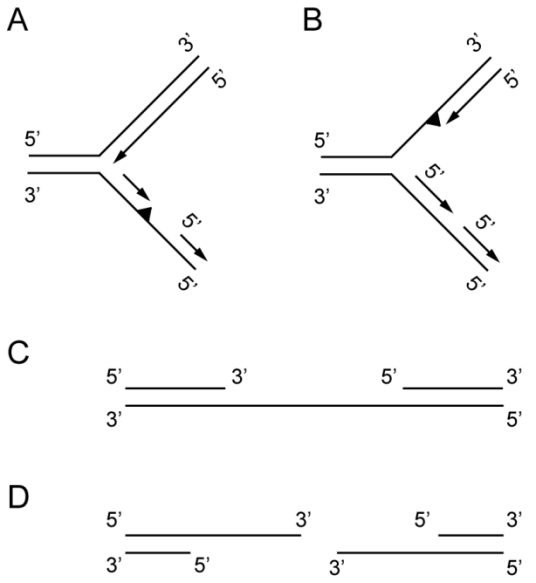

Figure 3: DNA structures that induce Mec1 activation. **(A)** Lesion (black triangle) in the lagging strand of the replication fork blocks the polymerase but not the helicase generating ssDNA regions with a dsDNA primer carrying a 5' free end. **(B)** Lesion in the leading strand of the replication fork also generates ssDNA. Repriming events generate the requisite dsDNA primer with a 5' free end to induce Mec1 activation. **(C)** UV-damage generates short ssDNA regions (30 nt) which are further resected to generate longer ssDNA regions (up to 2 kb) adjacent to dsDNA with a 5' end. **(D)** DSBs undergo resection to generate ssDNA stretches which are adjacent to a 5' end.

Mec1/ATR is essential for viability in several organisms from yeast to man and its loss causes lethality in early mice embryos (Brown and Baltimore, 2000). In contrast, Tel1/ATM is dispensable for cell viability (Shiloh and Ziv, 2013). However, mutations in *ATM* result in an elevated predisposition towards cancer and are found in 0.5 to 1.0% of the population (Renwick et al., 2006; Taylor et al., 1975). In fact, *ATM* is found to be mutated in a variety of cancers such as colorectal (Cancer Genome Atlas, 2012a), lung (Cancer Genome Atlas Research, 2012) and breast (Cancer Genome Atlas, 2012b), and is considered to be a tumor suppressor. On the other hand, cancer cells rarely carry mutations in *ATR* owing to the essential functions of ATR in maintaining genome integrity. Nevertheless, in some cancers, ATR may be a useful target for cancer therapy. Cancer cells replicate abnormally and are under a constant level of low replicative stress, accentuating the need for ATR for cell survival (Gorgoulis et al., 2005). Furthermore, some cancers have a dysfunctional DNA damage-induced G1 checkpoint owing to mutations in Rb, p53 or c-myc. This makes cancer cells over-dependent on the S-phase checkpoint which is regulated by the ATR kinase. Thus, by combining S-phase specific ATR inhibitors with DNA damaging agents to generate synthetic lethality, it is possible to selectively or preferentially kill cancer cells. Indeed, inhibition of the ATR kinase activity sensitizes cells to DNA damaging agents (Caporali et al., 2004; Cliby et al., 1998; Nghiem et al., 2002). These initial studies inspired the development of selective and potent ATR inhibitors such as VE-822, the first ATR inhibitor to enter clinical trials (Fokas et al., 2012).

Table 1: Conserved checkpoint proteins and their functions

S. cerevisiae	***S. pombe***	***H. sapiens***	**Function**
Mec1-Ddc2	Rad3-Rad26	ATR-ATRIP	Sensor signaling kinase
Tel1	Tel1	ATM	Sensor signaling kinase
Rfa1	Rad11/Rpa1	RPA70	ssDNA binding and protein-protein interactions
Rad24-RFC	Rad17-RFC	RAD17-RFC	9-1-1 clamp loader
Ddc1-Rad17-Mec3	Rad9-Rad1-Hus1	RAD9-RAD1-HUS1	Co-sensor and Mec1 activator
Dpb11	Cut5/Rad4	TopBP1	Mec1 activator
Dna2	Dna2	DNA2	Mec1 activator in S-phase
Mrc1	Mrc1	Claspin	Checkpoint mediator
Rad9	Crb2	53BP1, BRCA1	Checkpoint mediator
Sgs1	Rqh1	BLM	Rad53 activation
Rad53	Cds1	CHK2	Effector kinase
Chk1	Chk1	CHK1	Effector kinase
Mre11-Rad50-Xrs2	Mre11/Rad32-Rad50-Nbs1	MRE11-RAD50-NBS1	DSB resection, Tel1 recruitment
Exo1	Exo1	EXO1	NER gap resection

1. Mec1/ATR damage recognition

Being an apical DNA damage sensing kinase, Mec1 needs to rapidly localize to DNA damage sites and activate the DDR signaling cascade. The ability of Mec1 to respond to a wide spectrum of DNA damaging lesions and replication stress is largely dependent on the ability of Mec1 to recognize a common structural signal, replication protein A (RPA) bound to single-stranded DNA (ssDNA). This section reviews the current understanding of Mec1 recruitment to sites of DNA damage.

1.1. The ssDNA-RPA platform

Generation of long stretches of ssDNA is one of the earliest events and is a hallmark of DNA damage and replication stress. The functional uncoupling of replicative helicases and polymerases upon replication stress can expose up to 200 nucleotides (nt) of ssDNA (Sogo et al., 2002). End resection of DSBs for repair by HR and nuclease processing of NER intermediates of UV-induced lesions also generate long ssDNA gaps (Giannattasio et al., 2010; Paques and Haber, 1999), while the collision of a UV lesion with the replication fork can generate remarkably long ssDNA regions, extending up to 3 kb in length, as seen by electron microscopy (EM) (Lopes et al., 2006). R-loops or RNA:DNA hybrids that form as an aberrant intermediate of transcription, are a source of ssDNA and genomic instability (Skourti-Stathaki and Proudfoot, 2014). ssDNA is intrinsically more labile than dsDNA and tends to form secondary structures that might impede cellular processes. To prevent this, in the cell, most of the ssDNA generated during replication and repair is rapidly coated with the major ssDNA binding protein RPA (Alani et al., 1992).

RPA is a heterotrimeric complex consisting of the Rfa1, Rfa2 and Rfa3 subunits (RPA70, RPA32 and RPA14 in human). It was first described for its essential role in DNA replication (Wold and Kelly, 1988). Later, additional functions for RPA were uncovered in a wide array of processes, including DNA replication, recombination, repair, and DNA damage checkpoint activation (Zou et al., 2006). RPA primarily functions by protecting ssDNA from nucleases and secondary structure formation, but also by acting as a protein-protein interaction platform. RPA contains six oligosaccharide/oligonucleotide binding (OB) folds, each of which contains five β-strands forming a β-barrel structure that is present in other ssDNA binding proteins (Gomes et al., 1996). Four of the six OB-folds namely: N-OB, OB-A, OB-B and OB-C lie in the largest subunit Rfa1; one, OB-D, is present in the Rfa2 subunit, while OB-E lies in the smallest subunit, Rfa3 (Figure 4A). RPA binds ssDNA in three different modes depending on the length of ssDNA that it contacts (Figure 4B). Either it binds to 8 nt in a low-affinity mode that is initiated by OB-A and OB-B folds (Bochkarev et al., 1997), or it covers 12-23 nt in a medium-affinity mode that additionally involves the OB-C fold (Brill and Bastin-Shanower, 1998), or finally it contacts 30 nt in a high-affinity binding mode that involves the OB-D fold (Bastin-Shanower and Brill, 2001). RPA binds ssDNA strongly with a dissociation constant in the high picomolar range (Kim et al., 1994; Kim and Wold, 1995). Although a high resolution structure of the full length RPA has not yet been revealed, crystal structures of all RPA domains have been determined (Bochkareva et al., 2005; Fan and Pavletich, 2012; Feldkamp et al., 2014). These structural data along with nuclear magnetic resonance (NMR) and small-angle X-ray

scattering (SAXS) experiments suggest that RPA is a modular protein complex with the N-OB domain being structurally and dynamically independent from the rest of the RPA molecule (Brosey et al., 2015).

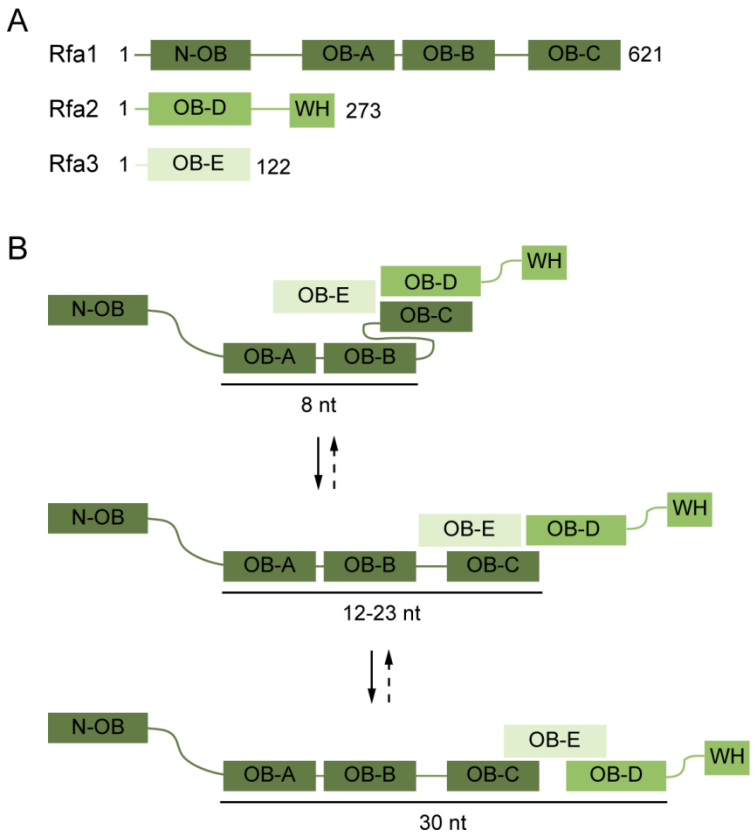

Figure 4: The OB domains of RPA bind ssDNA. **(A)** Domain organization of RPA. RPA comprises three subunits, Rfa1, Rfa2 and Rfa3, which are represented in different shades of green. OB: Oligosaccharide/oligonucleotide binding; and WH: Winged helix domains are indicated by boxes. **(B)** ssDNA binding modes of RPA. RPA binds ssDNA in the low affinity mode (8 nt), medium affinity mode (12-23 nt), and the high affinity mode (30 nt) involving different subunits of RPA.

Interestingly, the N-OB domain in the Rfa1 subunit interacts with multiple proteins in the DDR pathway including Ddc1, Ddc2, Dna2, Mre11-Rad50-Xrs2 (MRX), and Sgs1, as well as p53 in mammals (Bochkareva et al., 2005; Hegnauer et al., 2012; Lin et al., 1996; Seeber et al., 2016; Xu et al., 2008; Zhou et al., 2015). Early genetic analysis of yeast RPA identified *rfa1-t11*, a charge reversal K45E point mutation in the basic cleft of the N-OB fold (Umezu et al., 1998). *rfa1-t11* is about 1000-fold more sensitive than wild-type to DNA damage by UV-light and DNA alkylating agent MMS (Chen et al., 1998). The mutant is defective in recombination, but proficient in DNA replication (Soustelle et al., 2002). We recently showed that the K45E mutation disrupts a basic patch formed by the R44, K45 and R62 residues in the N-OB cleft (Seeber et al., 2016). In the same study, using genetic and biochemical analyses, we

showed that the MRX protein complex binds Rfa1, but not Rfa1-t11. In chapter 2, we elaborate on the interactions of Rfa1 and Rfa1-t11 with Ddc2 (ATRIP, ATR Interacting Protein, in human, and Rad26 in *S. pombe*), the regulatory partner of Mec1, and with Dna2, a nuclease-helicase involved in the maturation of Okazaki fragments. In conclusion, the ssDNA-RPA complex not only protects ssDNA in the cell, but also acts as a platform to recruit several proteins in the DDR pathway.

1.2. Mec1-Ddc2 recruitment to the ssDNA-RPA platform

The major mode of DNA damage recognition by Mec1-Ddc2 (ATR-ATRIP in human) occurs via the interaction of Ddc2 with the ssDNA-RPA platform (Zou and Elledge, 2003). Depletion of RPA in human cells and *Xenopus* egg extracts is defective in localizing ATR to sites of DNA damage and activating the ATR-mediated checkpoint pathway (Costanzo et al., 2003). The major interface of the Ddc2-RPA interaction involves the N-terminal 50 amino acid (aa) residues in Ddc2 (100 aa in ATRIP) and the N-OB domain of RPA subunit Rfa1 (Ball et al., 2007; Ball et al., 2005). NMR and mutagenesis experiments have proposed that a conserved acidic patch in the Ddc2 N-terminus is responsible for RPA binding and the disruption of this acidic patch reduced Ddc2 localization to DNA breaks and sensitized cells to DNA damage (Ball et al., 2007). The structural dissection of this interaction is presented in chapter 2. Notably, weaker RPA interacting domains in human ATRIP outside this N-terminal region may provide functional redundancy (Namiki and Zou, 2006).

If ssDNA-RPA is the major signal that recruits Mec1-Ddc2 and induces the DNA damage checkpoint activation, then normal replication processes which generate short ssDNA-RPA patches might activate Mec1 even in the absence of DNA damage. However, cells seem to tolerate the short ssDNA-RPA patches generated in S-phase and only when a certain threshold of ssDNA was reached, did Mec1 induce the checkpoint (Byun et al., 2005; Shimada et al., 2002) (Figure 5). Interestingly, the length of ssDNA generated correlates with Mec1/ATR mediated phosphorylation of major downstream effector kinase Chk1/CHK1 (Byun et al., 2005). The fact that Mec1 responds to different amounts of signal in different cell cycles supports the theory of a threshold signal for Mec1 activation (Shimada et al., 2002). The amount of the ssDNA-RPA signal required to breach this threshold, however, remains unclear. The ssDNA-RPA signal in the context of normal replication is kept at a minimum level by coupling DNA unwinding and DNA synthesis rates by the helicase and the polymerase, respectively. Functional uncoupling of the helicases and polymerases and subsequent generation of ssDNA-RPA can be achieved by treatment with MMS, DNA polymerase inhibitor aphidicolin, or hydroxyurea (HU), which inhibits ribonucleotide reductase and depletes deoxyribonucleotide (dNTP) pools. These drugs indeed activate the Mec1/ATR kinase dependent checkpoint (Walter and Newport, 2000). Interestingly, inhibition of DNA unwinding activity in the presence of DNA damage prevents Mec1/ATR-mediated checkpoint activation (Byun et al., 2005). This suggests that DNA damage *per se* is not sufficient to activate Mec1/ATR, but Mec1/ATR activation rather depends on the amount of ssDNA-RPA. Mec1/ATR can also be recruited by damage-specific repair proteins. For example, O^6-methyl G/T mispairing that is

recognized by mismatch repair proteins Msh2-Msh6 (MutSα) can specifically recruit ATR-ATRIP, and this is sufficient for CHK1 phosphorylation (Yoshioka et al., 2006). Msh2-Msh3 (MutSβ) that bind to hairpins in the ssDNA-RPA complex, can also form a complex with human ATR-ATRIP and promote ATR checkpoint function in response to replication associated DSBs (Burdova et al., 2015).

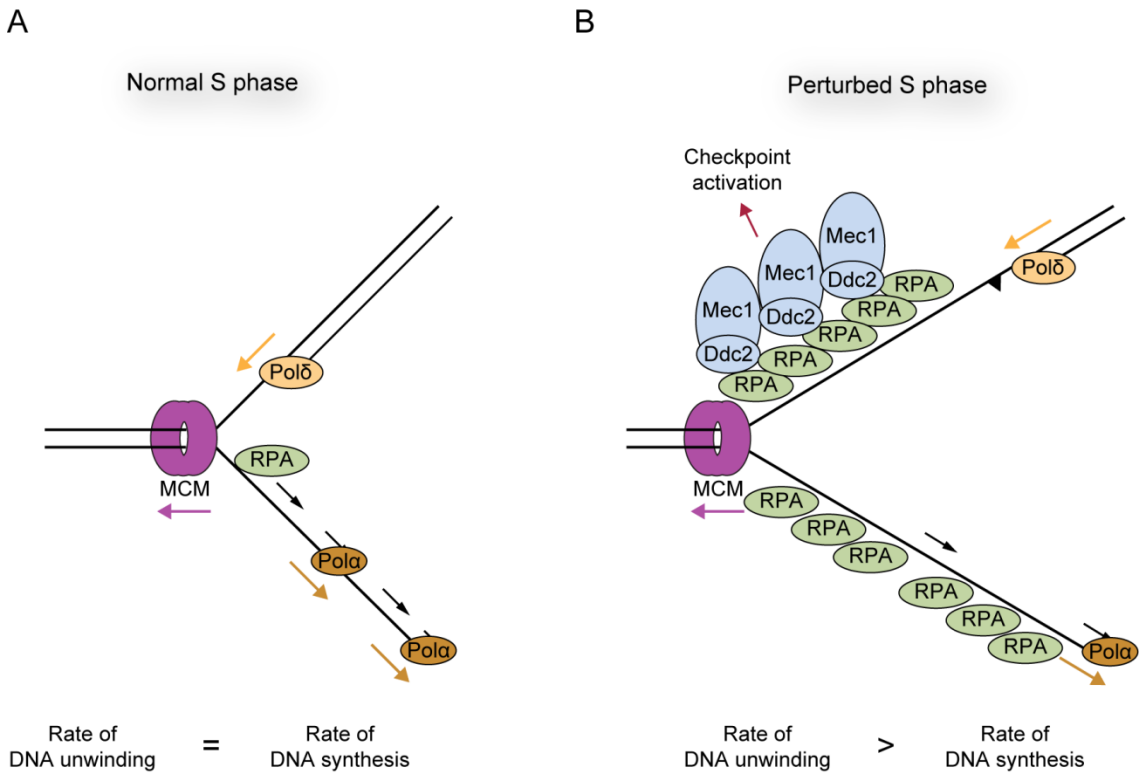

Figure 5: Model of ssDNA-RPA generation after helicase-polymerase uncoupling. **(A)** Under non-damaging conditions, the rate of DNA unwinding by the MCM (minichromosome maintenance) helicase is functionally coupled to the rate of DNA synthesis by the leading and the lagging strand polymerases. Therefore, the amount of ssDNA-RPA in an intact replication fork is minimal and below the threshold for Mec1-mediated checkpoint activation. **(B)** Under damaging conditions, polymerase movement is stalled; however, the helicase continues to unwind DNA generating long ssDNA-RPA regions. ssDNA-RPA recruits Mec1-Ddc2 and induces checkpoint activation.

2. Mec1/ATR activation

Mere recruitment of Mec1-Ddc2 is not sufficient for its activation. Mec1/ATR activation is regulated by several co-factors that act redundantly to ensure checkpoint induction. Misactivation of Mec1/ATR in the absence of DNA damage creates cell cycle blocks and induces cellular senescence (Toledo et al., 2008). Therefore, it is important to activate Mec1 at the right place and at the right time. This is reflected in the redundancy of Mec1 activation pathways and the independent sensing of DNA damage by Mec1-Ddc2 and its co-activators. The following section describes the mechanisms of Mec1 activation.

2.1. Mec1/ATR maturation: Folding and assembling the kinase

Before Mec1-Ddc2 is localized to and activated at sites of DNA damage or replication stress, it needs to be folded and assembled. This maturation of Mec1-Ddc2 occurs even in the absence of genomic insults. Mec1, like other PIKK proteins, is large (2,368 aa) and contains extensive N-terminal α-helical HEAT (Huntingtin, Elongation factor 3, A subunit of protein phosphatase 2A and TOR1) repeats. The proper folding and assembly of the Mec1-Ddc2 complex are mainly regulated by the Hsp90 chaperone that binds the nascent client protein Mec1-Ddc2 via the R2TP (Rvb1 and Rvb2, Tah1, and Pih1) and TTT (Tel2, Tti1 and Tti2) co-chaperone complexes (Hurov et al., 2010; Pal et al., 2014; Takai et al., 2007). The Hsp90-R2TP-TTT chaperone complex also regulates proper folding and assembly of other PIKKs owing to their large size and extensive HEAT repeats. In addition, post-translational modifications by the SUMO (Small Ubiquitin-like Modifier) ligase PIAS3 and the kinase Nek1 appear to prime Mec1/ATR for efficient DNA damage response (Figure 6) (Liu et al., 2013; Wu and Zou, 2016).

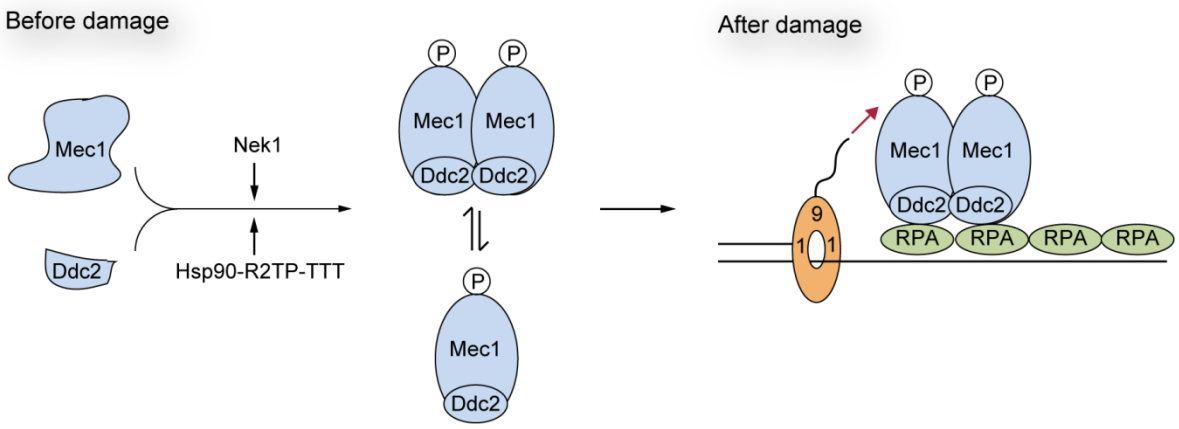

Figure 6: Model of Mec1-Ddc2 maturation and recruitment. Mec1-Ddc2 is folded and assembled, even before DNA damage, by the Hsp90-R2TP-TTT co-chaperone complex and priming kinase Nek1. After maturation, Mec1-Ddc2 complexes are recruited to sites of DNA damage through a direct interaction of Ddc2 and RPA. Recruited Mec1-Ddc2 is activated by the 9-1-1 checkpoint clamp and other factors (see Figure 7 for Mec1-Ddc2 activation).

2.2. Co-activators of Mec1/ATR

ssDNA-RPA generated at DNA damage sites or after replication stress is not sufficient for checkpoint induction by Mec1, but requires a double-stranded primer with a free 5‘ end (Figure 3) (MacDougall et al., 2007). The length of ssDNA adjacent to dsDNA positively correlates with Mec1 phosphorylation of Chk1. Such primed ssDNA structures containing long ssDNA tracts are formed as intermediates in various DNA repair processes and at stalled replication forks. However, during normal replication, such structures rarely feature long ssDNA tracts and therefore the threshold for Mec1/ATR activation might not be reached. The ds-ssDNA junction in the primed ssDNA structures recruits the Rad24-RFC clamp loader complex that binds the so-called 9-1-1 checkpoint clamp, which is a heterotrimeric ring-shaped protein complex containing Ddc1-Rad17-Mec3 in budding yeast (RAD9-HUS1-RAD1 in human and *S. pombe*) (Majka and Burgers, 2004). Crystal structures of the 9-1-1 clamp and the DNA polymerase associated trimeric sliding clamp PCNA (proliferating cell nuclear antigen) show structural similarity (Dore et al., 2009). However, distinct clamp loading complexes ensure specificity of 9-1-1 for 5’ junctions promoted by ssDNA-RPA, whereas PCNA gets recruited to 3’ junctions during normal DNA replication (Majka et al., 2006a). An important requirement of proper checkpoint signaling is the independent recruitment of the Mec1-Ddc2 and the 9-1-1 complexes to damage sites (Kondo et al., 2001; Melo et al., 2001). Under physiological salt concentrations, the 9-1-1 clamp, the clamp loader and the ssDNA-RPA platform are necessary for Mec1 phosphorylation of downstream target Rad53 (human Chk2, *S. pombe* Cds1) *in vitro* (Majka et al., 2006b). However, the Ddc1 subunit of the 9-1-1 clamp can directly activate Mec1 under low salt conditions i.e. 20 to 40 mM NaCl, in the absence of other factors. The Mec1 activation domain of Ddc1 lies in Ddc1’s poorly conserved unstructured C-terminal tail, and mutagenesis showed the requirement of two conserved aromatic residues in Ddc1, W352 and W544, for Mec1 activation *in vitro* (Navadgi-Patil and Burgers, 2009). In other organisms, however, direct activation of Mec1 by 9-1-1 is not conserved.

A conserved activator of Mec1/ATR is the essential replication protein Dpb11 (TopBP1 in human, Cut5/Rad4 in *S. pombe*). Through its multiple BRCA-1 C-terminal (BRCT) domains, yeast Dpb11 recognizes phosphorylated 9-1-1 subunit Ddc1 (residue T602), whereas human TopBP1 recognizes autophosphorylated ATR (residue T1989) (Delacroix et al., 2007; Furuya et al., 2004; Liu et al., 2011b). Once localized to damage sites, Dpb11 then activates Mec1-Ddc2 through an unstructured C-terminal tail (Navadgi-Patil and Burgers, 2008) and this activation is dependent on the interaction of the Dpb11 C-terminal tail with Ddc2 (Mordes et al., 2008). This tail is not conserved in human and instead ATR activation by TopBP1 is attributed to a region between the sixth and the seventh BRCT domains of TopBP1 (Kumagai et al., 2006). Like yeast, human ATR activation is promoted by TopBP1 interaction with ATRIP. Overexpression of this ATR-activating domain alone is sufficient to activate ATR. Additionally, tethering the ATR-activating domain to the PCNA clamp or the nucleosome, can bypass the requirement of the 9-1-1 clamp to activate ATR. Like Ddc1, the Dpb11 C-terminus and the TopBP1 ATR-activating domain harbor an unstructured tail that contains two conserved aromatic residues crucial for

Mec1/ATR activation. Although both Ddc1 and Dpb11 can activate Mec1 *in vitro*, their cellular function is most likely cell-cycle dependent. Whereas Ddc1 seems to activate Mec1 in G1-phase, Ddc1 and Dpb11 act redundantly to activate Mec1 in G2-phase (Navadgi-Patil and Burgers, 2009). Similarly, *S. pombe* Cut5 (ortholog of budding yeast Dpb11) is the predominant activator of Rad3 (Mec1 ortholog) in G1 (Lin et al., 2012). Contrasting reports show that Ddc1 and Dpb11 act redundantly in G1, whereas Ddc1 predominantly activates Mec1 in G2/M after UV damage (Puddu et al., 2011).

However, in S-phase cells, Mec1 can be activated even when the Mec1 activating domains of Ddc1 or Dpb11 are mutated. Biochemical screening of 39 proteins involved in DNA replication identified Dna2, a nuclease-helicase, as an S-phase specific Mec1 activator (Kumar and Burgers, 2013). Like Ddc1 and Dpb11, Dna2 harbors a Mec1-activating domain containing two aromatic residues (W128 and Y130) in an unstructured region. Mutations in *ddc1*, *dpb11*, and *dna2*, the three activators of Mec1, completely abolished the Mec1-mediated checkpoint in S-phase cells lacking the Tel1 kinase, Tel1 being a compensatory kinase of Mec1 (Sanchez et al., 1996). However, it is unknown whether human DNA2, like Ddc1 in yeast, activates ATR.

Recently, three separate studies identified a previously uncharacterized protein, ETAA1 (Ewing's tumor-associated antigen 1) as an activator of ATR in humans (Bass et al., 2016; Haahr et al., 2016; Lee et al., 2016). ETAA1 activation of ATR is independent of TopBP1 and simultaneous depletion of ETAA1 and TopBP1 results in synergistic lethality, abolishes ATR checkpoint signaling and results in genomic instability. While TopBP1 is recruited by the 9-1-1 and the MRE11-RAD50-NBS1 (MRN) complexes, ETAA1 is an RPA-binding protein (Feng et al., 2016). 9-1-1 preferentially binds 5' ds-ssDNA junctions *in vivo*, whereas RPA binds ssDNA. This might allow for different numbers and coverage of TopBP1 and ETAA1 proteins at DNA damage sites. Like other Mec1/ATR co-activators, ETAA1 contains an unstructured ATR-activating domain. Although, it is clear that an unstructured region containing two aromatic residues forms a motif that activates Mec1/ATR, the molecular details of how such a motif stimulates Mec1/ATR kinase activity are unclear.

Taken together, budding yeast contains at least three co-activators of Mec1: Ddc1, Dpb11 and Dna2 (Figure 7), whereas human cells contain at least two co-activators of ATR: TopBP1 and ETAA1. This redundancy of co-activators underscores the importance of a localized and timely activation of the Mec1/ATR checkpoint pathway. Indeed, artificial colocalization of Ddc1 and Mec1-Ddc2 induces Mec1 activation and checkpoint signaling even in the absence of DNA damage (Bonilla et al., 2008). Similarly, colocalization of Mrc1, a replisome component, and Mec1-Ddc2 is sufficient for Mec1 to phosphorylate Rad53 independent of co-activators Dpb11 and Ddc1 (Berens and Toczyski, 2012). Since misactivation of Mec1/ATR in the absence of DNA damage or replication stress can cause cellular senescence (Toledo et al., 2008), it is crucial that recruitment and activation of Mec1 are coupled and tightly regulated.

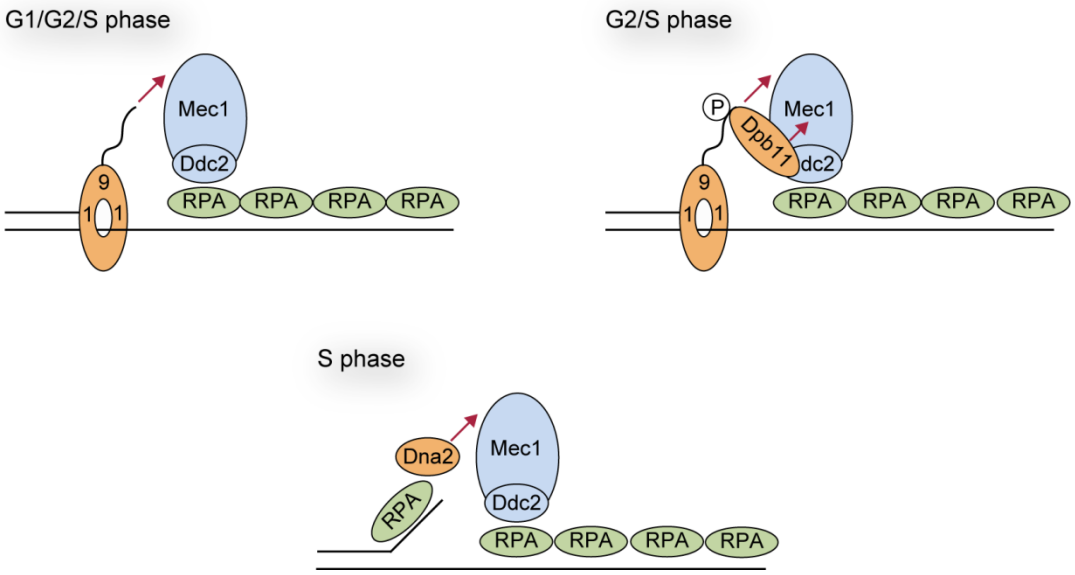

Figure 7: Cell-cycle dependent Mec1 activation. In budding yeast, the 9-1-1 checkpoint clamp activates Mec1 via two conserved aromatic residues (not shown) in the flexible C-terminal tail of the Ddc1 subunit. In G2 and S-phases, phosphorylated 9-1-1 recruits Dpb11, which activates Mec1 directly. In S-phase, Dna2 which is recruited to long 5' flaps generated during lagging strand synthesis, can activate Mec1.

2.3. Amplifying Mec1/ATR signaling

Once Mec1/ATR is properly recruited and activated, post-translational modifications further stimulate Mec1/ATR kinase activity and amplify the DNA damage signaling pathway. After DNA damage, PRP19, a ubiquitin ligase, binds ssDNA-RPA and deposits K63 poly-ubiquitin chains on the RPA32 subunit of RPA (Marechal et al., 2014; Wan and Huang, 2014). These K63 linked chains are recognized by ATRIP promoting further recruitment of ATR-ATRIP complexes. Mutants of *PRP19* defective in binding RPA or ubiquitin ligase activity, fail to efficiently phosphorylate ATR targets including RPA32 and Chk1. The PRP19-mediated signal amplification pathway is conserved in budding yeast. Similarly, RFWD3, another ubiquitin ligase gets recruited to RPA and ubiquitylates RPA in a DNA damage dependent manner to promote RPA and Chk1 phosphorylation (Elia et al., 2015; Liu et al., 2011a). In addition to ubiquitylation, SUMOylation strengthens Mec1/ATR signaling. Specifically, ATRIP modification by SUMO2/3 at K234 and K289 boosts the interaction of ATRIP with multiple proteins including ATR, RPA70, TopBP1 and the MRN complex (Wu et al., 2014). ATRIP carrying K234R and K289R mutations resulted in reduced ATR-ATRIP recruitment to damage sites and reduced Chk1 phosphorylation. Recently, it was shown that Sirtuin2 (SIRT2) interacts with and deacetylates K32 of ATRIP in response to replication stress (Zhang et al., 2016). Residue K32 lies in close proximity to the RPA-binding domain of ATRIP and K32 deacetylation promotes ATRIP binding to ssDNA-RPA, ATR autophosphorylation, and ultimately ATR checkpoint signaling.

2.4. Adaptor proteins for Mec1/ATR signaling

Adaptor or mediator proteins are a class of checkpoint proteins that act as regulatory nodes to activate specific signaling pathways. Rad9, the first checkpoint protein to be identified in budding yeast, is the prototypical adaptor. Rad9 (Crb2 in *S. pombe*) has no clear ortholog in higher organisms but is functionally homologous to BRCA1, 53BP1 and MDC1. Through its protein-protein interaction domains, Rad9 acts as an adaptor for Mec1-dependent Rad53 activation in the DNA damage checkpoint during G1 and G2/M phases, but not in the replication checkpoint in S-phase (Weinert et al., 1994). Rad9 localization to damage sites depends on the recognition of histone H3 lysine 79 methylation (H3K79me) by the Rad9 Tudor domain (Grenon et al., 2007), and histone H2A serine 129 phosphorylation (γ-H2A in yeast, γ-H2AX in human) by the Rad9 tandem BRCT domain (Hammet et al., 2007) (Figure 8). Methyltransferase Dot1 deposits the H3K79me mark, while Mec1 and Tel1 phosphorylate H2A serine 129 rapidly in response to DNA damage (Downs et al., 2000; Shroff et al., 2004; van Leeuwen et al., 2002). Furthermore, Rad9 itself is hyperphosphorylated by Mec1 and Tel1 in response to DNA damage (Vialard et al., 1998). Phosphorylated Rad9 is then recognized by the Rad53 forkhead-associated (FHA) domains, which increases the local concentration of Rad53 to damage sites (Sun et al., 1998). Mutations of Rad9 residues that are phosphorylated by Mec1 and Tel1, or mutations in Rad53 FHA domains, disrupt Rad9-Rad53 interaction and impair checkpoint activation (Lee et al., 2003; Schwartz et al., 2002). Thus, Rad9 acts as a mediator scaffold to localize Rad53 near the Mec1 kinase. In support of this model, one can bypass the requirement of Rad9 by creating a fusion of Rad53 to Mec1-Ddc2 (Lee et al., 2004). How Rad9 releases Rad53 to transduce the signal of damage once Rad53 is activated is unclear. The possibility of a negative feedback loop is suggested by the fact that Rad9 disassembles after it becomes phosphorylated by Rad53 (Usui et al., 2009). In conclusion, Rad9 is an adaptor for Rad53 activation in the DNA damage checkpoint in G1 and G2/M phases.

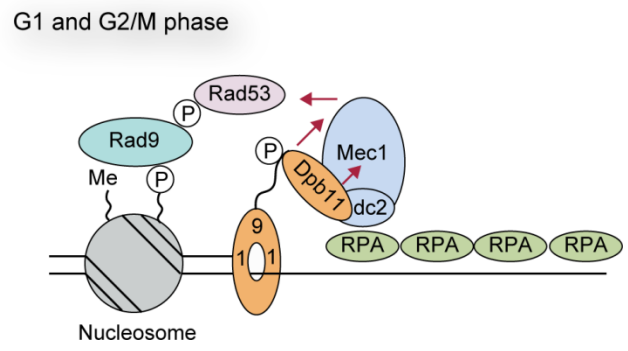

Figure 8: Rad9-dependent Rad53 activation. Upon DNA damage in G1 and G2-phases, nucleosome modifications H3K79me and γ-H2A, recruit the Rad9 adaptor protein. Rad9 gets phosphorylated in a Mec1/Tel1-dependent manner. Phosphorylated Rad9 localizes Rad53 close to Mec1-Ddc2 to promote Rad53 activation.

In S-phase, yeast Mrc1 (Claspin in human) mediates Rad53 activation (Alcasabas et al., 2001; Tanaka and Russell, 2001). Indeed, a *rad9*Δ *mrc1*Δ double mutant fails to activate Rad53 and induces synthetic lethality. Similarly, in human cells, Claspin interacts with Chk1 and promotes Chk1 phosphorylation (Chini and Chen, 2003; Kumagai and Dunphy, 2000). In addition to its role in checkpoint signaling, Mrc1/Claspin plays a role in DNA replication. Mrc1, along with Tof1-Csm3, localizes to replication forks under normal S-phase conditions, and travels with the fork to promote efficient replication (Osborn and Elledge, 2003). Upon encountering replication blocks, Mrc1 and Tof1-Csm3 form a stable replisome pausing complex (Katou et al., 2003). In addition, Mrc1 and Tof1-Csm3 interact with leading strand polymerase epsilon and the MCM replicative helicase and thus couple DNA synthesis and unwinding activities (Bando et al., 2009; Lou et al., 2008). Upon replication stress, Mrc1/Claspin gets phosphorylated by Mec1/ATR (Alcasabas et al., 2001). Alanine substitution mutations of the phosphorylated residues of Mrc1 render Mrc1 proficient in replication but defective in checkpoint function. Furthermore, yeast Mrc1 phosphorylation was shown to be important for Mec1 recruitment to stalled forks (Naylor et al., 2009). However, human Claspin was shown to act downstream of TopBP1 and depletion of Claspin selectively abrogated ATR's ability to phosphorylate Chk1, but not other ATR targets (Liu et al., 2006).

RecQ family helicase Sgs1 (human BLM, *S. pombe* Rqh1) is also involved in activating Rad53 in response to replication stress (Frei and Gasser, 2000) and this activity is independent of Sgs1 helicase function (Bjergbaek et al., 2005). Upon replication stress, Sgs1 is phosphorylated by Mec1-Ddc2 and this phosphorylation is recognized by the Rad53 FHA domain (Hegnauer et al., 2012). In addition, Sgs1 constitutively associates with replication forks (Cejka et al., 2010). Therefore, Sgs1 acts as a mediator to recruit Rad53 close to Mec1 at stalled forks. Whereas Sgs1 and Mrc1 are epistatic for Rad53 activation at stalled forks, Sgs1 and 9-1-1 act in parallel pathways and hence show synergy (Bjergbaek et al., 2005). In human cells, the Sgs1 ortholog BLM was also reported to be a target of ATR phosphorylation, and plays a role in recovery from replication stress (Davies et al., 2004).

In addition to Rad9, Mrc1 and Sgs1, which act as cell cycle specific adaptors of the Mec1-Rad53 signaling pathway, the Mec1/ATR pathway can also be regulated by damage-specific repair proteins. For example, Fanconi anemia pathway proteins, FANCM and FAAP24, which are recruited to inter-strand crosslinks, are implicated in Mec1/ATR activation independently of the Fanconi anemia core complex (Collis et al., 2008). NER proteins and the Exo1 exonuclease process UV-lesions to expose ssDNA which recruits RPA and activates Mec1/ATR (Giannattasio et al., 2010). Thus Mec1/ATR activation is regulated by a wide variety of context-specific regulators.

3. Mec1/ATR targets

Once Mec1/ATR is assembled and activated at sites of DNA damage or replication stress, it phosphorylates several targets and initiates a signaling cascade to control the cell-cycle, regulate origin firing and protect the replication fork while coordinating DNA repair and recovery (Friedel et al., 2009). Over the last decade, proteomics approaches have revealed numerous Mec1/ATR targets (Bastos de

Oliveira et al., 2015; Chen et al., 2010; Hustedt et al., 2015; Smolka et al., 2007). In this section, I will discuss some of the key targets that are essential in maintaining genome stability.

3.1. Rad53/CHK1: The major Mec1/ATR target

In budding yeast, there are two effector kinases downstream of Mec1, Rad53 (CHK2 in *S. pombe* and humans) and Chk1 (CHK1 in humans and *S. pombe*) (Sanchez et al., 1999). Rad53 is the major effector kinase in budding yeast, while in *S. pombe* and higher eukaryotes, CHK1 (Chk1 in budding yeast) assumes this role. Rad53/CHK1 is rapidly phosphorylated on multiple sites in a Mec1/ATR dependent manner upon DNA damage or replication stress and is a hallmark of an active Mec1/ATR checkpoint pathway (Pellicioli and Foiani, 2005). As described in section 2.4., Rad53 recruitment to Mec1 is dependent on adaptor proteins, Rad9 and Mrc1. In humans, adaptor protein Claspin brings CHK1 and ATR together. Following phosphorylation and activation, Rad53/CHK1 is released from chromatin and transmits the checkpoint signal throughout the cell (Smits et al., 2006). This is especially important because Mec1/ATR is considered to be a local kinase that acts at sites of DNA damage. An important target of Rad53 is the Dun1 kinase (Zhou and Elledge, 1993). A diphosphothreonine motif in the Rad53 kinase is recognized by the Dun1 FHA domain, allowing Rad53-dependent phosphorylation and activation of Dun1 (Bashkirov et al., 2003; Pike et al., 2003).

3.2. Cell cycle control

Rad53 and Chk1 phosphorylate several targets to arrest the cell cycle including Cdc5, a polo-like kinase involved in mitosis regulation, Pds1 (securin), which inhibits metaphase to anaphase transition, and the Bfa1-Bub2 GTPase activating protein complex, which inhibits mitotic exit (Hu et al., 2001; Sanchez et al., 1999; Smits et al., 2000). In *S. pombe* and higher organisms, CHK1 kinase phosphorylates and thereby inhibits all three CDC25 (Mih1 in *S. pombe*) phosphatase isoforms that function to activate cyclin-dependent kinases (CDKs) (Furnari et al., 1997; Sanchez et al., 1997; Uto et al., 2004).

A key mechanism of Mec1/ATR regulation of the cell cycle occurs through control of origin firing. Indeed, cells lacking Mec1 or Rad53 fire late origins prematurely and show loss of viability (Santocanale and Diffley, 1998; Shirahige et al., 1998). Rad53 phosphorylates and inactivates three DNA replication factors, Sld3, Dbf4 (the regulatory partner of the Cdc7 kinase), and helicase subunit Mcm4 (Lopez-Mosqueda et al., 2010; Sheu et al., 2014; Zegerman and Diffley, 2010). In agreement, mutations in all the three targets, Sld2-Sld3, Dbf4 and Mcm4, activated late origins prematurely, similar to cells lacking Mec1 or Rad53 (Sheu et al., 2016). In human cells, ATR/CHK1 phosphorylates Dbf4 and Treslin (related to budding yeast Sld3) (Heffernan et al., 2007). CDKs phosphorylate Sld2 and Sld3 to create a binding site for the BRCT domains of Dpb11 (Tanaka et al., 2007; Zegerman and Diffley, 2007). This Sld3-Dpb11-Sld2 complex is important for the loading and activation of the Cdc45-Mcm2-7-GINS (CMG) replicative helicase. In response to replication stress, Rad53/CHK1-dependent phosphorylation of Sld3/Treslin prevents the interaction of Sld3/Treslin and Dpb11/TopBP1, which prevents late origin firing (Boos et al., 2011; Guo et

al., 2015; Lopez-Mosqueda et al., 2010; Zegerman and Diffley, 2010). Thus, Mec1-Rad53 checkpoint signaling regulates cell cycle transitions to prevent duplication of an unrepaired genome.

In budding yeast, Mec1-Rad53 signaling activates the Dun1 kinase, which in turn phosphorylates and inhibits Sml1 and Dif1, inhibitors of ribonucleotide reductase (RNR) (Lee et al., 2008; Zhao and Rothstein, 2002). Thus, the Mec1-Rad53-Dun1 cascade causes an 8-fold increase in the dNTP pool, which facilitates cell survival in the face of DNA damage or replication stress (Chabes et al., 2003). Even under normal replication conditions, this pathway is important for dNTP regulation and cell survival. In fact, the lethality associated with *mec1* deletion in yeast is not due to its checkpoint function, but due to its role in dNTP level regulation (Desany et al., 1998; Zhao et al., 1998). Therefore, up-regulating dNTP pools by *sml1* deletion, is routinely used to suppress lethality associated with *mec1* or *rad53* deletions. Alternatively, increasing the RNR activity by deleting RNR inhibitors, such as *dif1*, *crt1* and *hug1*, or overexpressing *RNR1* or *RNR3* can also bypass *mec1* or *rad53* deletions (Basrai et al., 1999; Huang et al., 1998; Wu and Huang, 2008; Zhao et al., 1998). In higher organisms, however, Mec1/ATR does not play an essential role in dNTP regulation, although ATR promotes accumulation of RNR subunit RRM2 in human cells (D'Angiolella et al., 2012).

3.3. Replication fork protection

In addition to dNTP regulation, a crucial function of Mec1 is the maintenance of replication fork stability in response to replication stress. Early studies suggested that Mec1 regulation of cell cycle, transcription, and late origin firing only make modest contributions to cell viability. On the other hand, Mec1 checkpoint signaling is essential for avoiding irreversible breakdown of stalled replication forks termed as 'fork collapse' (Tercero et al., 2003). Collapsed forks contain large ssDNA regions and hemi-replicated intermediates which may give rise to reversed forks, as seen by electron microscopy of HU-treated cells lacking Rad53 (Sogo et al., 2002).

One mechanism of Mec1/ATR protection of stalled forks is through SMARCAL1. SMARCAL1 binds RPA and regresses stalled forks to promote fork restoration (Ciccia et al., 2009). Both too much and too little of SMARCAL1 activity causes replication-associated DNA damage (Bansbach et al., 2009). ATR phosphorylates a conserved serine residue in SMARCAL1 which regulates its DNA processing activity to prevent fork collapse (Couch et al., 2013). Selective ATR inhibition deregulates SMARCAL1 activity and induces fork collapse by causing aberrant fork structures that give rise to DSBs.

Mec1/ATR is important to maintain the replisome components at sites of origin following replication stress (Cobb et al., 2003; Tercero et al., 2003). Quantitative chromatin immunoprecipitation analysis of HU-arrested forks showed that leading and lagging strand polymerases and Cdc45 dissociate in cells lacking Mec1. Similar assays in cells lacking Rad53, however, only showed displacement of the MCM helicase but not the polymerases and Cdc45, highlighting the distinct roles played by Mec1 and Rad53 at stalled forks. Similarly, in higher eukaryotes, chromatin association of PCNA, CDC45 and the POLD2 and POLE

polymerases was reduced in ATR-deficient cells after treatment with replicative polymerase inhibitor aphidicolin (Ragland et al., 2013). However, genome-wide analysis of replication forks suggest that replisome stability at stalled forks might be independent of the Mec1/ATR checkpoint (De Piccoli et al., 2012). Deep sequencing analyses suggest that the replisome stays on chromatin but randomly slides away from the early initiating sites in HU-treated cells lacking Mec1 or Rad53. Recent studies using isolation of proteins on nascent DNA also suggest that replication stress in ATR-deficient cells does not cause replisome destabilization, but rather altered chromatin association of other fork-associated proteins (Dungrawala et al., 2015).

The Mec1 checkpoint pathway also regulates the activity of nucleases and helicases at perturbed forks. In budding yeast, Rad53 hyperphosphorylates DNA helicases Pif1 and Rrm3 to inhibit their activity at HU-challenged forks, and thus prevents fork reversal, chromosome fragmentation, and genome instability (Rossi et al., 2015). Similarly, human Chk1 prevents aberrant origin firing, apoptosis and incorrect fork processing by the Mus81/Eme1 endonuclease and the Rqh1 DNA helicase (Doe et al., 2002; Forment et al., 2011). Similarly, *S. pombe* Cds1 (Rad53 in budding yeast) prevents unscheduled Mus81/Eme1-mediated fork processing (Froget et al., 2008). In addition, Cds1 phosphorylates Dna2 on S220 after HU treatment and increases the chromatin association and nuclease activity of Dna2 to prevent fork reversal at stalled forks (Hu et al., 2012). The exonuclease Exo1 is also phosphorylated and inhibited by the checkpoint kinases (Morin et al., 2008). Interestingly, the major function of Rad53 at stalled forks is to prevent Exo1-dependent replication fork collapse, since cells lacking Exo1 almost completely rescued the sensitivity of cells lacking Rad53 after treatment with MMS (Segurado and Diffley, 2008). As described in section 2.4., the Sgs1 helicase gets phosphorylated by Mec1 and acts as an adaptor protein for Mec1-dependent activation of Rad53. In addition, Mec1 phosphorylation of Sgs1 also regulates Sgs1 helicase activity to prevent fork collapse (Cobb et al., 2005). Importantly, prevention of fork collapse is dependent on the helicase activity of Sgs1 and not just the role of Sgs1 in recruiting Rad53 to perturbed forks. Thus, checkpoint kinases target numerous nucleases and helicases to prevent abnormal fork processing that may hinder replication fork restart after repair of DNA damage.

3.4. Coordination of DNA repair

DNA repair is coupled to the DNA damage checkpoint and therefore an important class of Mec1/ATR targets includes proteins involved in DNA repair. Mec1/ATR induces phosphorylation of proteins involved in the regulation of homologous recombination such as RAD51, BRCA1, WRN (Werner syndrome ATP-dependent helicase) and BLM in humans (Davies et al., 2004; Pichierri et al., 2003; Sorensen et al., 2005; Tibbetts et al., 2000). Although the direct implication of these phosphorylation events is not fully understood, the function is most likely prevention of aberrant strand-exchange events (Meister et al., 2005). In human cells, ATR has been shown to phosphorylate NER protein XPA to regulate its intracellular localization (Wu et al., 2007). Additionally, yeast checkpoint protein Ddc1, part of the 9-1-1 clamp, physically interacts with Rad14 (XPA ortholog) (Giannattasio et al., 2004). Similarly, 9-1-1 also

interacts with BER factors including MYH, Polβ, NEIL1, TDG, Fen1 and DNA Ligase I, and stimulates their enzymatic activities (Balakrishnan et al., 2009; Chang and Lu, 2005; Gembka et al., 2007; Guan et al., 2007a; Guan et al., 2007b; Toueille et al., 2004; Wang et al., 2004). In *S. pombe*, Rad3 (Mec1 in budding yeast) dependent phosphorylation of Rad9 (Ddc1 in budding yeast) on T225 promotes Rad9 interaction with the post-replication repair protein Mms2 for efficient error-free repair and suppression of error-prone repair synthesis by translesion polymerases and strand invasion by Rhp51 (Kai et al., 2007). ATR signaling also targets the Fanconi-anemia protein FANCD2 to promote its localization to DNA damage for efficient inter-strand crosslink repair (Andreassen et al., 2004). Thus, Mec1/ATR signaling regulates DNA repair pathways in response to a variety of lesions.

4. Architecture of PIKKs

Phosphoinositide 3-kinase (PI3K)-related protein kinases (PIKKs) are a family of Ser/Thr protein kinases, whose kinase domains share homology with the PI3K lipid kinases, but lack lipid kinase activity (Baretic and Williams, 2014). Mammals express six PIKKs: ATR, ATM, mTOR (mammalian target of rapamycin), DNA-PK (DNA-dependent protein kinase), SMG1 and TRRAP. In budding yeast, the orthologs of four PIKK members, ATR (Mec1), ATM (Tel1), mTOR (Tor1p and Tor2p) and TRRAP (Tra1p) have been found, but that of SMG1 and DNA-PK are not known. These so-called “giant” kinases range in size between 2,547 and 4,128 aa in humans and share a common domain organization (Figure 9). The highly conserved kinase domain at the C-terminus is flanked by regions of sequence similarity called the FAT (FRAP, ATM, TRRAP) and the FATC (FAT C-terminus) domains. A large part of the N-terminus of the PIKKs consists of extensive α-solenoid helical HEAT repeats, as mentioned in section 2.1.

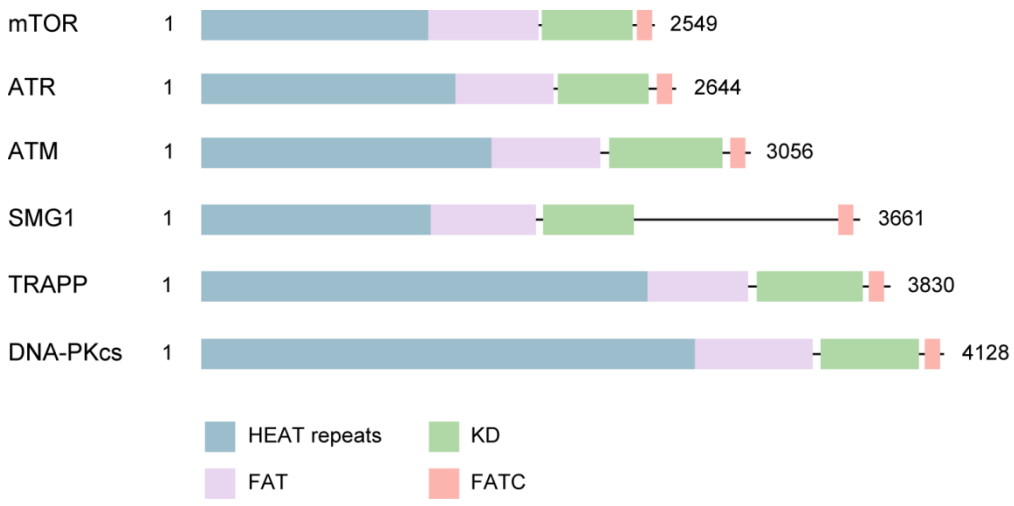

Figure 9: Domain organization of human PIKK proteins. The N-terminus is folded into α-helical HEAT repeats (shown in teal). HEAT repeats extend into a region of sequence similarity called FAT domain (shown in pink). KD represents the highly conserved kinase domain (shown in green). FATC is a highly conserved regulatory region at the C-terminus (shown in light orange).

Despite structural conservation, PIKKs serve diverse functions, reflecting their distinct subcellular distribution, substrate recognition and activation mechanisms, which depend on distinct regulatory subunits and co-activators (Table 2).

Table 2: Regulatory subunits and co-activators of major mammalian PIKKs. Yeast orthologs are mentioned in brackets.

PIKK	Regulatory subunit	Co-activator
ATR (Mec1)	ATRIP (Ddc2)	TopBP1/ETAA1 (Ddc1, Dpb11, Dna2)
ATM (Tel1)	NBS1 (Xrs2)	MRE11/RAD50 (Mre11/Rad50)
mTOR (Tor1p/Tor2p)	RAPTOR/RICTOR/mLST8 (Kog1/Tco89/Avo3/Lst8)	RHEB/TSC1/2/AMPK (Rhbp/Snf1)
DNA-PKcs (?)	Ku 70/80	Ku/DNA

Since their discovery in the mid-1990s, structural studies of PIKKs remained largely unsuccessful owing to their large size and complex architecture. The crystal structure of DNA-PKcs (DNA-PK catalytic subunit) at 6.6 Å resolution provided the first structural insights into PIKK architecture (Sibanda et al., 2010). The structure revealed that the α-helical HEAT repeats bend to form a hollow circular ring-like structure and allow the kinase domain to sit on top of it. A more detailed view of the PIKK architecture was provided with a high-resolution crystal structure of the mTOR C-terminus (encompassing the FAT/Kinase/FATC domains) in complex with accessory protein mLST8 (Yang et al., 2013). Surprisingly, the mTOR FAT domain was tightly associated with the kinase domain, while the highly conserved FATC domain interacted with the kinase activation loop. Moreover, structural analysis of the activation state of the kinase domain and mechanism of phosphotransfer, suggested that the crystallized kinase complex was intrinsically active even in the absence of additional regulatory subunits and shared the same catalytic mechanism as canonical protein kinases.

The last couple of years have seen a flurry of medium-resolution PIKK structures, largely owing to major advancements in the field of cryo-electron microscopy (cryo-EM). These cryo-EM structures include human mTORC1 (mTOR with subunits Raptor and mLST8) bound to a FK506 binding protein

(FKBP)-rapamycin complex at 5.9 Å resolution (Aylett et al., 2016), a 6 Å resolution structure of the full-length Tor–Lst8 complex from the thermotolerant yeast *Kluyveromyces marxianus* describing the complex topology of the HEAT repeats using domain insertions (Baretic et al., 2016) (Figure 10A), human mTORC1 at 4.4 Å resolution (Yang et al., 2016), *S. pombe* ATM/Tel1 at 8.7 Å resolution (Wang et al., 2016), closed and open conformations of human ATM dimers (Baretic et al., 2017), human DNA-PKcs at 4.4 Å resolution (Figure 10B) and the DNA-PK holoenzyme at 5.8 Å resolution (Sharif et al., 2017). In addition to the 6.6 Å resolution crystal structure of DNA-PKcs (Sibanda et al., 2010), the Blundell lab has recently published a 4.3 Å resolution crystal structure of DNA-PKcs in complex with residues 539 to 732 of Ku80 which suggests an allosteric mechanism modulating DNA DSB repair (Sibanda et al., 2017). Remarkably, Mec1/ATR structures have not been reported except for a 22 Å resolution negative-stain EM map of *S. cerevisiae* Mec1-Ddc2 (Sawicka et al., 2016).

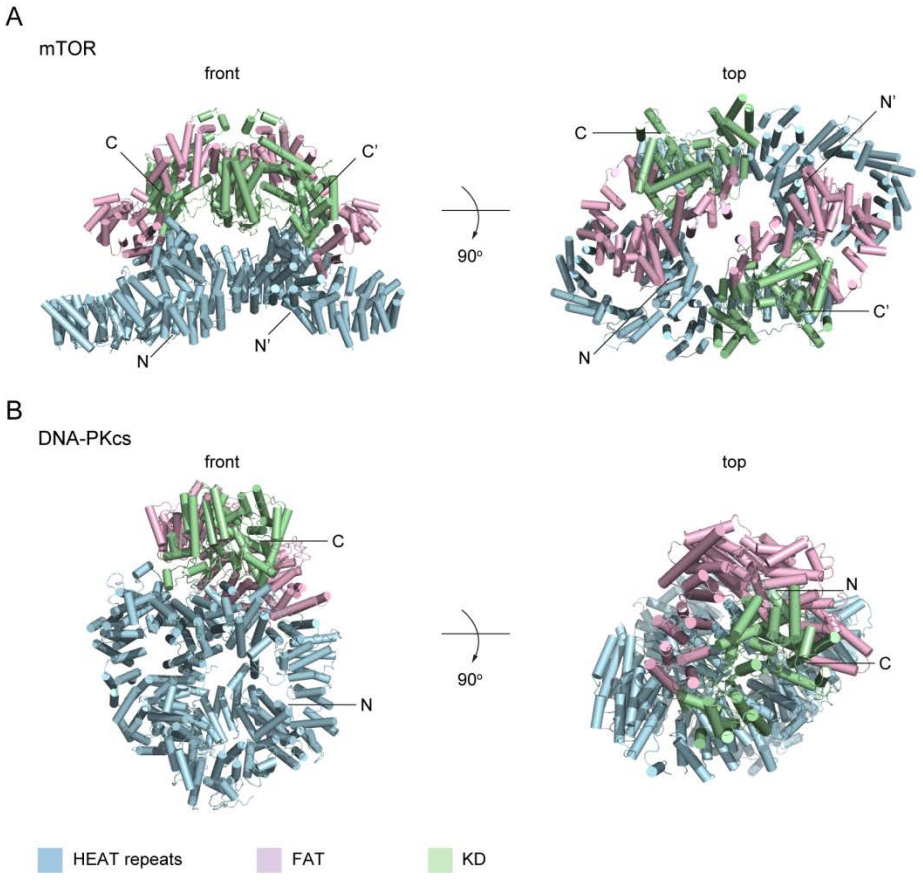

Figure 10: Structures of **(A)** Dimeric mTOR (PDB ID: 5FVM, Lst8 not shown) and **(B)** Monomeric DNA-PKcs (PDB ID: 5LUQ). Top and front views are shown. The N-terminal α-helical HEAT repeats are colored in teal. FAT domain is colored in pink. KD is colored in green. N and C termini are labeled.

A common theme that emerges from these structural studies is the oligomeric nature of PIKKs. DNA-PKcs, which is monomeric on gel filtration columns, was dimeric in the crystallographic asymmetric unit as well as in EM analysis. Thus, it is tempting to suggest that a DNA-PKcs dimer would align two broken DNA ends for ligation. Tel1/ATM, on the other hand, is catalytically inactive in its dimeric form. In response to DSBs, ATM is autophosphorylated on residue S1981, causing dissociation of inert dimers into catalytically active monomers (Bakkenist and Kastan, 2003). However, this dimer-monomer transition does not seem to be conserved in the case of ATR, since both ATR and ATRIP exist as oligomers before and after the induction of DNA damage (Ball and Cortez, 2005). These studies, however, were performed by tagging the proteins differentially, followed by immunoprecipitating with one tag and immunoblotting for the other tag. Therefore, we cannot rule out the possibility that ATR-ATRIP may co-exist as monomers and oligomers. In fact, overexpressed and purified budding yeast Mec1-Ddc2 was monomeric (19%) as well as dimeric (81%) in negative-stain EM experiments (Sawicka et al., 2016). Furthermore, support for both monomeric and dimeric Mec1-Ddc2 species, can be found in the literature (Bomgarden et al., 2004; Itakura et al., 2005; Kim et al., 2005; Unsal-Kacmaz and Sancar, 2004). Despite several efforts, the homodimerization of Mec1-Ddc2 is poorly understood. For example, complete information about the homodimerization interfaces between Mec1-Ddc2 molecules is missing. Moreover, the binding interface between Mec1 and Ddc2 remains unclear. An important unanswered question is whether Mec1-Ddc2 undergoes conformational changes that reflect its activity. Another open question is: How do the two conserved aromatic residues present in the multiple Mec1 co-activators stimulate Mec1 catalytic activity? Clearly, high resolution structures of Mec1-Ddc2 are needed to fill these knowledge gaps and provide detailed mechanistic insights into Mec1 kinase regulation.

Despite structural conservation, PIKKs perform diverse functions due to dissimilar localization, activation and substrate recognition, mostly as a result of their respective regulatory subunits. Indeed, Mec1 forms an enzyme complex with its regulatory subunit Ddc2, since the functions and stability of the proteins are inter-dependent (Cortez et al., 2001; Paciotti et al., 2000). Cells lacking Ddc2 phenotypically mimic cells lacking Mec1 in yeast and higher organisms (Edwards et al., 1999; Rouse and Jackson, 2000; Wakayama et al., 2001). Therefore, mechanistic insights into how Ddc2 regulates Mec1 recruitment and activation are crucial. In the recently published 22 Å resolution negative-stain EM-map (Sawicka et al., 2016), the proposed electron density for Ddc2 was calculated by subtracting the Mec1-Ddc2 density from the Tel1 density after fitting in the mTOR density from PDB ID: 5FLC. Although, Mec1, Tel1 and mTOR carry HEAT repeats at their N-termini, the low sequence similarity and variability in length of the HEAT repeats in these three kinases suggest that the architecture of the N-terminal HEAT repeats might be different. This is especially relevant considering Mec1, Tel1 and mTOR use their HEAT repeats to interact with their different substrates. Therefore, a comparison of the HEAT repeat densities might lead to problematic outcomes. Thus, it is possible that the proposed Ddc2 electron density in the negative-stain EM map may have been incorrectly assigned.

To gain structural insights into Mec1-Ddc2 assembly and activation at DNA damage sites, I carried out structural, biochemical and *in vivo* experiments on the homodimerization and recruitment domains of Ddc2.

References

Alani, E., Thresher, R., Griffith, J.D., and Kolodner, R.D. (1992). Characterization of DNA-binding and strand-exchange stimulation properties of y-RPA, a yeast single-strand-DNA-binding protein. J Mol Biol *227*, 54-71.

Alcasabas, A.A., Osborn, A.J., Bachant, J., Hu, F., Werler, P.J., Bousset, K., Furuya, K., Diffley, J.F., Carr, A.M., and Elledge, S.J. (2001). Mrc1 transduces signals of DNA replication stress to activate Rad53. Nat Cell Biol *3*, 958-965.

Andreassen, P.R., D'Andrea, A.D., and Taniguchi, T. (2004). ATR couples FANCD2 monoubiquitination to the DNA-damage response. Genes Dev *18*, 1958-1963.

Aylett, C.H., Sauer, E., Imseng, S., Boehringer, D., Hall, M.N., Ban, N., and Maier, T. (2016). Architecture of human mTOR complex 1. Science *351*, 48-52.

Bakkenist, C.J., and Kastan, M.B. (2003). DNA damage activates ATM through intermolecular autophosphorylation and dimer dissociation. Nature *421*, 499-506.

Balakrishnan, L., Brandt, P.D., Lindsey-Boltz, L.A., Sancar, A., and Bambara, R.A. (2009). Long patch base excision repair proceeds via coordinated stimulation of the multienzyme DNA repair complex. J Biol Chem *284*, 15158-15172.

Ball, H.L., and Cortez, D. (2005). ATRIP oligomerization is required for ATR-dependent checkpoint signaling. J Biol Chem *280*, 31390-31396.

Ball, H.L., Ehrhardt, M.R., Mordes, D.A., Glick, G.G., Chazin, W.J., and Cortez, D. (2007). Function of a conserved checkpoint recruitment domain in ATRIP proteins. Mol Cell Biol *27*, 3367-3377.

Ball, H.L., Myers, J.S., and Cortez, D. (2005). ATRIP binding to replication protein A-single-stranded DNA promotes ATR-ATRIP localization but is dispensable for Chk1 phosphorylation. Mol Biol Cell *16*, 2372-2381.

Bando, M., Katou, Y., Komata, M., Tanaka, H., Itoh, T., Sutani, T., and Shirahige, K. (2009). Csm3, Tof1, and Mrc1 form a heterotrimeric mediator complex that associates with DNA replication forks. J Biol Chem *284*, 34355-34365.

Bansbach, C.E., Betous, R., Lovejoy, C.A., Glick, G.G., and Cortez, D. (2009). The annealing helicase SMARCAL1 maintains genome integrity at stalled replication forks. Genes Dev *23*, 2405-2414.

Baretic, D., Berndt, A., Ohashi, Y., Johnson, C.M., and Williams, R.L. (2016). Tor forms a dimer through an N-terminal helical solenoid with a complex topology. Nat Commun *7*, 11016.

Baretic, D., Pollard, H.K., Fisher, D.I., Johnson, C.M., Santhanam, B., Truman, C.M., Kouba, T., Fersht, A.R., Phillips, C., and Williams, R.L. (2017). Structures of closed and open conformations of dimeric human ATM. Sci Adv *3*, e1700933.

Baretic, D., and Williams, R.L. (2014). PIKKs--the solenoid nest where partners and kinases meet. Curr Opin Struct Biol *29*, 134-142.

Bashkirov, V.I., Bashkirova, E.V., Haghnazari, E., and Heyer, W.D. (2003). Direct kinase-to-kinase signaling mediated by the FHA phosphoprotein recognition domain of the Dun1 DNA damage checkpoint kinase. Mol Cell Biol *23*, 1441-1452.

Basrai, M.A., Velculescu, V.E., Kinzler, K.W., and Hieter, P. (1999). NORF5/HUG1 is a component of the MEC1-mediated checkpoint response to DNA damage and replication arrest in Saccharomyces cerevisiae. Mol Cell Biol *19*, 7041-7049.
Bass, T.E., Luzwick, J.W., Kavanaugh, G., Carroll, C., Dungrawala, H., Glick, G.G., Feldkamp, M.D., Putney, R., Chazin, W.J., and Cortez, D. (2016). ETAA1 acts at stalled replication forks to maintain genome integrity. Nat Cell Biol *18*, 1185-1195.
Bastin-Shanower, S.A., and Brill, S.J. (2001). Functional analysis of the four DNA binding domains of replication protein A. The role of RPA2 in ssDNA binding. J Biol Chem *276*, 36446-36453.
Bastos de Oliveira, F.M., Kim, D., Cussiol, J.R., Das, J., Jeong, M.C., Doerfler, L., Schmidt, K.H., Yu, H., and Smolka, M.B. (2015). Phosphoproteomics reveals distinct modes of Mec1/ATR signaling during DNA replication. Mol Cell *57*, 1124-1132.
Berens, T.J., and Toczyski, D.P. (2012). Colocalization of Mec1 and Mrc1 is sufficient for Rad53 phosphorylation in vivo. Mol Biol Cell *23*, 1058-1067.
Bjergbaek, L., Cobb, J.A., Tsai-Pflugfelder, M., and Gasser, S.M. (2005). Mechanistically distinct roles for Sgs1p in checkpoint activation and replication fork maintenance. EMBO J *24*, 405-417.
Bochkarev, A., Pfuetzner, R.A., Edwards, A.M., and Frappier, L. (1997). Structure of the single-stranded-DNA-binding domain of replication protein A bound to DNA. Nature *385*, 176-181.
Bochkareva, E., Kaustov, L., Ayed, A., Yi, G.S., Lu, Y., Pineda-Lucena, A., Liao, J.C., Okorokov, A.L., Milner, J., Arrowsmith, C.H.*, et al.* (2005). Single-stranded DNA mimicry in the p53 transactivation domain interaction with replication protein A. Proc Natl Acad Sci U S A *102*, 15412-15417.
Bomgarden, R.D., Yean, D., Yee, M.C., and Cimprich, K.A. (2004). A novel protein activity mediates DNA binding of an ATR-ATRIP complex. J Biol Chem *279*, 13346-13353.
Bonilla, C.Y., Melo, J.A., and Toczyski, D.P. (2008). Colocalization of sensors is sufficient to activate the DNA damage checkpoint in the absence of damage. Mol Cell *30*, 267-276.
Boos, D., Sanchez-Pulido, L., Rappas, M., Pearl, L.H., Oliver, A.W., Ponting, C.P., and Diffley, J.F. (2011). Regulation of DNA replication through Sld3-Dpb11 interaction is conserved from yeast to humans. Curr Biol *21*, 1152-1157.
Brill, S.J., and Bastin-Shanower, S. (1998). Identification and characterization of the fourth single-stranded-DNA binding domain of replication protein A. Mol Cell Biol *18*, 7225-7234.
Brosey, C.A., Soss, S.E., Brooks, S., Yan, C., Ivanov, I., Dorai, K., and Chazin, W.J. (2015). Functional dynamics in replication protein A DNA binding and protein recruitment domains. Structure *23*, 1028-1038.
Brown, E.J., and Baltimore, D. (2000). ATR disruption leads to chromosomal fragmentation and early embryonic lethality. Genes Dev *14*, 397-402.
Burdova, K., Mihaljevic, B., Sturzenegger, A., Chappidi, N., and Janscak, P. (2015). The Mismatch-Binding Factor MutSbeta Can Mediate ATR Activation in Response to DNA Double-Strand Breaks. Mol Cell *59*, 603-614.
Byun, T.S., Pacek, M., Yee, M.C., Walter, J.C., and Cimprich, K.A. (2005). Functional uncoupling of MCM helicase and DNA polymerase activities activates the ATR-dependent checkpoint. Genes Dev *19*, 1040-1052.
Caldecott, K.W. (2008). Single-strand break repair and genetic disease. Nat Rev Genet *9*, 619-631.
Cancer Genome Atlas, N. (2012a). Comprehensive molecular characterization of human colon and rectal cancer. Nature *487*, 330-337.
Cancer Genome Atlas, N. (2012b). Comprehensive molecular portraits of human breast tumours. Nature *490*, 61-70.
Cancer Genome Atlas Research, N. (2012). Comprehensive genomic characterization of squamous cell lung cancers. Nature *489*, 519-525.

Caporali, S., Falcinelli, S., Starace, G., Russo, M.T., Bonmassar, E., Jiricny, J., and D'Atri, S. (2004). DNA damage induced by temozolomide signals to both ATM and ATR: role of the mismatch repair system. Mol Pharmacol *66*, 478-491.
Cejka, P., Cannavo, E., Polaczek, P., Masuda-Sasa, T., Pokharel, S., Campbell, J.L., and Kowalczykowski, S.C. (2010). DNA end resection by Dna2-Sgs1-RPA and its stimulation by Top3-Rmi1 and Mre11-Rad50-Xrs2. Nature *467*, 112-116.
Chabes, A., Georgieva, B., Domkin, V., Zhao, X., Rothstein, R., and Thelander, L. (2003). Survival of DNA damage in yeast directly depends on increased dNTP levels allowed by relaxed feedback inhibition of ribonucleotide reductase. Cell *112*, 391-401.
Chang, D.Y., and Lu, A.L. (2005). Interaction of checkpoint proteins Hus1/Rad1/Rad9 with DNA base excision repair enzyme MutY homolog in fission yeast, Schizosaccharomyces pombe. J Biol Chem *280*, 408-417.
Chapman, J.R., Taylor, M.R., and Boulton, S.J. (2012). Playing the end game: DNA double-strand break repair pathway choice. Mol Cell *47*, 497-510.
Chen, C., Umezu, K., and Kolodner, R.D. (1998). Chromosomal rearrangements occur in S. cerevisiae rfa1 mutator mutants due to mutagenic lesions processed by double-strand-break repair. Mol Cell *2*, 9-22.
Chen, S.H., Albuquerque, C.P., Liang, J., Suhandynata, R.T., and Zhou, H. (2010). A proteome-wide analysis of kinase-substrate network in the DNA damage response. J Biol Chem *285*, 12803-12812.
Chini, C.C., and Chen, J. (2003). Human claspin is required for replication checkpoint control. J Biol Chem *278*, 30057-30062.
Ciccia, A., Bredemeyer, A.L., Sowa, M.E., Terret, M.E., Jallepalli, P.V., Harper, J.W., and Elledge, S.J. (2009). The SIOD disorder protein SMARCAL1 is an RPA-interacting protein involved in replication fork restart. Genes Dev *23*, 2415-2425.
Cimprich, K.A., and Cortez, D. (2008). ATR: an essential regulator of genome integrity. Nat Rev Mol Cell Biol *9*, 616-627.
Cliby, W.A., Roberts, C.J., Cimprich, K.A., Stringer, C.M., Lamb, J.R., Schreiber, S.L., and Friend, S.H. (1998). Overexpression of a kinase-inactive ATR protein causes sensitivity to DNA-damaging agents and defects in cell cycle checkpoints. EMBO J *17*, 159-169.
Cobb, J.A., Bjergbaek, L., Shimada, K., Frei, C., and Gasser, S.M. (2003). DNA polymerase stabilization at stalled replication forks requires Mec1 and the RecQ helicase Sgs1. EMBO J *22*, 4325-4336.
Cobb, J.A., Schleker, T., Rojas, V., Bjergbaek, L., Tercero, J.A., and Gasser, S.M. (2005). Replisome instability, fork collapse, and gross chromosomal rearrangements arise synergistically from Mec1 kinase and RecQ helicase mutations. Genes Dev *19*, 3055-3069.
Collis, S.J., Ciccia, A., Deans, A.J., Horejsi, Z., Martin, J.S., Maslen, S.L., Skehel, J.M., Elledge, S.J., West, S.C., and Boulton, S.J. (2008). FANCM and FAAP24 function in ATR-mediated checkpoint signaling independently of the Fanconi anemia core complex. Mol Cell *32*, 313-324.
Cortez, D., Guntuku, S., Qin, J., and Elledge, S.J. (2001). ATR and ATRIP: partners in checkpoint signaling. Science *294*, 1713-1716.
Costanzo, V., Shechter, D., Lupardus, P.J., Cimprich, K.A., Gottesman, M., and Gautier, J. (2003). An ATR- and Cdc7-dependent DNA damage checkpoint that inhibits initiation of DNA replication. Mol Cell *11*, 203-213.
Couch, F.B., Bansbach, C.E., Driscoll, R., Luzwick, J.W., Glick, G.G., Betous, R., Carroll, C.M., Jung, S.Y., Qin, J., Cimprich, K.A*., et al.* (2013). ATR phosphorylates SMARCAL1 to prevent replication fork collapse. Genes Dev *27*, 1610-1623.
D'Angiolella, V., Donato, V., Forrester, F.M., Jeong, Y.T., Pellacani, C., Kudo, Y., Saraf, A., Florens, L., Washburn, M.P., and Pagano, M. (2012). Cyclin F-mediated degradation of ribonucleotide reductase M2 controls genome integrity and DNA repair. Cell *149*, 1023-1034.

Davies, S.L., North, P.S., Dart, A., Lakin, N.D., and Hickson, I.D. (2004). Phosphorylation of the Bloom's syndrome helicase and its role in recovery from S-phase arrest. Mol Cell Biol *24*, 1279-1291.
De Piccoli, G., Katou, Y., Itoh, T., Nakato, R., Shirahige, K., and Labib, K. (2012). Replisome stability at defective DNA replication forks is independent of S phase checkpoint kinases. Mol Cell *45*, 696-704.
Deans, A.J., and West, S.C. (2011). DNA interstrand crosslink repair and cancer. Nat Rev Cancer *11*, 467-480.
Delacroix, S., Wagner, J.M., Kobayashi, M., Yamamoto, K., and Karnitz, L.M. (2007). The Rad9-Hus1-Rad1 (9-1-1) clamp activates checkpoint signaling via TopBP1. Genes Dev *21*, 1472-1477.
Desany, B.A., Alcasabas, A.A., Bachant, J.B., and Elledge, S.J. (1998). Recovery from DNA replicational stress is the essential function of the S-phase checkpoint pathway. Genes Dev *12*, 2956-2970.
Doe, C.L., Ahn, J.S., Dixon, J., and Whitby, M.C. (2002). Mus81-Eme1 and Rqh1 involvement in processing stalled and collapsed replication forks. J Biol Chem *277*, 32753-32759.
Dore, A.S., Kilkenny, M.L., Rzechorzek, N.J., and Pearl, L.H. (2009). Crystal structure of the rad9-rad1-hus1 DNA damage checkpoint complex--implications for clamp loading and regulation. Mol Cell *34*, 735-745.
Downs, J.A., Lowndes, N.F., and Jackson, S.P. (2000). A role for Saccharomyces cerevisiae histone H2A in DNA repair. Nature *408*, 1001-1004.
Dungrawala, H., Rose, K.L., Bhat, K.P., Mohni, K.N., Glick, G.G., Couch, F.B., and Cortez, D. (2015). The Replication Checkpoint Prevents Two Types of Fork Collapse without Regulating Replisome Stability. Mol Cell *59*, 998-1010.
Edwards, R.J., Bentley, N.J., and Carr, A.M. (1999). A Rad3-Rad26 complex responds to DNA damage independently of other checkpoint proteins. Nat Cell Biol *1*, 393-398.
Elia, A.E., Wang, D.C., Willis, N.A., Boardman, A.P., Hajdu, I., Adeyemi, R.O., Lowry, E., Gygi, S.P., Scully, R., and Elledge, S.J. (2015). RFWD3-Dependent Ubiquitination of RPA Regulates Repair at Stalled Replication Forks. Mol Cell *60*, 280-293.
Fan, J., and Pavletich, N.P. (2012). Structure and conformational change of a replication protein A heterotrimer bound to ssDNA. Genes Dev *26*, 2337-2347.
Feldkamp, M.D., Mason, A.C., Eichman, B.F., and Chazin, W.J. (2014). Structural analysis of replication protein A recruitment of the DNA damage response protein SMARCAL1. Biochemistry *53*, 3052-3061.
Feng, S., Zhao, Y., Xu, Y., Ning, S., Huo, W., Hou, M., Gao, G., Ji, J., Guo, R., and Xu, D. (2016). Ewing Tumor-associated Antigen 1 Interacts with Replication Protein A to Promote Restart of Stalled Replication Forks. J Biol Chem *291*, 21956-21962.
Fokas, E., Prevo, R., Pollard, J.R., Reaper, P.M., Charlton, P.A., Cornelissen, B., Vallis, K.A., Hammond, E.M., Olcina, M.M., Gillies McKenna, W.*, et al.* (2012). Targeting ATR in vivo using the novel inhibitor VE-822 results in selective sensitization of pancreatic tumors to radiation. Cell Death Dis *3*, e441.
Forment, J.V., Blasius, M., Guerini, I., and Jackson, S.P. (2011). Structure-specific DNA endonuclease Mus81/Eme1 generates DNA damage caused by Chk1 inactivation. PLoS One *6*, e23517.
Frei, C., and Gasser, S.M. (2000). The yeast Sgs1p helicase acts upstream of Rad53p in the DNA replication checkpoint and colocalizes with Rad53p in S-phase-specific foci. Genes Dev *14*, 81-96.
Friedel, A.M., Pike, B.L., and Gasser, S.M. (2009). ATR/Mec1: coordinating fork stability and repair. Curr Opin Cell Biol *21*, 237-244.
Froget, B., Blaisonneau, J., Lambert, S., and Baldacci, G. (2008). Cleavage of stalled forks by fission yeast Mus81/Eme1 in absence of DNA replication checkpoint. Mol Biol Cell *19*, 445-456.
Furnari, B., Rhind, N., and Russell, P. (1997). Cdc25 mitotic inducer targeted by chk1 DNA damage checkpoint kinase. Science *277*, 1495-1497.
Furuya, K., Poitelea, M., Guo, L., Caspari, T., and Carr, A.M. (2004). Chk1 activation requires Rad9 S/TQ-site phosphorylation to promote association with C-terminal BRCT domains of Rad4TOPBP1. Genes Dev *18*, 1154-1164.

Gembka, A., Toueille, M., Smirnova, E., Poltz, R., Ferrari, E., Villani, G., and Hubscher, U. (2007). The checkpoint clamp, Rad9-Rad1-Hus1 complex, preferentially stimulates the activity of apurinic/apyrimidinic endonuclease 1 and DNA polymerase beta in long patch base excision repair. Nucleic Acids Res *35*, 2596-2608.
Giannattasio, M., Follonier, C., Tourriere, H., Puddu, F., Lazzaro, F., Pasero, P., Lopes, M., Plevani, P., and Muzi-Falconi, M. (2010). Exo1 competes with repair synthesis, converts NER intermediates to long ssDNA gaps, and promotes checkpoint activation. Mol Cell *40*, 50-62.
Giannattasio, M., Lazzaro, F., Longhese, M.P., Plevani, P., and Muzi-Falconi, M. (2004). Physical and functional interactions between nucleotide excision repair and DNA damage checkpoint. EMBO J *23*, 429-438.
Gomes, X.V., Henricksen, L.A., and Wold, M.S. (1996). Proteolytic mapping of human replication protein A: evidence for multiple structural domains and a conformational change upon interaction with single-stranded DNA. Biochemistry *35*, 5586-5595.
Gorgoulis, V.G., Vassiliou, L.V., Karakaidos, P., Zacharatos, P., Kotsinas, A., Liloglou, T., Venere, M., Ditullio, R.A., Jr., Kastrinakis, N.G., Levy, B.*, et al.* (2005). Activation of the DNA damage checkpoint and genomic instability in human precancerous lesions. Nature *434*, 907-913.
Grenon, M., Costelloe, T., Jimeno, S., O'Shaughnessy, A., Fitzgerald, J., Zgheib, O., Degerth, L., and Lowndes, N.F. (2007). Docking onto chromatin via the Saccharomyces cerevisiae Rad9 Tudor domain. Yeast *24*, 105-119.
Guan, X., Bai, H., Shi, G., Theriot, C.A., Hazra, T.K., Mitra, S., and Lu, A.L. (2007a). The human checkpoint sensor Rad9-Rad1-Hus1 interacts with and stimulates NEIL1 glycosylase. Nucleic Acids Res *35*, 2463-2472.
Guan, X., Madabushi, A., Chang, D.Y., Fitzgerald, M.E., Shi, G., Drohat, A.C., and Lu, A.L. (2007b). The human checkpoint sensor Rad9-Rad1-Hus1 interacts with and stimulates DNA repair enzyme TDG glycosylase. Nucleic Acids Res *35*, 6207-6218.
Guo, C., Kumagai, A., Schlacher, K., Shevchenko, A., Shevchenko, A., and Dunphy, W.G. (2015). Interaction of Chk1 with Treslin negatively regulates the initiation of chromosomal DNA replication. Mol Cell *57*, 492-505.
Haahr, P., Hoffmann, S., Tollenaere, M.A., Ho, T., Toledo, L.I., Mann, M., Bekker-Jensen, S., Raschle, M., and Mailand, N. (2016). Activation of the ATR kinase by the RPA-binding protein ETAA1. Nat Cell Biol *18*, 1196-1207.
Hammet, A., Magill, C., Heierhorst, J., and Jackson, S.P. (2007). Rad9 BRCT domain interaction with phosphorylated H2AX regulates the G1 checkpoint in budding yeast. EMBO Rep *8*, 851-857.
Heffernan, T.P., Unsal-Kacmaz, K., Heinloth, A.N., Simpson, D.A., Paules, R.S., Sancar, A., Cordeiro-Stone, M., and Kaufmann, W.K. (2007). Cdc7-Dbf4 and the human S checkpoint response to UVC. J Biol Chem *282*, 9458-9468.
Hegnauer, A.M., Hustedt, N., Shimada, K., Pike, B.L., Vogel, M., Amsler, P., Rubin, S.M., van Leeuwen, F., Guenole, A., van Attikum, H.*, et al.* (2012). An N-terminal acidic region of Sgs1 interacts with Rpa70 and recruits Rad53 kinase to stalled forks. EMBO J *31*, 3768-3783.
Hoeijmakers, J.H. (2009). DNA damage, aging, and cancer. N Engl J Med *361*, 1475-1485.
Hu, F., Wang, Y., Liu, D., Li, Y., Qin, J., and Elledge, S.J. (2001). Regulation of the Bub2/Bfa1 GAP complex by Cdc5 and cell cycle checkpoints. Cell *107*, 655-665.
Hu, J., Sun, L., Shen, F., Chen, Y., Hua, Y., Liu, Y., Zhang, M., Hu, Y., Wang, Q., Xu, W.*, et al.* (2012). The intra-S phase checkpoint targets Dna2 to prevent stalled replication forks from reversing. Cell *149*, 1221-1232.
Huang, M., Zhou, Z., and Elledge, S.J. (1998). The DNA replication and damage checkpoint pathways induce transcription by inhibition of the Crt1 repressor. Cell *94*, 595-605.

Hurov, K.E., Cotta-Ramusino, C., and Elledge, S.J. (2010). A genetic screen identifies the Triple T complex required for DNA damage signaling and ATM and ATR stability. Genes Dev *24*, 1939-1950.
Hustedt, N., Seeber, A., Sack, R., Tsai-Pflugfelder, M., Bhullar, B., Vlaming, H., van Leeuwen, F., Guenole, A., van Attikum, H., Srivas, R.*, et al.* (2015). Yeast PP4 interacts with ATR homolog Ddc2-Mec1 and regulates checkpoint signaling. Mol Cell *57*, 273-289.
Itakura, E., Sawada, I., and Matsuura, A. (2005). Dimerization of the ATRIP protein through the coiled-coil motif and its implication to the maintenance of stalled replication forks. Mol Biol Cell *16*, 5551-5562.
Jiricny, J. (2006). The multifaceted mismatch-repair system. Nat Rev Mol Cell Biol *7*, 335-346.
Kai, M., Furuya, K., Paderi, F., Carr, A.M., and Wang, T.S. (2007). Rad3-dependent phosphorylation of the checkpoint clamp regulates repair-pathway choice. Nat Cell Biol *9*, 691-697.
Katou, Y., Kanoh, Y., Bando, M., Noguchi, H., Tanaka, H., Ashikari, T., Sugimoto, K., and Shirahige, K. (2003). S-phase checkpoint proteins Tof1 and Mrc1 form a stable replication-pausing complex. Nature *424*, 1078-1083.
Kim, C., Paulus, B.F., and Wold, M.S. (1994). Interactions of human replication protein A with oligonucleotides. Biochemistry *33*, 14197-14206.
Kim, C., and Wold, M.S. (1995). Recombinant human replication protein A binds to polynucleotides with low cooperativity. Biochemistry *34*, 2058-2064.
Kim, S.M., Kumagai, A., Lee, J., and Dunphy, W.G. (2005). Phosphorylation of Chk1 by ATM- and Rad3-related (ATR) in Xenopus egg extracts requires binding of ATRIP to ATR but not the stable DNA-binding or coiled-coil domains of ATRIP. J Biol Chem *280*, 38355-38364.
Kondo, T., Wakayama, T., Naiki, T., Matsumoto, K., and Sugimoto, K. (2001). Recruitment of Mec1 and Ddc1 checkpoint proteins to double-strand breaks through distinct mechanisms. Science *294*, 867-870.
Kumagai, A., and Dunphy, W.G. (2000). Claspin, a novel protein required for the activation of Chk1 during a DNA replication checkpoint response in Xenopus egg extracts. Mol Cell *6*, 839-849.
Kumagai, A., Lee, J., Yoo, H.Y., and Dunphy, W.G. (2006). TopBP1 activates the ATR-ATRIP complex. Cell *124*, 943-955.
Kumar, S., and Burgers, P.M. (2013). Lagging strand maturation factor Dna2 is a component of the replication checkpoint initiation machinery. Genes Dev *27*, 313-321.
Lee, S.J., Duong, J.K., and Stern, D.F. (2004). A Ddc2-Rad53 fusion protein can bypass the requirements for RAD9 and MRC1 in Rad53 activation. Mol Biol Cell *15*, 5443-5455.
Lee, S.J., Schwartz, M.F., Duong, J.K., and Stern, D.F. (2003). Rad53 phosphorylation site clusters are important for Rad53 regulation and signaling. Mol Cell Biol *23*, 6300-6314.
Lee, Y.C., Zhou, Q., Chen, J., and Yuan, J. (2016). RPA-Binding Protein ETAA1 Is an ATR Activator Involved in DNA Replication Stress Response. Curr Biol *26*, 3257-3268.
Lee, Y.D., Wang, J., Stubbe, J., and Elledge, S.J. (2008). Dif1 is a DNA-damage-regulated facilitator of nuclear import for ribonucleotide reductase. Mol Cell *32*, 70-80.
Lin, S.J., Wardlaw, C.P., Morishita, T., Miyabe, I., Chahwan, C., Caspari, T., Schmidt, U., Carr, A.M., and Garcia, V. (2012). The Rad4(TopBP1) ATR-activation domain functions in G1/S phase in a chromatin-dependent manner. PLoS Genet *8*, e1002801.
Lin, Y.L., Chen, C., Keshav, K.F., Winchester, E., and Dutta, A. (1996). Dissection of functional domains of the human DNA replication protein complex replication protein A. J Biol Chem *271*, 17190-17198.
Lindahl, T., and Barnes, D.E. (2000). Repair of endogenous DNA damage. Cold Spring Harb Symp Quant Biol *65*, 127-133.
Liu, S., Bekker-Jensen, S., Mailand, N., Lukas, C., Bartek, J., and Lukas, J. (2006). Claspin operates downstream of TopBP1 to direct ATR signaling towards Chk1 activation. Mol Cell Biol *26*, 6056-6064.
Liu, S., Chu, J., Yucer, N., Leng, M., Wang, S.Y., Chen, B.P., Hittelman, W.N., and Wang, Y. (2011a). RING finger and WD repeat domain 3 (RFWD3) associates with replication protein A (RPA) and facilitates RPA-mediated DNA damage response. J Biol Chem *286*, 22314-22322.

Liu, S., Ho, C.K., Ouyang, J., and Zou, L. (2013). Nek1 kinase associates with ATR-ATRIP and primes ATR for efficient DNA damage signaling. Proc Natl Acad Sci U S A *110*, 2175-2180.
Liu, S., Shiotani, B., Lahiri, M., Marechal, A., Tse, A., Leung, C.C., Glover, J.N., Yang, X.H., and Zou, L. (2011b). ATR autophosphorylation as a molecular switch for checkpoint activation. Mol Cell *43*, 192-202.
Lopes, M., Foiani, M., and Sogo, J.M. (2006). Multiple mechanisms control chromosome integrity after replication fork uncoupling and restart at irreparable UV lesions. Mol Cell *21*, 15-27.
Lopez-Mosqueda, J., Maas, N.L., Jonsson, Z.O., Defazio-Eli, L.G., Wohlschlegel, J., and Toczyski, D.P. (2010). Damage-induced phosphorylation of Sld3 is important to block late origin firing. Nature *467*, 479-483.
Lou, H., Komata, M., Katou, Y., Guan, Z., Reis, C.C., Budd, M., Shirahige, K., and Campbell, J.L. (2008). Mrc1 and DNA polymerase epsilon function together in linking DNA replication and the S phase checkpoint. Mol Cell *32*, 106-117.
MacDougall, C.A., Byun, T.S., Van, C., Yee, M.C., and Cimprich, K.A. (2007). The structural determinants of checkpoint activation. Genes Dev *21*, 898-903.
Majka, J., Binz, S.K., Wold, M.S., and Burgers, P.M. (2006a). Replication protein A directs loading of the DNA damage checkpoint clamp to 5'-DNA junctions. J Biol Chem *281*, 27855-27861.
Majka, J., and Burgers, P.M. (2004). The PCNA-RFC families of DNA clamps and clamp loaders. Prog Nucleic Acid Res Mol Biol *78*, 227-260.
Majka, J., Niedziela-Majka, A., and Burgers, P.M. (2006b). The checkpoint clamp activates Mec1 kinase during initiation of the DNA damage checkpoint. Mol Cell *24*, 891-901.
Marechal, A., Li, J.M., Ji, X.Y., Wu, C.S., Yazinski, S.A., Nguyen, H.D., Liu, S., Jimenez, A.E., Jin, J., and Zou, L. (2014). PRP19 transforms into a sensor of RPA-ssDNA after DNA damage and drives ATR activation via a ubiquitin-mediated circuitry. Mol Cell *53*, 235-246.
Marteijn, J.A., Lans, H., Vermeulen, W., and Hoeijmakers, J.H. (2014). Understanding nucleotide excision repair and its roles in cancer and ageing. Nat Rev Mol Cell Biol *15*, 465-481.
Meister, P., Taddei, A., Vernis, L., Poidevin, M., Gasser, S.M., and Baldacci, G. (2005). Temporal separation of replication and recombination requires the intra-S checkpoint. J Cell Biol *168*, 537-544.
Melo, J.A., Cohen, J., and Toczyski, D.P. (2001). Two checkpoint complexes are independently recruited to sites of DNA damage in vivo. Genes Dev *15*, 2809-2821.
Mordes, D.A., Glick, G.G., Zhao, R., and Cortez, D. (2008). TopBP1 activates ATR through ATRIP and a PIKK regulatory domain. Genes Dev *22*, 1478-1489.
Morin, I., Ngo, H.P., Greenall, A., Zubko, M.K., Morrice, N., and Lydall, D. (2008). Checkpoint-dependent phosphorylation of Exo1 modulates the DNA damage response. EMBO J *27*, 2400-2410.
Namiki, Y., and Zou, L. (2006). ATRIP associates with replication protein A-coated ssDNA through multiple interactions. Proc Natl Acad Sci U S A *103*, 580-585.
Navadgi-Patil, V.M., and Burgers, P.M. (2008). Yeast DNA replication protein Dpb11 activates the Mec1/ATR checkpoint kinase. J Biol Chem *283*, 35853-35859.
Navadgi-Patil, V.M., and Burgers, P.M. (2009). The unstructured C-terminal tail of the 9-1-1 clamp subunit Ddc1 activates Mec1/ATR via two distinct mechanisms. Mol Cell *36*, 743-753.
Naylor, M.L., Li, J.M., Osborn, A.J., and Elledge, S.J. (2009). Mrc1 phosphorylation in response to DNA replication stress is required for Mec1 accumulation at the stalled fork. Proc Natl Acad Sci U S A *106*, 12765-12770.
Nghiem, P., Park, P.K., Kim Ys, Y.S., Desai, B.N., and Schreiber, S.L. (2002). ATR is not required for p53 activation but synergizes with p53 in the replication checkpoint. J Biol Chem *277*, 4428-4434.
Osborn, A.J., and Elledge, S.J. (2003). Mrc1 is a replication fork component whose phosphorylation in response to DNA replication stress activates Rad53. Genes Dev *17*, 1755-1767.

Paciotti, V., Clerici, M., Lucchini, G., and Longhese, M.P. (2000). The checkpoint protein Ddc2, functionally related to S. pombe Rad26, interacts with Mec1 and is regulated by Mec1-dependent phosphorylation in budding yeast. Genes Dev *14*, 2046-2059.
Pal, M., Morgan, M., Phelps, S.E., Roe, S.M., Parry-Morris, S., Downs, J.A., Polier, S., Pearl, L.H., and Prodromou, C. (2014). Structural basis for phosphorylation-dependent recruitment of Tel2 to Hsp90 by Pih1. Structure *22*, 805-818.
Paques, F., and Haber, J.E. (1999). Multiple pathways of recombination induced by double-strand breaks in Saccharomyces cerevisiae. Microbiol Mol Biol Rev *63*, 349-404.
Pellicioli, A., and Foiani, M. (2005). Signal transduction: how rad53 kinase is activated. Curr Biol *15*, R769-771.
Pichierri, P., Rosselli, F., and Franchitto, A. (2003). Werner's syndrome protein is phosphorylated in an ATR/ATM-dependent manner following replication arrest and DNA damage induced during the S phase of the cell cycle. Oncogene *22*, 1491-1500.
Pike, B.L., Yongkiettrakul, S., Tsai, M.D., and Heierhorst, J. (2003). Diverse but overlapping functions of the two forkhead-associated (FHA) domains in Rad53 checkpoint kinase activation. J Biol Chem *278*, 30421-30424.
Puddu, F., Piergiovanni, G., Plevani, P., and Muzi-Falconi, M. (2011). Sensing of replication stress and Mec1 activation act through two independent pathways involving the 9-1-1 complex and DNA polymerase epsilon. PLoS Genet *7*, e1002022.
Ragland, R.L., Patel, S., Rivard, R.S., Smith, K., Peters, A.A., Bielinsky, A.K., and Brown, E.J. (2013). RNF4 and PLK1 are required for replication fork collapse in ATR-deficient cells. Genes Dev *27*, 2259-2273.
Renwick, A., Thompson, D., Seal, S., Kelly, P., Chagtai, T., Ahmed, M., North, B., Jayatilake, H., Barfoot, R., Spanova, K.*, et al.* (2006). ATM mutations that cause ataxia-telangiectasia are breast cancer susceptibility alleles. Nat Genet *38*, 873-875.
Rossi, S.E., Ajazi, A., Carotenuto, W., Foiani, M., and Giannattasio, M. (2015). Rad53-Mediated Regulation of Rrm3 and Pif1 DNA Helicases Contributes to Prevention of Aberrant Fork Transitions under Replication Stress. Cell Rep *13*, 80-92.
Rouse, J., and Jackson, S.P. (2000). LCD1: an essential gene involved in checkpoint control and regulation of the MEC1 signalling pathway in Saccharomyces cerevisiae. EMBO J *19*, 5801-5812.
Sanchez, Y., Bachant, J., Wang, H., Hu, F., Liu, D., Tetzlaff, M., and Elledge, S.J. (1999). Control of the DNA damage checkpoint by chk1 and rad53 protein kinases through distinct mechanisms. Science *286*, 1166-1171.
Sanchez, Y., Desany, B.A., Jones, W.J., Liu, Q., Wang, B., and Elledge, S.J. (1996). Regulation of RAD53 by the ATM-like kinases MEC1 and TEL1 in yeast cell cycle checkpoint pathways. Science *271*, 357-360.
Sanchez, Y., Wong, C., Thoma, R.S., Richman, R., Wu, Z., Piwnica-Worms, H., and Elledge, S.J. (1997). Conservation of the Chk1 checkpoint pathway in mammals: linkage of DNA damage to Cdk regulation through Cdc25. Science *277*, 1497-1501.
Santocanale, C., and Diffley, J.F. (1998). A Mec1- and Rad53-dependent checkpoint controls late-firing origins of DNA replication. Nature *395*, 615-618.
Sawicka, M., Wanrooij, P.H., Darbari, V.C., Tannous, E., Hailemariam, S., Bose, D., Makarova, A.V., Burgers, P.M., and Zhang, X. (2016). The Dimeric Architecture of Checkpoint Kinases Mec1ATR and Tel1ATM Reveal a Common Structural Organization. J Biol Chem *291*, 13436-13447.
Schwartz, M.F., Duong, J.K., Sun, Z., Morrow, J.S., Pradhan, D., and Stern, D.F. (2002). Rad9 phosphorylation sites couple Rad53 to the Saccharomyces cerevisiae DNA damage checkpoint. Mol Cell *9*, 1055-1065.
Seeber, A., Hegnauer, A.M., Hustedt, N., Deshpande, I., Poli, J., Eglinger, J., Pasero, P., Gut, H., Shinohara, M., Hopfner, K.P.*, et al.* (2016). RPA Mediates Recruitment of MRX to Forks and Double-Strand Breaks to Hold Sister Chromatids Together. Mol Cell *64*, 951-966.

Segurado, M., and Diffley, J.F. (2008). Separate roles for the DNA damage checkpoint protein kinases in stabilizing DNA replication forks. Genes Dev *22*, 1816-1827.
Sharif, H., Li, Y., Dong, Y., Dong, L., Wang, W.L., Mao, Y., and Wu, H. (2017). Cryo-EM structure of the DNA-PK holoenzyme. Proc Natl Acad Sci U S A *114*, 7367-7372.
Sheu, Y.J., Kinney, J.B., Lengronne, A., Pasero, P., and Stillman, B. (2014). Domain within the helicase subunit Mcm4 integrates multiple kinase signals to control DNA replication initiation and fork progression. Proc Natl Acad Sci U S A *111*, E1899-1908.
Sheu, Y.J., Kinney, J.B., and Stillman, B. (2016). Concerted activities of Mcm4, Sld3, and Dbf4 in control of origin activation and DNA replication fork progression. Genome Res *26*, 315-330.
Shiloh, Y., and Ziv, Y. (2013). The ATM protein kinase: regulating the cellular response to genotoxic stress, and more. Nat Rev Mol Cell Biol *14*, 197-210.
Shimada, K., Pasero, P., and Gasser, S.M. (2002). ORC and the intra-S-phase checkpoint: a threshold regulates Rad53p activation in S phase. Genes Dev *16*, 3236-3252.
Shirahige, K., Hori, Y., Shiraishi, K., Yamashita, M., Takahashi, K., Obuse, C., Tsurimoto, T., and Yoshikawa, H. (1998). Regulation of DNA-replication origins during cell-cycle progression. Nature *395*, 618-621.
Shroff, R., Arbel-Eden, A., Pilch, D., Ira, G., Bonner, W.M., Petrini, J.H., Haber, J.E., and Lichten, M. (2004). Distribution and dynamics of chromatin modification induced by a defined DNA double-strand break. Curr Biol *14*, 1703-1711.
Sibanda, B.L., Chirgadze, D.Y., Ascher, D.B., and Blundell, T.L. (2017). DNA-PKcs structure suggests an allosteric mechanism modulating DNA double-strand break repair. Science *355*, 520-524.
Sibanda, B.L., Chirgadze, D.Y., and Blundell, T.L. (2010). Crystal structure of DNA-PKcs reveals a large open-ring cradle comprised of HEAT repeats. Nature *463*, 118-121.
Skourti-Stathaki, K., and Proudfoot, N.J. (2014). A double-edged sword: R loops as threats to genome integrity and powerful regulators of gene expression. Genes Dev *28*, 1384-1396.
Smits, V.A., Klompmaker, R., Arnaud, L., Rijksen, G., Nigg, E.A., and Medema, R.H. (2000). Polo-like kinase-1 is a target of the DNA damage checkpoint. Nat Cell Biol *2*, 672-676.
Smits, V.A., Reaper, P.M., and Jackson, S.P. (2006). Rapid PIKK-dependent release of Chk1 from chromatin promotes the DNA-damage checkpoint response. Curr Biol *16*, 150-159.
Smolka, M.B., Albuquerque, C.P., Chen, S.H., and Zhou, H. (2007). Proteome-wide identification of in vivo targets of DNA damage checkpoint kinases. Proc Natl Acad Sci U S A *104*, 10364-10369.
Sogo, J.M., Lopes, M., and Foiani, M. (2002). Fork reversal and ssDNA accumulation at stalled replication forks owing to checkpoint defects. Science *297*, 599-602.
Sorensen, C.S., Hansen, L.T., Dziegielewski, J., Syljuasen, R.G., Lundin, C., Bartek, J., and Helleday, T. (2005). The cell-cycle checkpoint kinase Chk1 is required for mammalian homologous recombination repair. Nat Cell Biol *7*, 195-201.
Soustelle, C., Vedel, M., Kolodner, R., and Nicolas, A. (2002). Replication protein A is required for meiotic recombination in Saccharomyces cerevisiae. Genetics *161*, 535-547.
Sun, Z., Hsiao, J., Fay, D.S., and Stern, D.F. (1998). Rad53 FHA domain associated with phosphorylated Rad9 in the DNA damage checkpoint. Science *281*, 272-274.
Takai, H., Wang, R.C., Takai, K.K., Yang, H., and de Lange, T. (2007). Tel2 regulates the stability of PI3K-related protein kinases. Cell *131*, 1248-1259.
Tanaka, K., and Russell, P. (2001). Mrc1 channels the DNA replication arrest signal to checkpoint kinase Cds1. Nat Cell Biol *3*, 966-972.
Tanaka, S., Umemori, T., Hirai, K., Muramatsu, S., Kamimura, Y., and Araki, H. (2007). CDK-dependent phosphorylation of Sld2 and Sld3 initiates DNA replication in budding yeast. Nature *445*, 328-332.

Taylor, A.M., Harnden, D.G., Arlett, C.F., Harcourt, S.A., Lehmann, A.R., Stevens, S., and Bridges, B.A. (1975). Ataxia telangiectasia: a human mutation with abnormal radiation sensitivity. Nature *258*, 427-429.
Tercero, J.A., Longhese, M.P., and Diffley, J.F. (2003). A central role for DNA replication forks in checkpoint activation and response. Mol Cell *11*, 1323-1336.
Tibbetts, R.S., Cortez, D., Brumbaugh, K.M., Scully, R., Livingston, D., Elledge, S.J., and Abraham, R.T. (2000). Functional interactions between BRCA1 and the checkpoint kinase ATR during genotoxic stress. Genes Dev *14*, 2989-3002.
Toledo, L.I., Murga, M., Gutierrez-Martinez, P., Soria, R., and Fernandez-Capetillo, O. (2008). ATR signaling can drive cells into senescence in the absence of DNA breaks. Genes Dev *22*, 297-302.
Toueille, M., El-Andaloussi, N., Frouin, I., Freire, R., Funk, D., Shevelev, I., Friedrich-Heineken, E., Villani, G., Hottiger, M.O., and Hubscher, U. (2004). The human Rad9/Rad1/Hus1 damage sensor clamp interacts with DNA polymerase beta and increases its DNA substrate utilisation efficiency: implications for DNA repair. Nucleic Acids Res *32*, 3316-3324.
Umezu, K., Sugawara, N., Chen, C., Haber, J.E., and Kolodner, R.D. (1998). Genetic analysis of yeast RPA1 reveals its multiple functions in DNA metabolism. Genetics *148*, 989-1005.
Unsal-Kacmaz, K., and Sancar, A. (2004). Quaternary structure of ATR and effects of ATRIP and replication protein A on its DNA binding and kinase activities. Mol Cell Biol *24*, 1292-1300.
Usui, T., Foster, S.S., and Petrini, J.H. (2009). Maintenance of the DNA-damage checkpoint requires DNA-damage-induced mediator protein oligomerization. Mol Cell *33*, 147-159.
Uto, K., Inoue, D., Shimuta, K., Nakajo, N., and Sagata, N. (2004). Chk1, but not Chk2, inhibits Cdc25 phosphatases by a novel common mechanism. EMBO J *23*, 3386-3396.
van Leeuwen, F., Gafken, P.R., and Gottschling, D.E. (2002). Dot1p modulates silencing in yeast by methylation of the nucleosome core. Cell *109*, 745-756.
Vialard, J.E., Gilbert, C.S., Green, C.M., and Lowndes, N.F. (1998). The budding yeast Rad9 checkpoint protein is subjected to Mec1/Tel1-dependent hyperphosphorylation and interacts with Rad53 after DNA damage. EMBO J *17*, 5679-5688.
Wakayama, T., Kondo, T., Ando, S., Matsumoto, K., and Sugimoto, K. (2001). Pie1, a protein interacting with Mec1, controls cell growth and checkpoint responses in Saccharomyces cerevisiae. Mol Cell Biol *21*, 755-764.
Walter, J., and Newport, J. (2000). Initiation of eukaryotic DNA replication: origin unwinding and sequential chromatin association of Cdc45, RPA, and DNA polymerase alpha. Mol Cell *5*, 617-627.
Wan, L., and Huang, J. (2014). The PSO4 protein complex associates with replication protein A (RPA) and modulates the activation of ataxia telangiectasia-mutated and Rad3-related (ATR). J Biol Chem *289*, 6619-6626.
Wang, W., Brandt, P., Rossi, M.L., Lindsey-Boltz, L., Podust, V., Fanning, E., Sancar, A., and Bambara, R.A. (2004). The human Rad9-Rad1-Hus1 checkpoint complex stimulates flap endonuclease 1. Proc Natl Acad Sci U S A *101*, 16762-16767.
Wang, X., Chu, H., Lv, M., Zhang, Z., Qiu, S., Liu, H., Shen, X., Wang, W., and Cai, G. (2016). Structure of the intact ATM/Tel1 kinase. Nat Commun *7*, 11655.
Weinert, T.A., Kiser, G.L., and Hartwell, L.H. (1994). Mitotic checkpoint genes in budding yeast and the dependence of mitosis on DNA replication and repair. Genes Dev *8*, 652-665.
Wold, M.S., and Kelly, T. (1988). Purification and characterization of replication protein A, a cellular protein required for in vitro replication of simian virus 40 DNA. Proc Natl Acad Sci U S A *85*, 2523-2527.
Wu, C.S., Ouyang, J., Mori, E., Nguyen, H.D., Marechal, A., Hallet, A., Chen, D.J., and Zou, L. (2014). SUMOylation of ATRIP potentiates DNA damage signaling by boosting multiple protein interactions in the ATR pathway. Genes Dev *28*, 1472-1484.

Wu, C.S., and Zou, L. (2016). The SUMO (Small Ubiquitin-like Modifier) Ligase PIAS3 Primes ATR for Checkpoint Activation. J Biol Chem *291*, 279-290.
Wu, X., and Huang, M. (2008). Dif1 controls subcellular localization of ribonucleotide reductase by mediating nuclear import of the R2 subunit. Mol Cell Biol *28*, 7156-7167.
Wu, X., Shell, S.M., Liu, Y., and Zou, Y. (2007). ATR-dependent checkpoint modulates XPA nuclear import in response to UV irradiation. Oncogene *26*, 757-764.
Xu, X., Vaithiyalingam, S., Glick, G.G., Mordes, D.A., Chazin, W.J., and Cortez, D. (2008). The basic cleft of RPA70N binds multiple checkpoint proteins, including RAD9, to regulate ATR signaling. Mol Cell Biol *28*, 7345-7353.
Yang, H., Rudge, D.G., Koos, J.D., Vaidialingam, B., Yang, H.J., and Pavletich, N.P. (2013). mTOR kinase structure, mechanism and regulation. Nature *497*, 217-223.
Yang, H., Wang, J., Liu, M., Chen, X., Huang, M., Tan, D., Dong, M.Q., Wong, C.C., Wang, J., Xu, Y.*, et al.* (2016). 4.4 A Resolution Cryo-EM structure of human mTOR Complex 1. Protein Cell *7*, 878-887.
Yoshioka, K., Yoshioka, Y., and Hsieh, P. (2006). ATR kinase activation mediated by MutSalpha and MutLalpha in response to cytotoxic O6-methylguanine adducts. Mol Cell *22*, 501-510.
Zegerman, P., and Diffley, J.F. (2007). Phosphorylation of Sld2 and Sld3 by cyclin-dependent kinases promotes DNA replication in budding yeast. Nature *445*, 281-285.
Zegerman, P., and Diffley, J.F. (2010). Checkpoint-dependent inhibition of DNA replication initiation by Sld3 and Dbf4 phosphorylation. Nature *467*, 474-478.
Zhang, H., Head, P.E., Daddacha, W., Park, S.H., Li, X., Pan, Y., Madden, M.Z., Duong, D.M., Xie, M., Yu, B.*, et al.* (2016). ATRIP Deacetylation by SIRT2 Drives ATR Checkpoint Activation by Promoting Binding to RPA-ssDNA. Cell Rep *14*, 1435-1447.
Zhao, X., Muller, E.G., and Rothstein, R. (1998). A suppressor of two essential checkpoint genes identifies a novel protein that negatively affects dNTP pools. Mol Cell *2*, 329-340.
Zhao, X., and Rothstein, R. (2002). The Dun1 checkpoint kinase phosphorylates and regulates the ribonucleotide reductase inhibitor Sml1. Proc Natl Acad Sci U S A *99*, 3746-3751.
Zhou, C., Pourmal, S., and Pavletich, N.P. (2015). Dna2 nuclease-helicase structure, mechanism and regulation by Rpa. Elife *4*.
Zhou, Z., and Elledge, S.J. (1993). DUN1 encodes a protein kinase that controls the DNA damage response in yeast. Cell *75*, 1119-1127.
Zou, L., and Elledge, S.J. (2003). Sensing DNA damage through ATRIP recognition of RPA-ssDNA complexes. Science *300*, 1542-1548.
Zou, Y., Liu, Y., Wu, X., and Shell, S.M. (2006). Functions of human replication protein A (RPA): from DNA replication to DNA damage and stress responses. J Cell Physiol *208*, 267-273.

Chapter 2:

Structural basis of Mec1-Ddc2-RPA assembly and activation on single-stranded DNA at sites of damage

Ishan Deshpande[1,2], Andrew Seeber[1], Kenji Shimada[1], Jeremy J. Keusch[1], Heinz Gut[1], Susan M. Gasser[1,2]

[1]Friedrich Miescher Institute for Biomedical Research (FMI), Maulbeerstrasse 66, 4058 Basel, Switzerland
[2]University of Basel, Faculty of Natural Sciences, Klingelbergstrasse 50, CH-4056 Basel, Switzerland

Published in *Mol Cell*, 2017, 68(2):431-455.

Summary

Mec1-Ddc2 (ATR-ATRIP) is a key DNA damage-sensing kinase that is recruited through the single-stranded (ss) DNA binding replication protein A (RPA) to initiate the DNA damage checkpoint response. Activation of ATR-ATRIP in the absence of DNA damage is lethal. Therefore, it is important that damage-specific recruitment precedes kinase activation, which is achieved at least in part by Mec1-Ddc2 homodimerization. Here we report a structural, biochemical and functional characterization of the yeast Mec1-Ddc2-RPA assembly. High resolution co-crystal structures of Ddc2-Rfa1 and Ddc2-Rfa1-t11 (K45E mutant) N-termini, and of the Ddc2 coiled-coil domain (CCD) provide insight into Mec1-Ddc2 homodimerization and damage-site targeting. Based on our structural and functional findings, we present a Mec1-Ddc2-RPA-ssDNA composite structural model. By way of validation, we show that RPA-dependent recruitment of Mec1-Ddc2 is crucial for maintaining its homodimeric state at ssDNA, and that Ddc2's recruitment domain and CCD are important for Mec1-dependent survival of UV-light induced DNA damage.

Molecular Cell
Article

Structural Basis of Mec1-Ddc2-RPA Assembly and Activation on Single-Stranded DNA at Sites of Damage

Ishan Deshpande,[1,2] Andrew Seeber,[1] Kenji Shimada,[1] Jeremy J. Keusch,[1] Heinz Gut,[1] and Susan M. Gasser[1,2,3,*]
[1]Friedrich Miescher Institute for Biomedical Research (FMI), Maulbeerstrasse 66, 4058 Basel, Switzerland
[2]University of Basel, Faculty of Natural Sciences, Klingelbergstrasse 50, 4056 Basel, Switzerland
[3]Lead Contact
*Correspondence: susan.gasser@fmi.ch
https://doi.org/10.1016/j.molcel.2017.09.019

SUMMARY

Mec1-Ddc2 (ATR-ATRIP) is a key DNA-damage-sensing kinase that is recruited through the single-stranded (ss) DNA-binding replication protein A (RPA) to initiate the DNA damage checkpoint response. Activation of ATR-ATRIP in the absence of DNA damage is lethal. Therefore, it is important that damage-specific recruitment precedes kinase activation, which is achieved at least in part by Mec1-Ddc2 homodimerization. Here, we report a structural, biochemical, and functional characterization of the yeast Mec1-Ddc2-RPA assembly. High-resolution co-crystal structures of Ddc2-Rfa1 and Ddc2-Rfa1-t11 (K45E mutant) N termini and of the Ddc2 coiled-coil domain (CCD) provide insight into Mec1-Ddc2 homodimerization and damage-site targeting. Based on our structural and functional findings, we present a Mec1-Ddc2-RPA-ssDNA composite structural model. By way of validation, we show that RPA-dependent recruitment of Mec1-Ddc2 is crucial for maintaining its homodimeric state at ssDNA and that Ddc2's recruitment domain and CCD are important for Mec1-dependent survival of UV-light-induced DNA damage.

INTRODUCTION

Genome integrity is crucial for the survival of eukaryotic organisms. It is maintained by an evolutionarily conserved and meticulously coordinated network of pathways, collectively known as the DNA damage response (DDR). *Ataxia telangiectasia* mutated and Rad3 related (ATR, or Mec1 in budding yeast) and *ataxia telangiectasia* mutated (ATM, or Tel1 in budding yeast) are apical kinases of two key DDR signaling cascades. In contrast to ATM/Tel1, which is dispensable for viability (Shiloh and Ziv, 2013), ATR/Mec1 is essential in a number of organisms. Notably, its loss is early embryonic lethal in mice (Brown and Baltimore, 2000; Liu et al., 2000). In budding yeast, the lethality ensuing from loss of Mec1 can be suppressed by upregulating ribonucleotide reductase through a *sml1* deletion (Zhao et al., 1998). Although viable, *mec1*Δ *sml1*Δ cells nonetheless remain extremely sensitive to DNA-damaging agents.

Mec1 forms a complex with its regulatory subunit Ddc2 (ATRIP in human), and the function and stability of the two proteins are completely dependent on each other (Cortez et al., 2001; Paciotti et al., 2000). In other words, loss of the catalytic subunit, Mec1, and of the regulatory subunit Ddc2 yield identical phenotypes in face of a wide variety of genomic insults, including replication stress, base adducts, UV-induced nucleotide damage, and double-strand breaks (DSBs) (Cortez et al., 2001; Edwards et al., 1999; Paciotti et al., 2000; Rouse and Jackson, 2002; Wakayama et al., 2001). Upon activation, Mec1-Ddc2 phosphorylates over 100 substrates (Bastos de Oliveira et al., 2015; Hustedt et al., 2015), initiating a signaling cascade that controls DNA repair and fork restart as well as cell-cycle progression, replisome stability, and deoxynucleotide triphosphate (dNTP) levels (Friedel et al., 2009).

DNA damage or replication stress exposes long stretches of single-stranded (ss) DNA, which are rapidly bound by replication protein A (RPA) to form an ssDNA-RPA complex (Alani et al., 1992). The ssDNA-RPA platform recruits Mec1-Ddc2 (Dubrana et al., 2007; Rouse and Jackson, 2002; Zou and Elledge, 2003); however, this recruitment is not sufficient to induce Mec1 activation. In *Xenopus* egg extracts, ATR/Mec1-dependent checkpoint activation required the presence of double-stranded (ds) DNA adjacent to the ssDNA stretch, a structure recognized by the so-called 9-1-1 clamp (MacDougall et al., 2007). Similarly, the long unstructured C-terminal tail of 9-1-1 subunit Ddc1 can activate Mec1 kinase in vitro (Majka et al., 2006a), as well as in vivo, when artificially targeted together with Ddc2 to an integrated array of binding sites (Bonilla et al., 2008). Mec1-dependent phosphorylation of Ddc1 in turn recruits Dpb11 (TopBP1 in human), which further activates Mec1/ATR (Furuya et al., 2004; Kumagai et al., 2006; Puddu et al., 2008).

The hierarchy of factors contributing to Mec1 activation is influenced by the cell cycle. In G1 phase, Ddc1 is the predominant activator and in S/G2, Ddc1 and Dpb11 act redundantly (Navadgi-Patil and Burgers, 2009), whereas the Dna2 and Sgs1 helicases also contribute to activate Mec1 in S phase cells (Frei and Gasser, 2000; Kumar and Burgers, 2013). This redundancy underscores the significance of a localized and timely activation of Mec1-Ddc2, which is a highly relevant feature of

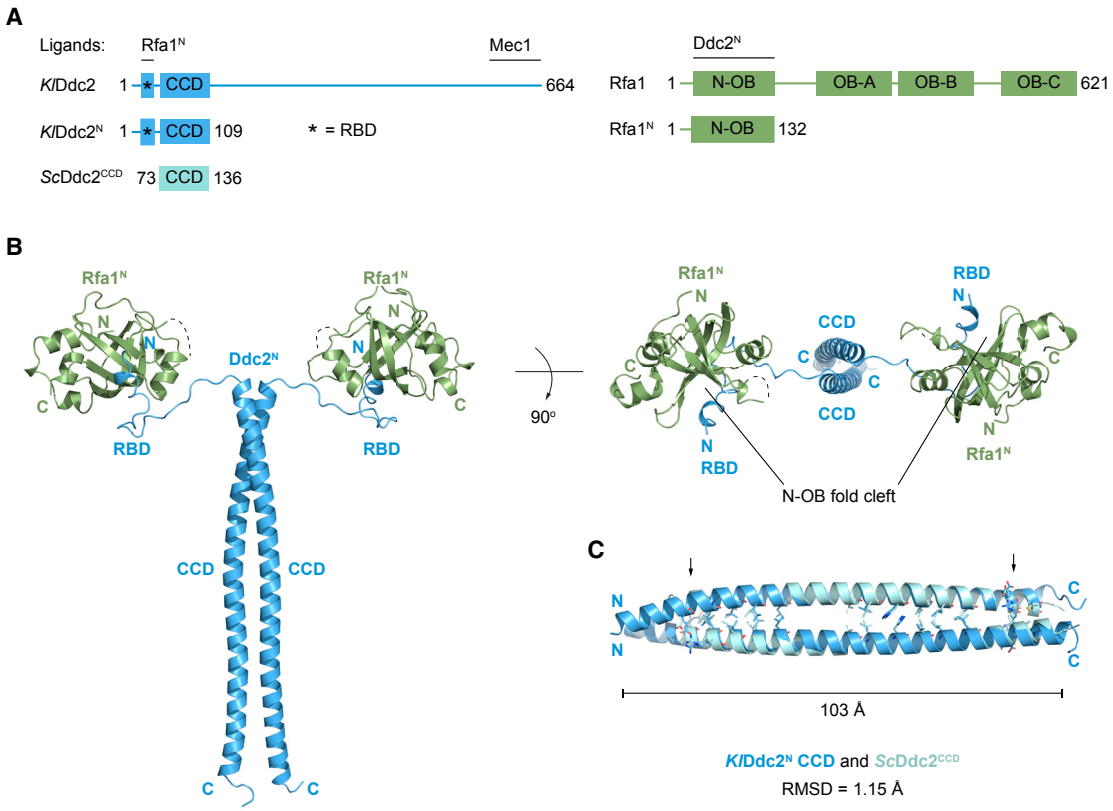

Figure 1. Architecture of the Ddc2^{N}-Rfa1^{N} Complex

(A) Schematic diagram of Ddc2 and Rfa1 constructs used for crystallization. CCD, coiled-coil domain; *Kl*, *Kluyveromyces lactis*; OB, oligonucleotide/oligosaccharide binding; RBD (denoted by *), Rfa1-binding domain; *Sc*, *Saccharomyces cerevisiae*. Black bars above protein segments indicate protein-protein interactions.

(B) Crystal structure of the Ddc2^{N}-Rfa1^{N} complex in cartoon representation; *Sc*Rfa1^{N} is colored in green and *Kl*Ddc2^{N} in blue. Two loops lacking electron density due to flexibility are indicated by dashed lines. RBD, CCD, and N-terminal OB (N-OB) fold cleft are highlighted.

(C) Superposition of the crystal structure of *Sc*Ddc2^{CCD} (cyan) onto the CCD of *Kl*Ddc2^{N} (blue) in cartoon representation. Residues involved in dimerization are shown as colored sticks. Salt bridges are indicated by arrows. Length of the CCD is indicated. RMSD, root-mean-square deviation.

See also Figure S1.

the kinase, given that Mec1 activation in the absence of damage causes cellular senescence (Toledo et al., 2008).

In the DDR pathway, Ddc2 plays a crucial, non-redundant role in checkpoint activation, and cells lacking Ddc2, like those lacking Mec1, are non-viable. Deletion analysis within the *DDC2* gene identified an RPA-binding domain (RBD) at its N terminus (Ball and Cortez, 2005; Kim et al., 2005), which is followed by a predicted CCD (Ball and Cortez, 2005; Itakura et al., 2005) and a Mec1 interaction domain in the C terminus that is essential for cell viability (Wakayama et al., 2001; Figure 1A). The RBD interacts with the N-terminal oligonucleotide/oligosaccharide (N-OB) domain of RPA's largest subunit (Rfa1 in yeast; RPA70 in human), which serves as a platform for interaction with multiple DDR proteins, including Ddc1, Dna2, Mre11-Rad50-Xrs2 (MRX), and Sgs1 in yeast, as well as p53 in mammals (Hegnauer et al., 2012; Lin et al., 1996; Seeber et al., 2016; Xu et al., 2008; Zhou et al., 2015). Due to the lack of structural information for Ddc2, it remained unclear how Ddc2 recognizes or binds the Rfa1 N-OB domain, although a theoretical model has been proposed (Ball et al., 2007). Interestingly, a yeast mutant in which the Rfa1 N-OB domain carries a charge reversal mutation (K45E; or *rfa-t11*) renders cells defective in recombination and DNA repair but proficient in replication (Chen et al., 1998; Seeber et al., 2016; Soustelle et al., 2002; Umezu et al., 1998).

Like the RBD of Ddc2, its CCD is well studied on a functional, but not structural, level. The CCD of the human homolog ATRIP was needed for ATRIP oligomerization, stable ATR-ATRIP complex formation, ATRIP's recruitment to DNA lesions, and the activation of checkpoint signaling (Ball and Cortez, 2005; Itakura et al., 2005). Interestingly, replacing the ATRIP CCD with a heterologous dimerization domain restored stable ATRIP oligomerization, complex formation, and recruitment, but not checkpoint activation (Ball and Cortez, 2005), arguing that oligomerization per se is not sufficient for ATR-ATRIP activation. Surprisingly, however, deletion of the Ddc2 CCD in *S. cerevisiae* did not yield an obvious phenotype (Bandhu et al., 2014). In conclusion, it remained unclear how the structure of Ddc2's RBD and CCD might contribute to the assembly of Mec1-Ddc2 complexes at sites of damage.

Here, we present crystal structures of Ddc2^{CCD}, Ddc2$^{RBD+CCD}$-Rfa1^{N-OB}, and Ddc2$^{RBD+CCD}$-Rfa1^{N-OB}-t11 complexes and analyze the functional role of Ddc2 N-terminal domains in vitro and in vivo. Importantly, our Ddc2-Rfa1 crystal structure provides the missing link to existing structural data, allowing us to propose a mode of assembly for Mec1-Ddc2 on the ssDNA-RPA platform at sites of DNA damage. On the functional side, we reveal a complete dependency on the Ddc2 N terminus for cell survival following inefficient repair of UV-induced damage and generation of ssDNA gaps. Our model provides an explanation of how recruitment to ssDNA can itself contribute to dimerization and activation of the Mec1-Ddc2 complex. It also suggests a role for the Ddc2 CCD as a structural spacer, allowing Mec1 to selectively phosphorylate targets locally.

RESULTS

Architecture of the Ddc2^{N}-Rfa1^{N} Complex

To gain structural insights into recruitment and oligomerization of Mec1-Ddc2 by RPA, we co-crystallized Ddc2^{N}, residues 1–109 from the budding yeast *Kluyveromyces lactis*, and Rfa1^{N}, residues 1–132 from *Saccharomyces cerevisiae* (Figure 1A), and determined its crystal structure at 1.9 Å resolution (Figure 1B). High sequence conservation (33% identity; Figure S1) allowed us to substitute *Kl*Ddc2^{N} for *Sc*Ddc2^{N} to obtain well-diffracting crystals. Ddc2^{N} includes the RBD (residues 10–30) and the CCD (residues 35–109) connected by a short linker. Rfa1^{N} contains a five-stranded beta barrel N-OB fold flanked by two flexible loops, forming a basic-hydrophobic cleft. The structure of the Ddc2^{N}-Rfa1^{N} complex was experimentally determined by single-wavelength anomalous diffraction (SAD) using selenomethionine-labeled Rfa1^{N} (Table 1). The complex crystallized in space group $P2_12_12_1$ with four protein chains per asymmetric unit. The entire Ddc2 CCD dimerizes to form a parallel coiled-coil, which allows two Ddc2 RBDs to interact with two Rfa1^{N} molecules, creating the A_2B_2 stoichiometry. Because RPA molecules coat ssDNA in a "beads on a string" fashion (Alani et al., 1992), it is reasonable to propose that the two Rfa1^{N} molecules in our crystal structure resemble two adjacent RPA molecules on a physiological stretch of ssDNA. Thus, the A_2B_2 architecture of the Ddc2^{N}-Rfa1^{N} complex could represent the biological assembly of homodimers of the Mec1-Ddc2 heterodimer on ssDNA-RPA.

Ddc2^{N} Homodimerizes through the CCD

The Ddc2 CCD is formed by two 103-Å-long parallel α helices and creates a 2-fold symmetry axis running along the center of the CCD (Figure 1B). The CCD homodimer is stabilized by classical hydrophobic knobs-into-holes leucine side-chain interactions at both ends, where additional polar side chains interact. The CCD opens up in the middle section, where polar side chains Asp65, Gln68, or His79 occupy the center, allowing access of solvent. To validate the CCD arrangement present in the *K. lactis* protein, we also determined the crystal structure of *Sc*Ddc2^{CCD} (*S. cerevisiae* Ddc2 CCD; residues 73–136) at 2.1 Å resolution (Table 1) and found that the crystallographic *Sc*Ddc2^{CCD} homodimer and the *K. lactis* CCD superimpose well (root-mean-square deviation [RMSD] = 1.15 Å), with all structural features of dimerization being conserved (Figure 1C). This is consistent with the sequence conservation (39% identity) of the two Ddc2 CCDs (Figure S1). In conclusion, the CCD is an extended helix (103 Å) that homodimerizes in a parallel orientation, thus being well-positioned to serve an architectural role in the enzyme complex.

Ddc2^{N} Binds Rfa1^{N} by Polar and Hydrophobic Interactions

The conserved acidic-hydrophobic motif in the *Kl*Ddc2 RBD interacts with the basic-hydrophobic cleft of *Sc*Rfa1^{N} (Figure S2A). The Ddc2 RBD, formed by residues 10–30 (Figure 2A), consists of a short α helix (residues 12–15) followed by a rigid proline-rich turn (residues 16–28), which together contribute to a buried surface area of ~850 Å^2 in the Ddc2^{N}-Rfa1^{N} complex (Figures 2B and S2B). Detailed protein-protein interface analysis by proteins, interfaces, structures, and assemblies (PISA) (Krissinel and Henrick, 2007) identified key residues on both proteins, highlighting the dual polar-hydrophobic character of the interaction. The Rfa1^{N}-interacting residues of *Kl*Ddc2 RBD are mostly conserved in *Sc*Ddc2 RBD (blue circles, Figure 2A).

The Ddc2^{N}-Rfa1^{N} interface can be classified into four spatially distinct regions (panels 1–4, Figure 2C). To confirm these and extend the analysis to *Sc*Ddc2^{N}, we determined the dissociation constant (K_d) using microscale thermophoresis (MST) of Cy5-labeled *Sc*Ddc2 RBD (residues 7–27) and *Sc*Rfa1^{N} that was either wild-type (WT) or carried alanine substitutions that were predicted to weaken the interaction (labeled Rfa1^{N} KREK for K58A, R62A, E86A, and K95A). The *Sc*Ddc2 RBD peptide bound *Sc*Rfa1^{N} WT with nanomolar affinity (K_d = 0.43 ± 0.08 μM), whereas *Sc*Rfa1^{N} KREK failed to interact with *Sc*Ddc2 RBD (Figure 2D). In conclusion, Ddc2^{N} binds Rfa1^{N} by polar and hydrophobic interactions with a moderately high affinity, and the residues involved for this interaction are conserved.

Ddc2 Interacts with Rfa1-t11 Mutant Protein

The *rfa1-t11* strain carries a K45E mutation close to the Ddc2-RPA interface, which renders cells defective in recombination and repair after damage by UV light, hydroxyurea (HU), Zeocin, and methyl methanesulfonate (MMS) but still able to carry out unperturbed DNA replication (Chen et al., 1998; Soustelle et al., 2002; Umezu et al., 1998). The K45E substitution indeed disrupts a positively charged patch in the basic-hydrophobic cleft of Rfa1^{N}, compromising the binding of MRX to RPA (Seeber et al., 2016). Although the Rfa1-t11 mutant protein failed to recruit Ddc2 to ssDNA in vitro (Zou and Elledge, 2003) and compromised Mec1 focus formation at an induced DSB (Dubrana et al., 2007), it was not defective in Ddc2 recruitment to HU-stalled replication forks in vivo (Kanoh et al., 2006), nor was checkpoint activation by HU treatment compromised (Seeber et al., 2016). To investigate whether the K45E mutation in Rfa1^{N} alters its interaction with Ddc2, we performed MST using Cy5-labeled *Sc*Ddc2 RBD and purified *Sc*Rfa1^{N}-t11. We found that the *Sc*Ddc2 RBD peptide bound *Sc*Rfa1^{N}-t11 with a 6-fold weaker affinity of K_d = 2.61 ± 0.37 μM (Figure 3A) compared to *Sc*Rfa1^{N} WT. This difference in affinity might explain the defect of the *rfa1-t11* mutant in

Table 1. Crystallographic Data Collection and Refinement Statistics

	$Ddc2^N$-$Rfa1^N$ Se-Met peak	$Ddc2^N$-$Rfa1^N$-t11	*Sc*$Ddc2^{CCD}$
Data collection			
Space group	$P2_12_12_1$	$P2_12_12_1$	$P222_1$
Unit cell: *a, b, c* (Å)	34.05, 94.94, 170.47	34.42, 94.59, 170.84	116.94, 19.89, 30.80
Unit cell: α, β, γ (°)	90.0, 90.0, 90.0	90.0, 90.0, 90.0	90.0, 90.0, 90.0
Resolution range (Å)[a]	50.00–1.94 (1.99–1.94)	50.00–2.38 (2.45–2.38)	50.00–2.10 (2.15–2.10)
Wavelength (Å)	0.9794	1.0000	1.0001
Completeness (%)[a]	98.0 (91.3)	92.1 (69.9)	99.8 (98.5)
Redundancy[a]	11.4 (11.0)	3.77 (2.92)	6.08 (5.72)
R_{sym}[a]	0.110 (1.573)	0.139 (0.919)	0.090 (0.856)
$I/\sigma(I)$[a]	12.1 (1.6)	5.87 (0.99)	13.23 (2.19)
CC (1/2) (%)[a]	99.9 (60.5)	99.3 (35.5)	99.9 (70.6)
Unique reflections	41,015	21,408	4,644
Refinement			
R_{work}	0.185	0.201	0.228
R_{free}	0.220	0.261	0.270
Resolution range (Å)	48.76–1.94	47.29–2.38	38.98–2.10
Reflections (all)	41,015	21,407	4,644
Reflections (test set)	2,046 (5%)	1,071 (5%)	558 (12%)
Number of atoms			
Overall	3,915	3,673	561
Protein	3,706	3,578	516
Solvent	202	95	45
B Factors (Å^2)			
Overall	50.9	57.1	51.8
Protein	50.8	57.3	52.4
Solvent	52.6	50.9	44.9
RMSD			
Bond lengths (Å)	0.01	0.01	0.01
Bond angles (°)	1.03	1.13	1.15
Ramachandran plot			
Allowed (%)	99.2	99.8	100
Outliers (%)	0.8	0.2	0

RMSD, root-mean-square deviation
[a]Values in parentheses refer to the highest-resolution shell

recruiting Ddc2 to ssDNA reported earlier (Zou and Elledge, 2003), although Rfa1-t11 still binds Ddc2 with significant affinity.

Recently, an N-terminal peptide (residues 1–20) of human Dna2, a nuclease-helicase, was co-crystallized with the human RPA N-OB domain (Zhou et al., 2015; PDB: 5EAY). R41 of human Rfa1, equivalent to K45 of yeast Rfa1 (mutated in *rfa1-t11*), was involved in a salt bridge with E6 of Dna2. Based on sequence alignments, we hypothesized that residues 355–372 of yeast Dna2 might interact with $Rfa1^N$ in an *rfa1-t11*-sensitive manner. To test this hypothesis, we performed MST using Cy5-labeled *Sc*Dna2 RBD (residues 355–372) and purified *Sc*$Rfa1^N$ WT or *Sc*$Rfa1^N$-t11. The *Sc*Dna2 RBD peptide bound *Sc*$Rfa1^N$ WT with an affinity of K_d = 118 ± 8 μM (Figure 3A) but failed to bind *Sc*$Rfa1^N$-t11 (Figure S4A). Similarly, we have previously shown that a peptide of the MRX complex (Rad50 residues 145–162) binds $Rfa1^N$ with an affinity of K_d = 63 ± 7 μM in an *rfa1-t11*-sensitive manner (Seeber et al., 2016). In conclusion, the basic cleft compromised by the *rfa1-t11* allele affects some, but not all, $Rfa1^N$ ligands. Whereas the Rfa1-Dna2 and Rfa1-MRX interactions are strongly compromised by the mutation, the Ddc2 RBD shows only minor sensitivity to the K45E substitution, arguing that Ddc2 binds $Rfa1^N$ in a distinct manner.

We next determined the crystal structure of $Ddc2^N$ in complex with $Rfa1^N$-t11 at 2.4 Å resolution (Table 1). Similar to WT $Ddc2^N$-$Rfa1^N$, the $Ddc2^N$-$Rfa1^N$-t11 complex crystallized in the $P2_12_12_1$ packing with comparable unit cell constants and contained the same A_2B_2 oligomer (Figure S3). There were no significant conformational changes in the overall arrangement

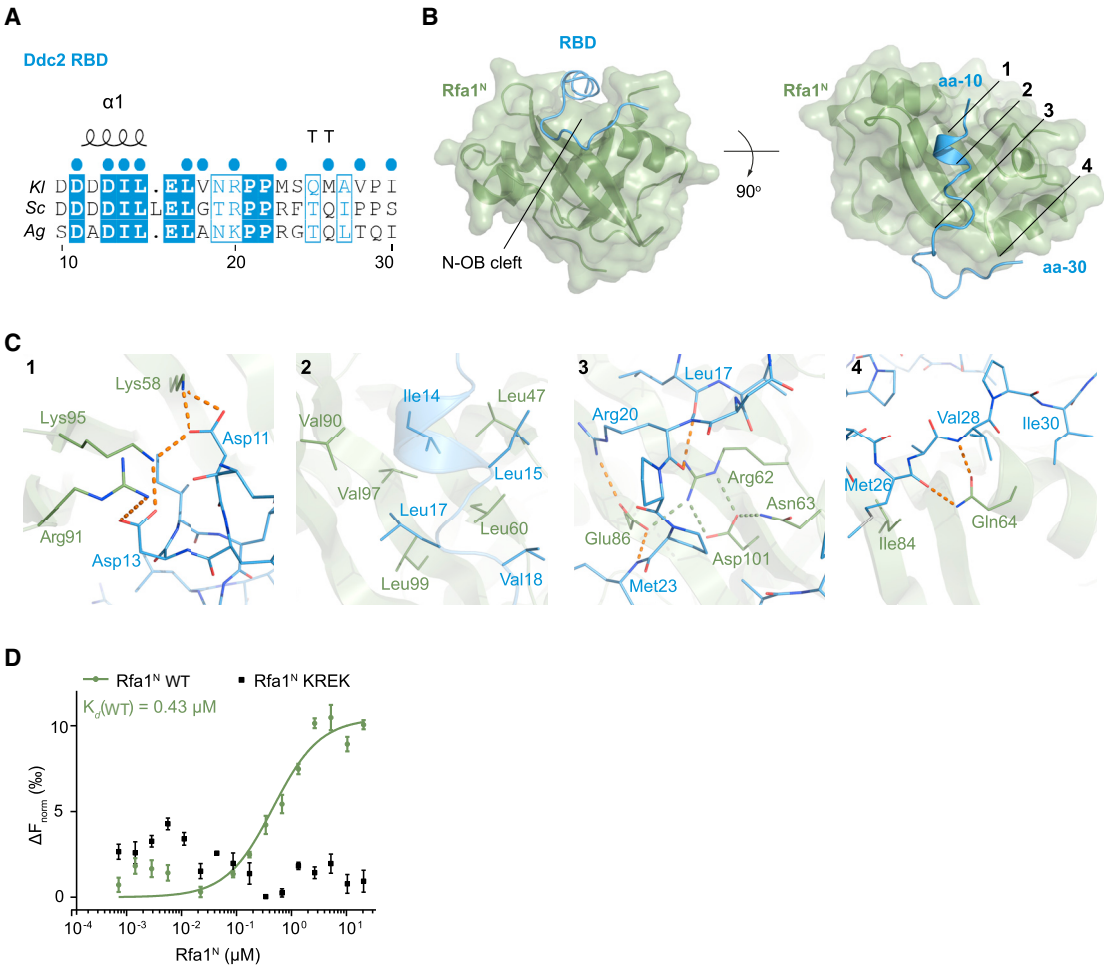

Figure 2. Ddc2^N Binds Rfa1^N by Polar and Hydrophobic Interactions

(A) Multiple sequence alignment of Ddc2 RBD (residues 10–30); *Ag*, *A. gossypii*. Secondary structure elements of the *Kl*Ddc2 RBD present in the crystal structure are indicated at the top (α, α helix; TT, turn). Blue dots represent residues that interact with *Sc*Rfa1^N. Identical and highly conserved residues are colored and bordered in blue, respectively.

(B) Structural overview of *Kl*Ddc2 RBD (blue) binding to *Sc*Rfa1^N (green) in cartoon representation. *Sc*Rfa1^N is also shown as transparent surface. Sub-interfaces of the Ddc2^N-Rfa1^N complex are numbered 1–4.

(C) Close-up view of the Ddc2^N-Rfa1^N sub-interfaces (panels 1–4). Residues involved in binding are displayed as colored sticks. Inter-molecular polar interactions are highlighted as orange dashed lines, whereas intra-molecular polar interactions are in green.

(D) Microscale thermophoresis (MST) analysis of binding of Cy5-labeled *Sc*Ddc2 RBD to *Sc*Rfa1^N WT (wild-type) (green curve) and *Sc*Rfa1^N KREK (K58A, R62A, E86A, and K95A; black data points). K_d represents dissociation constant. ΔF_{norm} (‰) represents change in fluorescence during thermophoresis normalized to initial fluorescence. Data are represented as mean ± SEM from three independent measurements.

See also Figure S2.

of domains or mode of binding. In the WT Ddc2^N-Rfa1^N structure, K45 is found in a short 3_{10} helix toward the end of a loop that connects the first and second β strand of the N-OB-fold β-barrel, lining one side of the Ddc2 RBD binding cleft. The K45 side chain was not involved in Ddc2^N binding and in fact pointed away from the Ddc2 RBD, as did the E45 side chain in the mutant crystal structure (Figure 3B), explaining why Rfa1^N-t11 is capable of binding Ddc2^N. To confirm this, we tested Ddc2^N-Rfa1^N-t11 binding in aqueous pull-down experiments. Purified histidine-tagged Rfa1^N and Rfa1^N-t11 proteins were immobilized on Ni^{2+} magnetic beads and incubated with purified untagged *Sc*Ddc2^N. Eluates were analyzed on SDS-PAGE and by mass spectrometry. *Sc*Ddc2^N was recovered with both Rfa1^N WT and Rfa1^N-t11 proteins (lanes 5 and 7, Figure 3C), but not in the presence of beads alone (lane 8, Figure 3C). This was confirmed by subjecting eluates to mass spectrometry.

After characterizing the Ddc2^N-Rfa1^N-t11 interaction in vitro, we tested the interaction in vivo using budding yeast strains, in which the endogenous *DDC2* locus was replaced by a C-terminal *DDC2-GFP* fusion in either a WT *RFA1* or *rfa1-t11* background. We performed immunoprecipitation with anti-GFP antibody and probed for Rfa1 using a polyclonal anti-Rfa1 antibody. Bolstering our structural and biochemical findings, Rfa1-t11 precipitated with Ddc2-GFP as efficiently as WT Rfa1

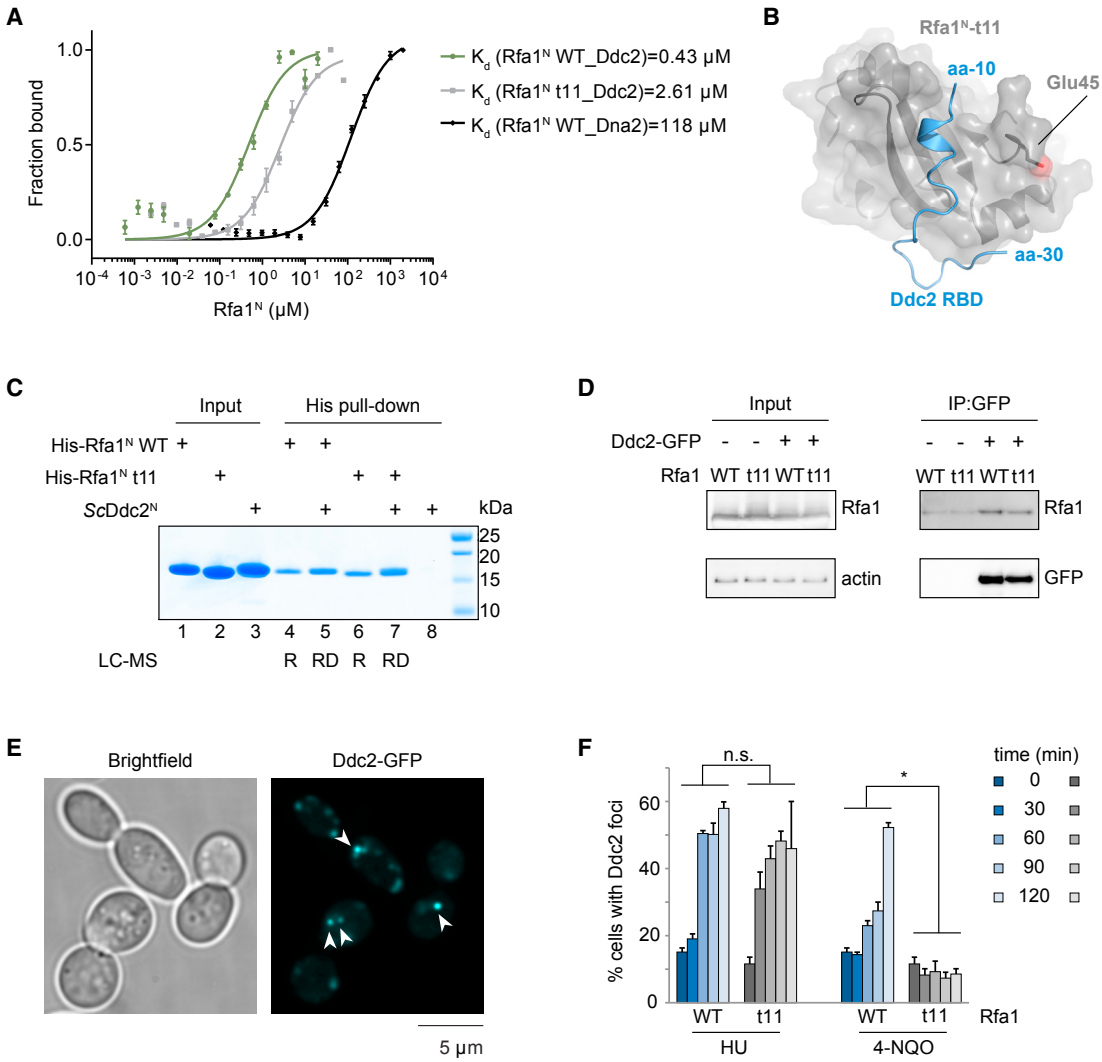

Figure 3. Ddc2 Interacts with Rfa1-t11 Mutant Protein

(A) MST analysis of binding of Cy5-labeled *Sc*Ddc2 RBD to *Sc*Rfa1^{N} WT (green curve; from Figure 2D) and *Sc*Rfa1^{N}-t11 (gray curve) and Cy5-labeled *Sc*Dna2 RBD to *Sc*Rfa1^{N} WT(black curve). K_d represents dissociation constant. ΔF_{norm} values were divided by the amplitude of the saturation level, resulting in the fraction bound (from 0 to 1) for each data point. Data are represented as mean ± SEM from three independent measurements.

(B) Detailed view of the binding of Ddc2 RBD to Rfa1^{N}-t11 as present in the Ddc2^{N}-Rfa1^{N}-t11 crystal structure (see also Figure S3). Ddc2 RBD is displayed as blue cartoon whereas Rfa1^{N}-t11 is shown as gray cartoon and transparent surface. The side chain of residue E45 (K45E mutation in *rfa1-t11*) is displayed as atom-type colored stick.

(C) In vitro pull-down: purified WT or K45E His-*Sc*Rfa1^{N} proteins were immobilized on Ni^{2+} magnetic beads and incubated with purified untagged *Sc*Ddc2^{N}. Eluates were subjected to SDS-PAGE and LC-MS. LC-MS identification of *Sc*Rfa1 is represented as R; LC-MS identification of both *Sc*Rfa1 and *Sc*Ddc2 is represented as RD.

(D) In vivo immunoprecipitation: extracts from cycling cultures of haploid *S. cerevisiae* (strains GA-1981, 4968, 9149, and 9828; see also Table S1) were subjected to anti-GFP immunoprecipitation (IP) in the presence of Benzonase. Shown are the western blots performed with indicated antibodies. Quantification is shown in Figure S4B.

(E and F) *DDC2-GFP* cells carrying either RFA1-wt or *rfa1-t11* alleles (strains GA-8705 and 9828; see also Table S1) were exposed to 0.2 M HU or 0.5 μg/mL 4-NQO for 0, 30, 60, 90, and 120 min prior to fixation for microscopy. (E) Example images of S phase cells exposed to 0.5 μg/mL 4-NQO for 120 min show Ddc2 foci (white arrowheads). (F) Quantification of S phase cells containing Ddc2-GFP foci is shown (N = 3 and n ≥ 100 per N; N indicates independent experiments and n indicates number of cells counted). n.s., not significant; *p < 0.05 (chi-square test). Data are represented as mean ± SD from three independent experiments.

See also Figures S3 and S4 and Table S1.

(Figures 3D and S4B) and neither bound to GFP alone. We minimized any impact that contaminating nucleic acids might have on the Ddc2-Rfa1-t11 interaction by performing the binding assay in the presence of the nuclease Benzonase.

To extend this analysis to DNA-damage-specific recruitment of Ddc2, we analyzed Ddc2-GFP foci formation by exposing WT and *rfa1-t11* cells expressing *DDC2-GFP* to either 0.2 M HU (which causes replication stress) or 0.5 μg/mL

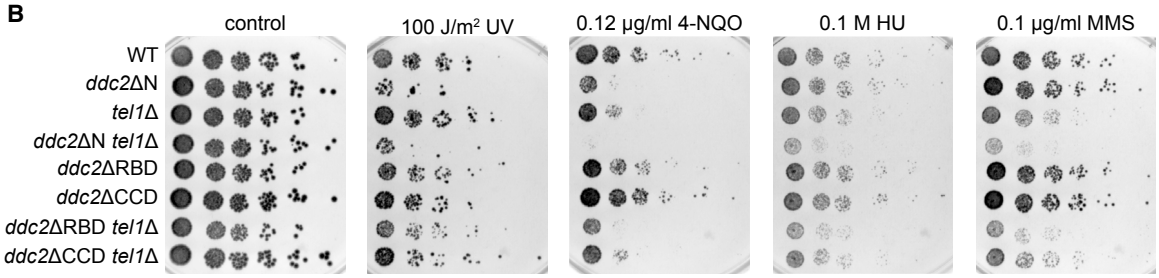

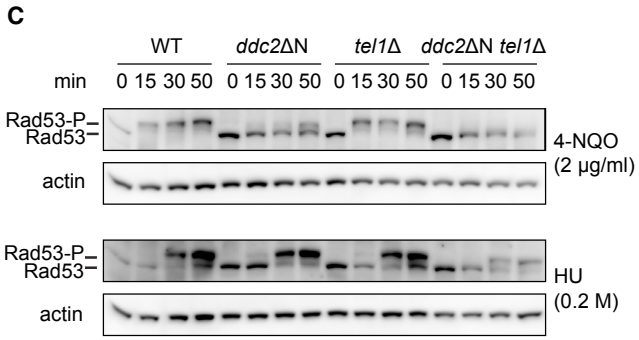

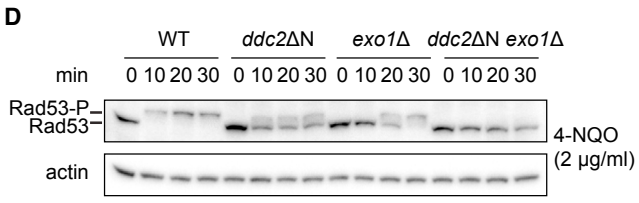

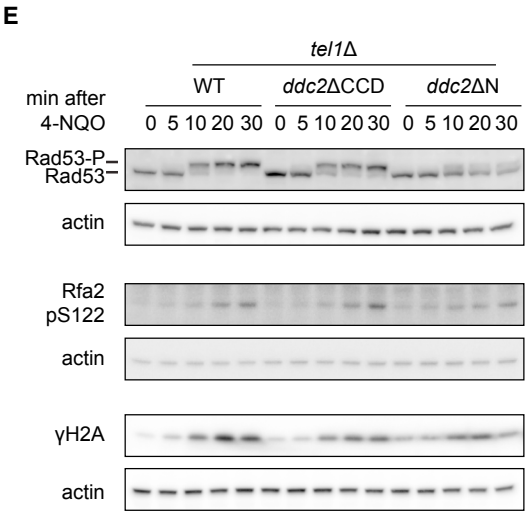

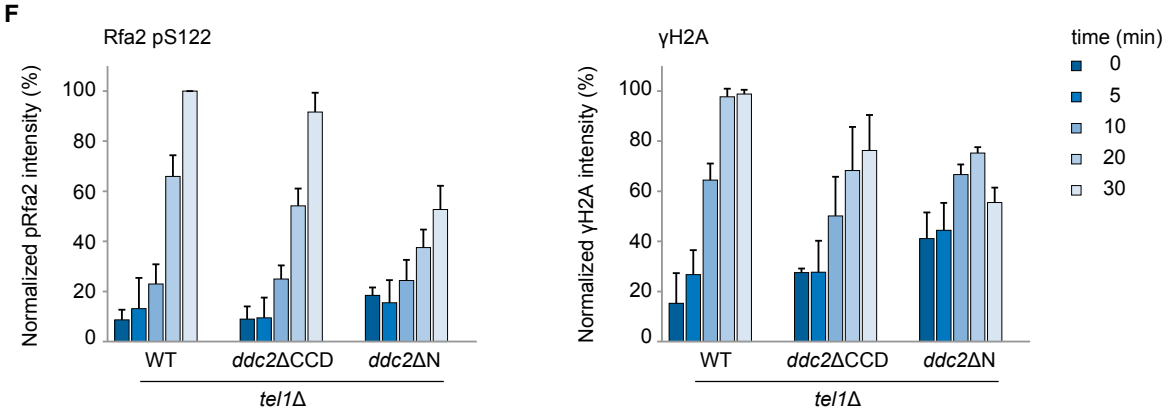

(legend on next page)

4-Nitroquinoline N-oxide (4-NQO), a UV-mimetic agent. As expected, after damage induction, Ddc2-GFP formed distinct sub-nuclear foci (Figure 3E). Consistent with the in vitro data, we could not measure significant differences in Ddc2 focus formation between *rfa1-t11* mutant and WT *RFA1* strains after treatment with HU (Figure 3F). However, upon treatment with 4-NQO, we measured a significant reduction in Ddc2 foci formation in the *rfa1-t11* strain (Figure 3F). Whereas UV-induced thymine dimers can be repaired by short-patch nucleotide excision repair (NER), obviating the need for checkpoint activation, it has been shown that unrepaired UV/4-NQO damage generates ssDNA (Giannattasio et al., 2010; Lopes et al., 2006), consistent with the strong Ddc2 focus formation that we observe in WT yeast after 4-NQO exposure (Figure 3F). Intriguingly, the sensitivity of *rfa1-t11* for growth on 0.01 M HU or 30 J/m^2 UV was additive with *ddc2*ΔN (Ddc2 lacking both RBD and CCD, i.e., residues 2–136; Figure S4C), arguing that compromised growth may not be due to defective Mec1-Ddc2 binding, in contrast to the epistasis observed between *rfa1-t11* and MRX mutations (Seeber et al., 2016). This argues that the *rfa1-t11* phenotypes, particularly on HU or UV, may well reflect the loss of binding of Rfa1-t11 to MRX or Dna2, but probably not to Ddc2.

Ddc2 RBD and CCD Function Additively under DNA Damage Conditions

We next examined the roles of the Ddc2 N terminus in the survival of DNA damage in vivo. We created isogenic *ddc2* alleles expressed from the endogenous promoter lacking residues 2–56 (*ddc2*ΔRBD), residues 58–136 (*ddc2*ΔCCD), or lacking both domains, i.e., residues 2–136 (*ddc2*ΔN; Figure 4A). Because Tel1 kinase (ATM in humans) is functionally redundant with Mec1 kinase for Rad53 activation in budding yeast (Morrow et al., 1995), we also created the above-mentioned *ddc2* mutants in strains lacking Tel1. Growth was scored by plating a dilution series of cultures on YPAD agar plates with and without exposure to UV light, 4-NQO, HU, or MMS. In the absence of Tel1, *ddc2*ΔN was highly sensitive to all tested damaging agents (row 4, Figure 4B), and it was hyper-sensitive to UV light and UV-mimetic 4-NQO, even in the presence of Tel1 kinase (row 2, Figure 4B). This suggests that Ddc2^N is involved in Mec1-dependent survival in response to a variety of DNA damage types. The sensitivity of the single-domain mutants, *ddc2*ΔRBD and *ddc2*ΔCCD, to all damaging agents was masked by Tel1, yet in its absence, they showed severe sensitivity to DNA damage (last two rows, Figure 4B). Nonetheless, single-domain deletions were not as sensitive as the combined deletion, suggesting that the RBD and the CCD are additive for Ddc2^N function.

To assess whether the sensitivity of *ddc2*ΔN cells stems from a defect in checkpoint induction, we monitored the phosphorylation-dependent activation of Rad53 by a phospho-upshift on a western blot. *ddc2*ΔN cells had strongly delayed and reduced Rad53 phosphorylation after exposure to 2 μg/mL 4-NQO, especially 15–30 min post-damage (Figure 4C). In contrast, the kinetics of Rad53 phosphorylation in *ddc2*ΔN cells on HU was nearly comparable to that of WT. This was true even in the absence of Tel1: *ddc2*ΔN *tel1Δ* cells completely failed to phosphorylate Rad53 after exposure to 4-NQO, whereas *tel1Δ* cells do (Figure 4C). We note that, although the N-terminal tail of Ddc2ΔN was partially degraded (data not shown), the protein was able to function as a co-factor of Mec1, as demonstrated by cell survival on high HU concentrations and robust checkpoint induction. Because *ddc2*ΔN was defective in Rad53 activation on 4-NQO, we tested whether the 4-NQO sensitivity of *ddc2*ΔN can only be attributed to defective Rad53 signaling. We examined epistasis between *ddc2*ΔN and *rad53*Δ mutants in cells lacking *sml1* at low 4-NQO concentrations, because *rad53*Δ mutants fail to grow at higher 4-NQO levels (Figure S5A). We observed that the *ddc2*ΔN *rad53*Δ double mutant was more sensitive than *rad53*Δ single mutant, suggesting that the 4-NQO sensitivity of *ddc2*ΔN cannot be only ascribed to defective Rad53 signaling. In conclusion, the Ddc2 RBD and the CCD are important for survival after DNA damage by UV and the UV-mimetic drug 4-NQO and for proficient Mec1 signaling to Rad53 and possibly other targets.

UV lesions are exclusively repaired by a "cut and patch"-type reaction called NER. Exo1, a 5′-3′ exonuclease, captures NER intermediates stabilized by impediments in repair synthesis and converts the initial 24- to 30-nucleotide (nt) ssDNA gap into a long (>500 nt) ssDNA gap, which triggers the DNA damage checkpoint response (Giannattasio et al., 2010). During S phase, replication forks running into UV lesions generate remarkably long ssDNA regions, up to 3 kb in length (Lopes et al., 2006). A study suggests that checkpoint activation by Mec1-Ddc2 in response to replication fork-stalling UV lesions is mainly triggered by ssDNA expanded by Exo1 (N. García-Rodríguez and H. Ulrich, personal communication). To test whether the 4-NQO sensitivity of *ddc2*ΔN arises from defective Mec1-Ddc2 recruitment to the ssDNA-RPA platform generated by Exo1 activity, we monitored Rad53 phosphorylation and cell survival in *ddc2*ΔN, *exo1*Δ, and

Figure 4. Ddc2 RBD and CCD Function Additively under DNA Damage Conditions

(A) Schematic diagram of *Sc*Ddc2 mutants used in this study and integrated into isogenic yeast strains.

(B) DNA damage sensitivity of *ddc2* mutants. A 5-fold dilution series of isogenic yeast strains with indicated genotypes (see also Table S1) on YPAD plates without or with 100 J/m^2 UV light, 0.12 μg/mL 4-NQO, 0.1 M HU, or 0.1 μg/mL MMS. Plates were incubated at 30°C for two days.

(C) Rad53 phosphorylation of strains used in (B) monitored by western blotting with anti-Rad53 antibody after synchronization in the G1 phase of the cell cycle (by α-factor) and release for indicated times into either 2 μg/mL 4-NQO or 0.2 M HU.

(D) Rad53 phosphorylation of isogenic strains GA-1981, 6354, 9479, and 9970 (see also Table S1) monitored as in Figure 4C.

(E) Isogenic strains GA-8163, 9485, and 9417 (see also Table S1) were synchronized in the G1 phase of the cell cycle (by α-factor) and released for indicated times into 2 μg/mL 4-NQO. Lysates were probed with anti-Rad53 antibody (Santa Cruz Biotechnology), anti-phospho-S122-Rfa2 antibody (Rockland), and anti-phospho-S129-H2A antibody (Sigma).

(F) Quantification of the intensities of Rfa2 phospho-S122 and H2A phospho-S129 normalized to actin loading control. Data are represented as mean ± SD from two independent experiments.

See also Figure S5 and Table S1.

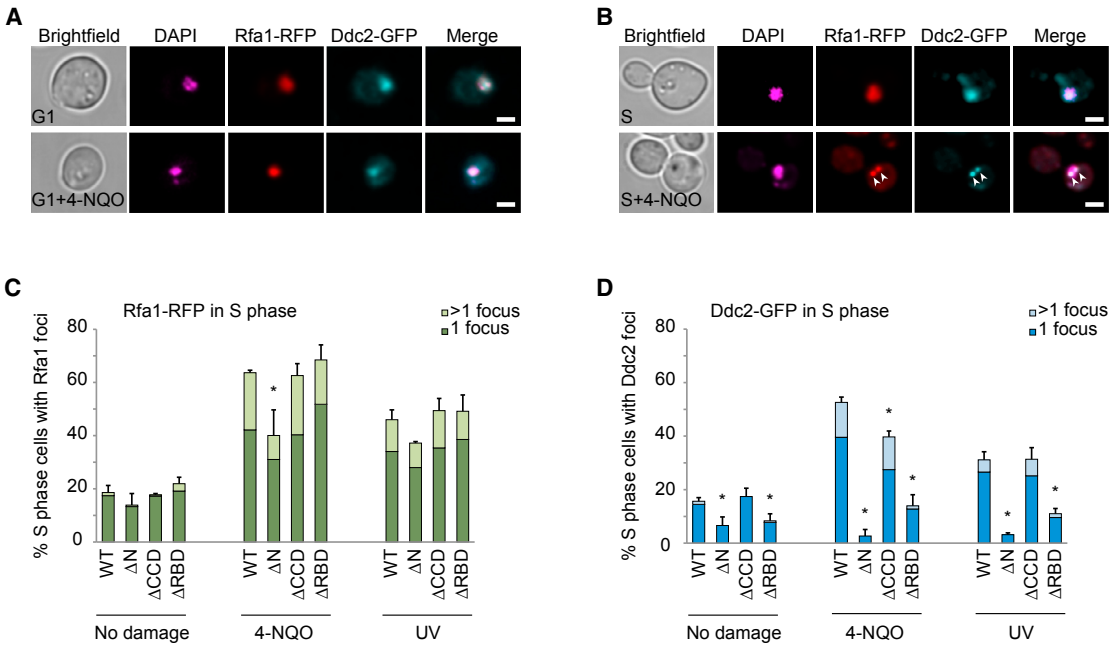

Figure 5. Ddc2 RBD and CCD Are Critical for Ddc2 Recruitment to 4-NQO and UV Damage Sites in S Phase

RFA1-RFP cells carrying indicated *ddc2* N-terminal truncations tagged with GFP (strains GA-8705, 9961, 9963, and 9965; see also Table S1) were either untreated or treated with 0.5 μg/mL 4-NQO or 100 J/m^2 UV 2 hr prior to fixation for microscopy.

(A) Images of *RFA1-RFP DDC2-GFP* G1 phase cells ± 4-NQO treatment. The scale bar represents 2 μm.

(B) Images of *RFA1-RFP DDC2-GFP* S phase cells ± 4-NQO treatment. White arrowheads indicate Rfa1 and Ddc2 foci and their colocalization (lower panel). The scale bar represents 2 μm.

(C) Quantification of S phase cells containing Rfa1-RFP foci. Data are represented as mean ± SD from three independent experiments where greater than 100 cells were counted. *$p < 0.005$ (chi-square test).

(D) Quantification of S phase cells containing Ddc2-GFP foci. Data are represented as mean ± SD from three independent experiments where greater than 100 cells were counted. *$p < 0.0005$ (chi-square test).

See also Table S1.

*ddc2*ΔN *exo1*Δ mutants upon 4-NQO treatment. In the presence of Exo1, Rad53 phosphorylation was strongly reduced and delayed in *ddc2*ΔN cells, whereas, in the absence of Exo1, *ddc2*ΔN cells failed to phosphorylate Rad53, even after 30 min of 4-NQO treatment (Figure 4D). However, *ddc2*ΔN mutation did not further sensitize *exo1*Δ mutants (Figure S5B), indicating that ssDNA generated by Exo1 is crucial for the Mec1-Ddc2 function for survival after 4-NQO and UV-induced damage, which is not necessarily correlated with Rad53 activation (Figure 4D).

Next, we tested whether the Ddc2 N terminus, especially the 103-Å-long CCD, would serve not only as a recruitment domain but also as a structural spacer that might allow Mec1 to selectively phosphorylate DNA-bound targets in *cis* while remaining bound to ssDNA-RPA. In *ddc2*ΔCCD and *ddc2*ΔN mutants lacking Tel1, we monitored phosphorylation of three Mec1 substrates following treatment with 2 μg/mL 4-NQO (Figure 4E). First, we scored Rad53 phosphorylation, as Rad53 diffuses freely and its phosphorylation should not be dependent on a structural spacer. Indeed, in this case, the *ddc2*ΔCCD mutant was as proficient as WT Ddc2 for Rad53 phosphorylation, whereas *ddc2*ΔN was deficient. Next, we tested the phosphorylation of S122 in the RPA subunit 2 (Rfa2-S122), which is localized to ssDNA sites. Again, *ddc2*ΔCCD cells modified S122 efficiently, with only a minor reduction over WT cells, whereas *ddc2*ΔN cells showed a significant reduction (39% of the *ddc2*ΔCCD level; Figures 4E and 4F). On the other hand, for the phosphorylation of histone H2A on S129 (γH2A), which, as part of a nucleosome, would sit further from the site of Mec1-Ddc2 binding than Rfa2, reduced levels in both *ddc2*ΔCCD and *ddc2*ΔN cells were observed (29% as compared to WT). This is consistent with the notion that the long CCD of Ddc2 allows Mec1 to reach targets that are further away from damage sites, such as γH2A, providing a degree of substrate selectivity to the RPA-bound Mec1 kinase.

Ddc2 RBD and CCD Are Critical for Ddc2 Focus Formation after 4-NQO or UV Damage in S Phase

To measure Ddc2 recruitment to 4-NQO damage sites quantitatively in *ddc2* mutants, we generated red fluorescent protein (RFP)-tagged Rfa1 and GFP-tagged Ddc2 in WT and Ddc2 mutants. All fusion proteins were C-terminally tagged and expressed from their endogenous loci under the genomic promoter. Consistent with previous reports, G1 phase cells rarely form Rfa1/Ddc2 foci, regardless of 4-NQO or UV treatment (Figure 5A; Lisby et al., 2004). S phase cells, however, showed punctate sub-nuclear Rfa1/Ddc2 foci in 15%–20% untreated cells, indicative of endogenous damage, and both markers showed an increase in focus number after 4-NQO or UV, as

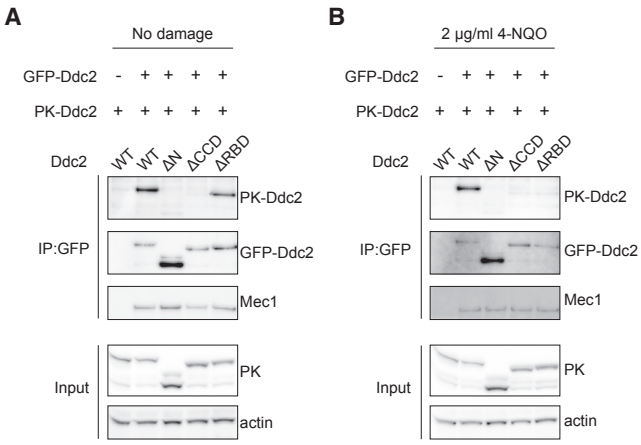

Figure 6. Ddc2 RBD Is Essential for Homodimerization under Damage Conditions

Extracts from cycling cultures of diploid *S. cerevisiae* strains GA-9842, 9843, 9844, 9845, and 9846 (see also Table S1) were subjected to anti-GFP IP and western blotting with indicated antibodies in the absence of DNA damage (A) or after 30 min exposure to 2 μg/mL 4-NQO (B).
See also Figure S6 and Table S1.

expected (Figures 5B–5D). When examining the Ddc2 mutants, we found that Rfa1-RFP foci still increased 2- to 3-fold upon 4-NQO or UV treatment in WT, *ddc2*ΔRBD, and *ddc2*ΔCCD strains, whereas *ddc2*ΔN cells showed a reduction, but not complete loss, upon 4-NQO treatment (denoted by asterisk, Figure 5C). This may indicate a feedforward amplification loop, in which RPA-dependent Mec1-Ddc2 recruitment to 4-NQO damage sites promotes further RPA recruitment. In the case of Ddc2 foci, however, despite a 3-fold increase in cells containing Ddc2 foci on 4-NQO (Figure 5D), neither *ddc2*ΔN nor *ddc2*ΔRBD cells showed an increase in Ddc2 foci on damage. In the *ddc2*ΔCCD strain on 4-NQO, the increase occurred and was slightly attenuated versus WT cells, whereas after UV, the increase was equal to WT. Combined with the survival studies, this suggests that the interaction of the Ddc2 RBD with Rfa1 is crucial for recruitment to 4-NQO or UV damage sites, whereas the CCD is more important for survival than for recruitment.

Ddc2 RBD Is Essential for Homodimerization under Damage Conditions

To examine the roles of these subdomains in homodimerization, we performed pull-down studies. Recent work has shown the co-existence of monomer-dimer species (Mec1-Ddc2 and $[Mec1\text{-}Ddc2]_2$), when Mec1-Ddc2 was overexpressed and purified under physiological salt concentrations (Andersen, 2017; Sawicka et al., 2016). Discrepancies in the literature regarding the size of the Mec1-Ddc2 complex may argue for a dynamic equilibrium between pools of Mec1-Ddc2 and $(Mec1\text{-}Ddc2)_2$ (Bomgarden et al., 2004; Itakura et al., 2005; Kim et al., 2005; Majka et al., 2006b; Unsal-Kaçmaz and Sancar, 2004). Congruently, in our hands, size-exclusion chromatography coupled with multi-angle light scattering (SEC-MALS) analysis showed that recombinant *Sc*Ddc2^{N} and *Sc*Ddc2^{CCD} were monomeric (Figures S6A and S6B), suggesting that the Ddc2 CCD is not a constitutive dimer. To test whether the Ddc2 CCD is nonetheless important for homodimerization in vivo, we created WT, *ddc2*ΔN, *ddc2*ΔRBD, and *ddc2*ΔCCD strains in a diploid background, wherein one endogenous allele of *DDC2* was C-terminally GFP tagged and the other allele was C-terminally PK tagged. In the absence of DNA damage, immunoprecipitation of WT GFP-Ddc2 co-precipitated WT PK-Ddc2; however, PK-Ddc2ΔN did not co-precipitate with GFP-Ddc2ΔN (Figure 6A). Importantly, PK-Ddc2ΔRBD, but not PK-Ddc2ΔCCD, was recovered from immunoprecipitates of GFP-Ddc2ΔRBD and GFP-Ddc2ΔCCD, respectively, arguing that the CCD, but not the RBD, is essential for Ddc2 homodimerization in the absence of DNA damage. All the mutant forms of Ddc2 tested here retain the ability to associate with Mec1 and form a Mec1-Ddc2 heterodimer.

We next tested whether the response to DNA damage would alter the observed domain-dependent interaction. From the lysates of cells treated with 2 μg/mL 4-NQO, PK-Ddc2ΔRBD was not as efficiently recovered in immunoprecipitates of GFP-Ddc2ΔRBD as the WT Ddc2 (Figure 6B). This indicates that the Ddc2 RBD promotes Ddc2 homodimerization in the presence of UV-mimetic stress, but not in the absence of the damage. On the other hand, the Ddc2 CCD is essential for homodimerization both in the presence and absence of damage. Of course, these experiments do not exclude that interactions between the Mec1 moieties could also contribute to homodimerization of the Mec1-Ddc2 heterodimer, i.e., to the $(Mec1\text{-}Ddc2)_2$ assembly.

DISCUSSION

Assembly of Mec1-Ddc2 on ssDNA-RPA

Our structural, biochemical, and in vivo findings allowed us to define the structural building blocks to model the higher-order Mec1-Ddc2 assembly on ssDNA-RPA at sites of DNA damage. The Ddc2^{N}-Rfa1^{N} crystal structure provides the missing link between the crystal structure of the ssDNA-RPA complex (Fan and Pavletich, 2012; PDB: 4GNX) and the negative-stain electron microscopy (EM) map of a homodimer of heterodimeric Mec1-Ddc2 (Sawicka et al., 2016; EMDB-4085). Specifically, the RPA construct in the crystal structure of ssDNA-RPA lacks the Rfa1 N-OB domain that is present in our Ddc2^{N}-Rfa1^{N} crystal structure. Similarly, the thin and long Ddc2 CCD dimer (6 × 103 Å) is absent in the ~22-Å negative-stain $(Mec1\text{-}Ddc2)_2$ map. Indeed, Ddc2^{N} is expected to be masked or averaged out due to the weak contrast of the thin CCD and its conformational flexibility.

To ascertain the position of Ddc2^{N} with respect to the Mec1-Ddc2 core complex, we tagged the N terminus of *Kl*Ddc2 with residues 840–978 of the *Sc*Sir3 winged helix dimerization domain (Sir3wH) (Oppikofer et al., 2013). We then co-expressed and purified Sir3wH-Ddc2 with *Kl*Mec1^{N} (residues 1–341) and subjected the Sir3wH-Ddc2-Mec1^{N} homodimeric complex to negative-stain EM to gain structural information. 2D class averages of $(Sir3wH\text{-}Ddc2\text{-}Mec1^{N})_2$ showed strong contrast for dimeric Sir3wH and core domains of Ddc2-Mec1^{N} but weak contrast for Ddc2^{N} (located between globular domains of Ddc2-Mec1^{N} and Sir3wH; Figure S7A). Our EM analysis confirmed two things. First, in agreement with the earlier

$(Mec1\text{-}Ddc2)_2$ negative-stained images (Sawicka et al., 2016), the Ddc2 N terminus showed poor contrast, reflecting its small diameter. Second, the Ddc2 N terminus—made visible through its fusion to Sir3wH—was positioned away from the Ddc2-$Mec1^N$ globular core. This allowed us to model the recruitment of $(Mec1\text{-}Ddc2)_2$ to ssDNA-RPA by compiling the following structural data: the crystal structure of the ssDNA-RPA complex lacking Rfa2wH and $Rfa1^N$—PDB: 4GNX; the negative-stain EM map of $(Mec1\text{-}Ddc2)_2$—EMD-4085; and the crystal structure of $Ddc2^N$-$Rfa1^N$ complex (this study). We assembled these in a to-scale composite model (Figures 7 and S7B), which illustrates the recruitment of $(Mec1\text{-}Ddc2)_2$ to two adjacent ssDNA-bound RPA molecules.

According to this model, $Ddc2^N$ would serve not only as a recruitment domain but also as a structural spacer, allowing the large $(Mec1\text{-}Ddc2)_2$ core module to move without encountering the DNA and thus preventing steric clashes with the assembly and disassembly of DNA repair and damage-processing complexes that must interact with the damage sites. This model also allows Mec1 kinase to phosphorylate multiple spatially distinct substrates while remaining bound, gaining flexibility from two long unstructured linkers. The first 50-residue-long linker is found between the Rfa1 N-OB and OB-A domains and can reach a maximum distance of ~158 Å. This linker was in fact reported to be highly flexible (Brosey et al., 2015). The second linker, between $Ddc2^N$ and the Mec1-Ddc2 globular core, is 64 residues long and maximally ~210 Å long. Both linkers show little amino acid conservation, yet their existence is conserved and their lengths increase from yeast to man. This is consistent with the proposed function as a flexible spacer. Our model reveals that two adjacent ssDNA-bound RPA molecules recruit one $(Mec1\text{-}Ddc2)_2$ entity to form the principal building block of the Mec1-Ddc2 higher-order assembly.

Our data suggest that $Ddc2^N$ is a non-constitutive homodimer. Due to the presence of long linkers in Ddc2 and RPA that flank $Ddc2^N$, it is reasonable to propose that $Ddc2^N$ homodimerization is independent of the Mec1-Ddc2 globular core homodimerization. Because the binding affinity of the RBD-$Rfa1^N$ interaction (K_d = 0.43 μM) was much higher than that of $Ddc2^N$ homodimerization, we propose that Ddc2 recruitment to ssDNA-RPA arrays increases the local concentration of the Ddc2 N terminus, promoting its homodimerization. The model reinforces our finding that the Ddc2 RBD becomes critical to maintain Ddc2 homodimerization only in response to DNA damage. Another explanation of the RBD-dependent homodimerization of Mec1-Ddc2 could be that the activation of Mec1-Ddc2 at damage sites, e.g., binding of Mec1-Ddc2 to Dpb11, induces a conformational change that weakens the Mec1-Ddc2 core homodimerization, increasing the dependency of Mec1-Ddc2 homodimerization on the Ddc2 N terminus. This may be a regulatory feature that helps prevent improper Mec1 activation in the absence of sufficiently long stretches of ssDNA. Indeed, in human cells, ATR failed to phosphorylate downstream effectors when the ATRIP CCD was replaced by the constitutively homodimeric GCN4 CCD (Ball and Cortez, 2005). A further means to regulate Mec1 activation could be recognition of homodimeric Ddc2 CCD by Mec1 co-activators, such as Dpb11 and 9-1-1.

Exo1-Dependent Assembly of $(Mec1\text{-}Ddc2)_2$ Molecules on ssDNA-RPA after UV Damage

RPA binds ssDNA in three different modes, depending on the length of ssDNA that it contacts: either the 8-nt low-affinity mode; the 12- to 23-nt medium-affinity mode; or the 30-nt high-affinity mode (Bochkareva et al., 2001). Because two RPA molecules bind one $(Mec1\text{-}Ddc2)_2$ entity, we expect 60 nt (high-affinity mode) to be the minimum length of ssDNA that is required to assemble $(Mec1\text{-}Ddc2)_2$ efficiently. Indeed, it was reported that, in the presence of RPA, Ddc2 binds more efficiently to 75-nt ssDNA (space for two RPA molecules) than it does to 50-nt or 30-nt ssDNA (space for one RPA molecule; Zou and Elledge, 2003). Thus, it is clear that Mec1-Ddc2 is efficiently recruited to an Exo1-expanded ssDNA gap, where long arrays of RPA bound to ssDNA in high-affinity mode are present. Of course, Mec1 recruitment and activation on ssDNA is dependent on the $Ddc2^N$-$Rfa1^N$ interaction, and *ddc2*ΔN cells showed greatly delayed and reduced Rad53 phosphorylation upon 4-NQO treatment (Figure 4D). Notably, Rad53 was still phosphorylated at low levels. On the other hand, in *exo1*Δ cells, the initial 24- to 30-nt gap cannot be elongated and long RPA-Mec1-Ddc2 arrays cannot build up. Congruently, we observed delayed and reduced Rad53 phosphorylation, hinting at a weak recruitment and dimerization mode for Mec1-Ddc2, even to the 24- to 30-nt short gap. It is imaginable that one Mec1-Ddc2 homodimer binds to two of the three RPA molecules that could occupy the initial 24- to 30-nt gap generated during NER in the 8-nt low-affinity mode. Such a scenario could still trigger weak and delayed Rad53 phosphorylation. Together, these mechanistic insights explain why *ddc2*ΔN and *exo1*Δ were additive for Rad53 phosphorylation upon 4-NQO treatment and that the delayed and reduced Rad53 activation in the case of *ddc2*ΔN is dependent on Exo1.

Interestingly, the additivity of *ddc2*ΔN and *exo1*Δ for Rad53 phosphorylation does not reflect on cell survival in our drop assays (Figure S5B). Nonetheless, the epistasis between *ddc2*ΔN and *exo1*Δ on survival assays suggests that Exo1-dependent ssDNA formation is crucial to fulfill Mec1-Ddc2 function in response to UV damage. This discrepancy between Rad53 activation and cell survival assays may reflect the distinct natures of the two experiments; Rad53 phosphorylation was done in liquid cultures acutely exposed to 4-NQO, whereas, for the drop assay, colonies were continuously exposed to 4-NQO for two days on plates, where both Exo1 and Mec1-Ddc2 may be involved in an alternative rescue pathway. Taken together, we suggest that, in the presence of UV lesions, Exo1 extends short unrepaired ssDNA gaps to recruit Mec1-Ddc2 efficiently by means of the $Ddc2^N$-$Rfa1^N$ interaction, promoting checkpoint induction and survival (Figure 7A). This occurs, apparently, in S phase cells.

Activation of $(Mec1\text{-}Ddc2)_2$ on ssDNA-RPA at DNA Damage Sites

Finally, we extrapolated our composite to-scale model to mimic Mec1-Ddc2 activation on ssDNA-RPA after DNA damage (Figure 7B; see STAR Methods for assembly details). The model recapitulates the role of $Ddc2^N$ as both a recruitment and spacer module that may allow Mec1 kinase to phosphorylate spatially

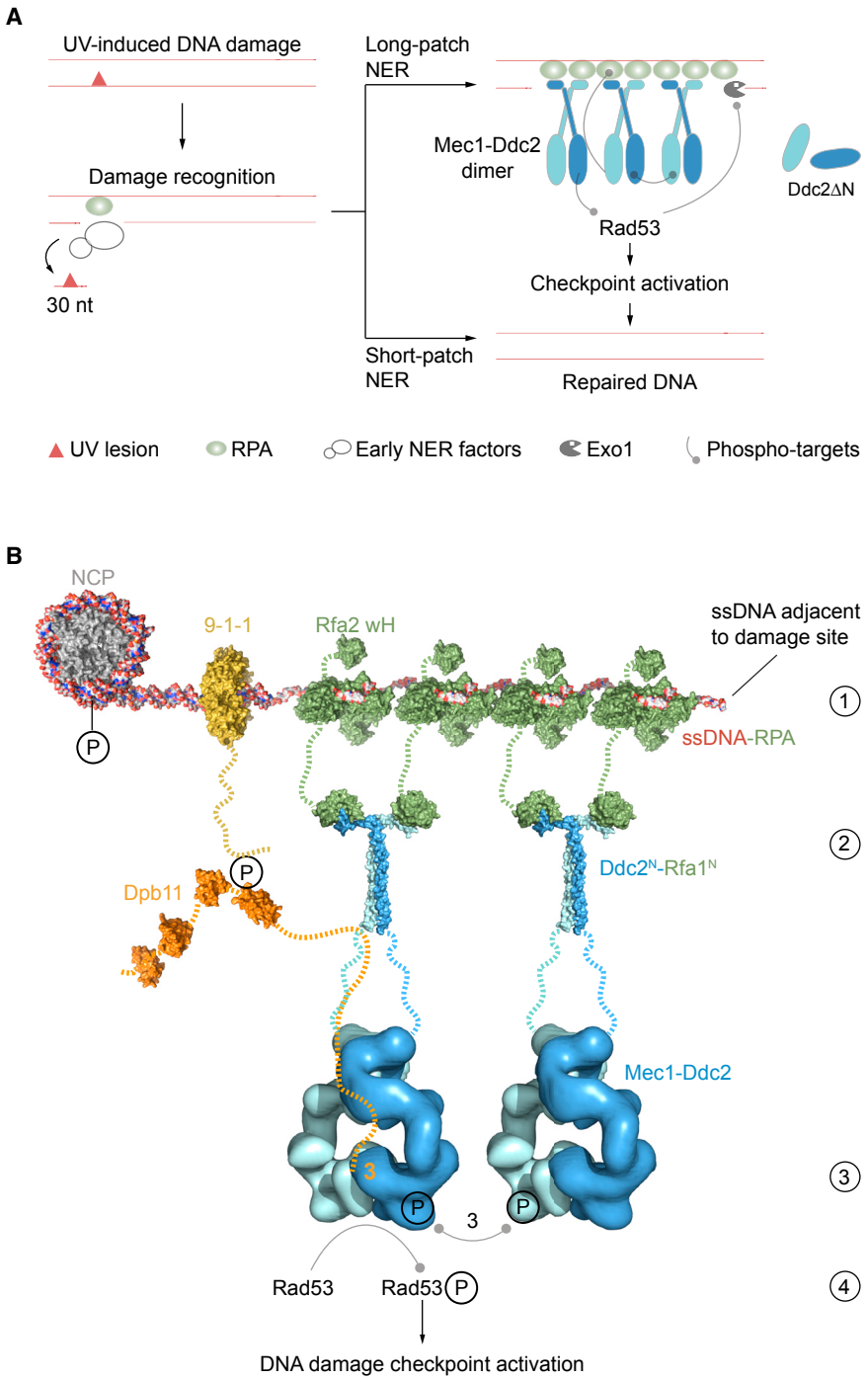

Figure 7. Assembly and Activation of Mec1-Ddc2-RPA at DNA Damage Sites

(A) Schematic diagram of the DNA damage response to a UV lesion. In the first step, early NER factors recognize the damage and excise a 24- to 30-nt gap containing the lesion. In the second step, the NER reaction is completed by gap-filling DNA synthesis and ligation (short-patch NER). An impediment between these two steps, e.g., replication fork or opposing lesion, allows Exo1 exonuclease to process the 24- to 30-nt gap and generate long ssDNA gaps, which recruit Mec1-Ddc2 via the $Ddc2^{N}$-$Rfa1^{N}$ interaction. Mec1 induces checkpoint activation by phosphorylating multiple substrates, including Rad53, RPA, and Exo1, to allow DNA repair (long-patch NER).

(B) To-scale composite structural model of the Mec1-Ddc2-RPA assembly (see also Figure S7B) and activation at DNA damage sites (see STAR Methods for assembly details). (1) indicates the ssDNA-RPA platform, (2) indicates assembly of $(Mec1\text{-}Ddc2)_2$ on the ssDNA-RPA platform via $Ddc2^{N}$-$Rfa1^{N}$, (3) indicates activation of Mec1 kinase, and (4) indicates phosphorylation of Rad53 and checkpoint induction.

See also Figure S7.

distinct targets, including proximal or readily diffusing targets like RPA and Rad53, but also more distal substrates like histone H2A, 9-1-1, and Dpb11, thanks to the extended CCD and the long unstructured linkers (dotted lines; see also Figure S7B). The capacity of Ddc2 for spatial flexibility may also facilitate an efficient activation of Mec1 by the long unstructured C-terminal tails of either the Ddc1 subunit in the 9-1-1 clamp or of Dpb11. The model is consistent with the notion that the recruitments of 9-1-1-Dpb11 and/or $(Mec1\text{-}Ddc2)_2$ to damage are largely independent events (Kondo et al., 2001; Melo et al., 2001), which may reduce the likelihood of untimely Mec1 activation. Once activated, Mec1-Ddc2 appears to remain bound and act locally on substrates in the vicinity, given that it forms a bright focus at the site of damage (Dubrana et al., 2007). Thus, the structures presented here and the composite model of the Mec1-Ddc2 higher-order assembly on ssDNA-RPA that they enabled have elucidated structural features of the enzyme complex that have functional implications for the activation and target recognition of this kinase. We find that these unusual Mec1/ATR characteristics are crucial for the maintenance of genomic integrity in face of genomic insult.

STAR★METHODS

Detailed methods are provided in the online version of this paper and include the following:

- KEY RESOURCES TABLE
- CONTACT FOR REAGENT AND RESOURCE SHARING
- METHOD DETAILS
  - Protein engineering and purification from *E. coli*
  - Protein engineering and purification from *Sf*9
  - Crystallization
  - Data collection and structure determination
  - Molecular mass measurement by SEC-MALS
  - Microscale thermophoresis
  - Immunoprecipitation and western blotting
  - Yeast drop assays
  - Fluorescence microscopy
  - Negative-stain electron microscopy
  - Modeling structural assemblies
- QUANTIFICATION AND STATISTICAL ANALYSES
  - MST binding assay
  - Immunoblots
  - Fluorescence microscopy
- DATA AND SOFTWARE AVAILABILITY
  - Accession Numbers

SUPPLEMENTAL INFORMATION

Supplemental Information includes seven figures and one table and can be found with this article online at https://doi.org/10.1016/j.molcel.2017.09.019.

AUTHOR CONTRIBUTIONS

I.D. designed and performed most experiments including protein expression, purification, crystallization, EM, MST, and yeast assays, analyzed data, and wrote the manuscript; A.S. performed fluorescence microscopy; K.S. supervised and performed yeast experiments with I.D.; J.J.K. performed SEC-MALS, MST, and purified protein; I.D. and H.G. determined crystal structures; and H.G. and S.M.G. outlined the project, supervised I.D., evaluated experiments, and wrote the manuscript.

ACKNOWLEDGMENTS

This work was supported by the Swiss Cancer League (KFS-3062-08-2012), Swiss National Science Foundation, (31003A 138334) and Novartis Research Foundation. Part of this work was performed at the X06DA and X10SA beamlines of the Swiss Light Source, Paul Scherrer Institute, Villigen. We thank D. Hess for mass spectrometry analysis and S. Cavadini and A. Graff for help with electron microscopy. We also thank U. Rass and N. Thomae for proofreading the manuscript and the Gasser laboratory for discussions.

Received: May 24, 2017
Revised: August 18, 2017
Accepted: September 14, 2017
Published: October 12, 2017

REFERENCES

Abdulrahman, W., Uhring, M., Kolb-Cheynel, I., Garnier, J.M., Moras, D., Rochel, N., Busso, D., and Poterszman, A. (2009). A set of baculovirus transfer vectors for screening of affinity tags and parallel expression strategies. Anal. Biochem. *385*, 383–385.

Adams, P.D., Afonine, P.V., Bunkóczi, G., Chen, V.B., Echols, N., Headd, J.J., Hung, L.W., Jain, S., Kapral, G.J., Grosse Kunstleve, R.W., et al. (2011). The Phenix software for automated determination of macromolecular structures. Methods *55*, 94–106.

Alani, E., Thresher, R., Griffith, J.D., and Kolodner, R.D. (1992). Characterization of DNA-binding and strand-exchange stimulation properties of y-RPA, a yeast single-strand-DNA-binding protein. J. Mol. Biol. *227*, 54–71.

Andersen, K.R. (2017). Insights into Rad3 kinase recruitment from the crystal structure of the DNA damage checkpoint protein Rad26. J. Biol. Chem. *292*, 8149–8157.

Ball, H.L., and Cortez, D. (2005). ATRIP oligomerization is required for ATR-dependent checkpoint signaling. J. Biol. Chem. *280*, 31390–31396.

Ball, H.L., Ehrhardt, M.R., Mordes, D.A., Glick, G.G., Chazin, W.J., and Cortez, D. (2007). Function of a conserved checkpoint recruitment domain in ATRIP proteins. Mol. Cell. Biol. *27*, 3367–3377.

Bandhu, A., Kang, J., Fukunaga, K., Goto, G., and Sugimoto, K. (2014). Ddc2 mediates Mec1 activation through a Ddc1- or Dpb11-independent mechanism. PLoS Genet. *10*, e1004136.

Bastos de Oliveira, F.M., Kim, D., Cussiol, J.R., Das, J., Jeong, M.C., Doerfler, L., Schmidt, K.H., Yu, H., and Smolka, M.B. (2015). Phosphoproteomics reveals distinct modes of Mec1/ATR signaling during DNA replication. Mol. Cell *57*, 1124–1132.

Berrow, N.S., Alderton, D., Sainsbury, S., Nettleship, J., Assenberg, R., Rahman, N., Stuart, D.I., and Owens, R.J. (2007). A versatile ligation-independent cloning method suitable for high-throughput expression screening applications. Nucleic Acids Res. *35*, e45.

Bochkareva, E., Belegu, V., Korolev, S., and Bochkarev, A. (2001). Structure of the major single-stranded DNA-binding domain of replication protein A suggests a dynamic mechanism for DNA binding. EMBO J. *20*, 612–618.

Bomgarden, R.D., Yean, D., Yee, M.C., and Cimprich, K.A. (2004). A novel protein activity mediates DNA binding of an ATR-ATRIP complex. J. Biol. Chem. *279*, 13346–13353.

Bonilla, C.Y., Melo, J.A., and Toczyski, D.P. (2008). Colocalization of sensors is sufficient to activate the DNA damage checkpoint in the absence of damage. Mol. Cell *30*, 267–276.

Bricogne, G. (2011). BUSTER version 2.11.4 (Global Phasing).

Brosey, C.A., Soss, S.E., Brooks, S., Yan, C., Ivanov, I., Dorai, K., and Chazin, W.J. (2015). Functional dynamics in replication protein A DNA binding and protein recruitment domains. Structure *23*, 1028–1038.

Brown, E.J., and Baltimore, D. (2000). ATR disruption leads to chromosomal fragmentation and early embryonic lethality. Genes Dev. *14*, 397–402.

Chen, C., Umezu, K., and Kolodner, R.D. (1998). Chromosomal rearrangements occur in S. cerevisiae rfa1 mutator mutants due to mutagenic lesions processed by double-strand-break repair. Mol. Cell *2*, 9–22.

Chen, V.B., Arendall, W.B., 3rd, Headd, J.J., Keedy, D.A., Immormino, R.M., Kapral, G.J., Murray, L.W., Richardson, J.S., and Richardson, D.C. (2010). MolProbity: all-atom structure validation for macromolecular crystallography. Acta Crystallogr. D Biol. Crystallogr. *66*, 12–21.

Cortez, D., Guntuku, S., Qin, J., and Elledge, S.J. (2001). ATR and ATRIP: partners in checkpoint signaling. Science *294*, 1713–1716.

Cowtan, K. (2006). The Buccaneer software for automated model building. 1. Tracing protein chains. Acta Crystallogr. D Biol. Crystallogr. *62*, 1002–1011.

Dore, A.S., Kilkenny, M.L., Rzechorzek, N.J., and Pearl, L.H. (2009). Crystal structure of the rad9-rad1-hus1 DNA damage checkpoint complex–implications for clamp loading and regulation. Mol, Cell *34*, 735–745.

Dubrana, K., van Attikum, H., Hediger, F., and Gasser, S.M. (2007). The processing of double-strand breaks and binding of single-strand-binding proteins RPA and Rad51 modulate the formation of ATR-kinase foci in yeast. J. Cell Sci. *120*, 4209–4220.

Edwards, R.J., Bentley, N.J., and Carr, A.M. (1999). A Rad3-Rad26 complex responds to DNA damage independently of other checkpoint proteins. Nat. Cell Biol. *1*, 393–398.

Emsley, P., Lohkamp, B., Scott, W.G., and Cowtan, K. (2010). Features and development of Coot. Acta Crystallogr. D Biol. Crystallogr. *66*, 486–501.

Fan, J., and Pavletich, N.P. (2012). Structure and conformational change of a replication protein A heterotrimer bound to ssDNA. Genes Dev. *26*, 2337–2347.

Feldkamp, M.D., Mason, A.C., Eichman, B.F., and Chazin, W.J. (2014). Structural analysis of replication protein A recruitment of the DNA damage response protein SMARCAL1. Biochemistry *53*, 3052–3061.

Frei, C., and Gasser, S.M. (2000). The yeast Sgs1p helicase acts upstream of Rad53p in the DNA replication checkpoint and colocalizes with Rad53p in S-phase-specific foci. Genes Dev. *14*, 81–96.

Friedel, A.M., Pike, B.L., and Gasser, S.M. (2009). ATR/Mec1: coordinating fork stability and repair. Curr. Opin. Cell Biol. *21*, 237–244.

Furuya, K., Poitelea, M., Guo, L., Caspari, T., and Carr, A.M. (2004). Chk1 activation requires Rad9 S/TQ-site phosphorylation to promote association with C-terminal BRCT domains of Rad4TOPBP1. Genes Dev. *18*, 1154–1164.

Giannattasio, M., Follonier, C., Tourrière, H., Puddu, F., Lazzaro, F., Pasero, P., Lopes, M., Plevani, P., and Muzi-Falconi, M. (2010). Exo1 competes with repair synthesis, converts NER intermediates to long ssDNA gaps, and promotes checkpoint activation. Mol. Cell *40*, 50–62.

Hegnauer, A.M., Hustedt, N., Shimada, K., Pike, B.L., Vogel, M., Amsler, P., Rubin, S.M., van Leeuwen, F., Guénolé, A., van Attikum, H., et al. (2012). An N-terminal acidic region of Sgs1 interacts with Rpa70 and recruits Rad53 kinase to stalled forks. EMBO J. *31*, 3768–3783.

Hohn, M., Tang, G., Goodyear, G., Baldwin, P.R., Huang, Z., Penczek, P.A., Yang, C., Glaeser, R.M., Adams, P.D., and Ludtke, S.J. (2007). SPARX, a new environment for Cryo-EM image processing. J. Struct. Biol. *157*, 47–55.

Hustedt, N., Seeber, A., Sack, R., Tsai-Pflugfelder, M., Bhullar, B., Vlaming, H., van Leeuwen, F., Guénolé, A., van Attikum, H., Srivas, R., et al. (2015). Yeast PP4 interacts with ATR homolog Ddc2-Mec1 and regulates checkpoint signaling. Mol. Cell *57*, 273–289.

Itakura, E., Sawada, I., and Matsuura, A. (2005). Dimerization of the ATRIP protein through the coiled-coil motif and its implication to the maintenance of stalled replication forks. Mol. Biol. Cell *16*, 5551–5562.

Kabsch, W. (2010). Xds. Acta Crystallogr. D Biol. Crystallogr. *66*, 125–132.

Kanoh, Y., Tamai, K., and Shirahige, K. (2006). Different requirements for the association of ATR-ATRIP and 9-1-1 to the stalled replication forks. Gene *377*, 88–95.

Kim, S.M., Kumagai, A., Lee, J., and Dunphy, W.G. (2005). Phosphorylation of Chk1 by ATM- and Rad3-related (ATR) in Xenopus egg extracts requires binding of ATRIP to ATR but not the stable DNA-binding or coiled-coil domains of ATRIP. J. Biol. Chem. *280*, 38355–38364.

Kondo, T., Wakayama, T., Naiki, T., Matsumoto, K., and Sugimoto, K. (2001). Recruitment of Mec1 and Ddc1 checkpoint proteins to double-strand breaks through distinct mechanisms. Science *294*, 867–870.

Krissinel, E., and Henrick, K. (2007). Inference of macromolecular assemblies from crystalline state. J. Mol. Biol. *372*, 774–797.

Kumagai, A., Lee, J., Yoo, H.Y., and Dunphy, W.G. (2006). TopBP1 activates the ATR-ATRIP complex. Cell *124*, 943–955.

Kumar, S., and Burgers, P.M. (2013). Lagging strand maturation factor Dna2 is a component of the replication checkpoint initiation machinery. Genes Dev. *27*, 313–321.

Lin, Y.L., Chen, C., Keshav, K.F., Winchester, E., and Dutta, A. (1996). Dissection of functional domains of the human DNA replication protein complex replication protein A. J. Biol. Chem. *271*, 17190–17198.

Lisby, M., Barlow, J.H., Burgess, R.C., and Rothstein, R. (2004). Choreography of the DNA damage response: spatiotemporal relationships among checkpoint and repair proteins. Cell *118*, 699–713.

Liu, Q., Guntuku, S., Cui, X.S., Matsuoka, S., Cortez, D., Tamai, K., Luo, G., Carattini-Rivera, S., DeMayo, F., Bradley, A., et al. (2000). Chk1 is an essential kinase that is regulated by Atr and required for the G(2)/M DNA damage checkpoint. Genes Dev. *14*, 1448–1459.

Lopes, M., Foiani, M., and Sogo, J.M. (2006). Multiple mechanisms control chromosome integrity after replication fork uncoupling and restart at irreparable UV lesions. Mol. Cell *21*, 15–27.

MacDougall, C.A., Byun, T.S., Van, C., Yee, M.C., and Cimprich, K.A. (2007). The structural determinants of checkpoint activation. Genes Dev. *21*, 898–903.

Majka, J., Binz, S.K., Wold, M.S., and Burgers, P.M. (2006a). Replication protein A directs loading of the DNA damage checkpoint clamp to 5′-DNA junctions. J. Biol. Chem. *281*, 27855–27861.

Majka, J., Niedziela-Majka, A., and Burgers, P.M. (2006b). The checkpoint clamp activates Mec1 kinase during initiation of the DNA damage checkpoint. Mol. Cell *24*, 891–901.

McCoy, A.J., Grosse-Kunstleve, R.W., Adams, P.D., Winn, M.D., Storoni, L.C., and Read, R.J. (2007). Phaser crystallographic software. J. Appl. Cryst. *40*, 658–674.

Melo, J.A., Cohen, J., and Toczyski, D.P. (2001). Two checkpoint complexes are independently recruited to sites of DNA damage in vivo. Genes Dev. *15*, 2809–2821.

Morrow, D.M., Tagle, D.A., Shiloh, Y., Collins, F.S., and Hieter, P. (1995). TEL1, an S. cerevisiae homolog of the human gene mutated in ataxia telangiectasia, is functionally related to the yeast checkpoint gene MEC1. Cell *82*, 831–840.

Navadgi-Patil, V.M., and Burgers, P.M. (2009). A tale of two tails: activation of DNA damage checkpoint kinase Mec1/ATR by the 9-1-1 clamp and by Dpb11/TopBP1. DNA Repair (Amst.) *8*, 996–1003.

Oppikofer, M., Kueng, S., Keusch, J.J., Hassler, M., Ladurner, A.G., Gut, H., and Gasser, S.M. (2013). Dimerization of Sir3 via its C-terminal winged helix domain is essential for yeast heterochromatin formation. EMBO J. *32*, 437–449.

Paciotti, V., Clerici, M., Lucchini, G., and Longhese, M.P. (2000). The checkpoint protein Ddc2, functionally related to S. pombe Rad26, interacts with Mec1 and is regulated by Mec1-dependent phosphorylation in budding yeast. Genes Dev. *14*, 2046–2059.

Pettersen, E.F., Goddard, T.D., Huang, C.C., Couch, G.S., Greenblatt, D.M., Meng, E.C., and Ferrin, T.E. (2004). UCSF Chimera–a visualization system for exploratory research and analysis. J. Comput. Chem. *25*, 1605–1612.

Puddu, F., Granata, M., Di Nola, L., Balestrini, A., Piergiovanni, G., Lazzaro, F., Giannattasio, M., Plevani, P., and Muzi-Falconi, M. (2008). Phosphorylation of the budding yeast 9-1-1 complex is required for Dpb11 function in the full activation of the UV-induced DNA damage checkpoint. Mol. Cell. Biol. *28*, 4782–4793.

Rouse, J., and Jackson, S.P. (2002). Interfaces between the detection, signaling, and repair of DNA damage. Science *297*, 547–551.

Sawicka, M., Wanrooij, P.H., Darbari, V.C., Tannous, E., Hailemariam, S., Bose, D., Makarova, A.V., Burgers, P.M., and Zhang, X. (2016). The dimeric architecture of checkpoint kinases Mec1ATR and Tel1ATM reveal a common structural organization. J. Biol. Chem. *291*, 13436–13447.

Seeber, A., Hegnauer, A.M., Hustedt, N., Deshpande, I., Poli, J., Eglinger, J., Pasero, P., Gut, H., Shinohara, M., Hopfner, K.P., et al. (2016). RPA mediates recruitment of MRX to forks and double-strand breaks to hold sister chromatids together. Mol. Cell *64*, 951–966.

Shiloh, Y., and Ziv, Y. (2013). The ATM protein kinase: regulating the cellular response to genotoxic stress, and more. Nat. Rev. Mol. Cell Biol. *14*, 197–210.

Soustelle, C., Vedel, M., Kolodner, R., and Nicolas, A. (2002). Replication protein A is required for meiotic recombination in Saccharomyces cerevisiae. Genetics *161*, 535–547.

Tang, G., Peng, L., Baldwin, P.R., Mann, D.S., Jiang, W., Rees, I., and Ludtke, S.J. (2007). EMAN2: an extensible image processing suite for electron microscopy. J. Struct. Biol. *157*, 38–46.

Terwilliger, T.C., Adams, P.D., Read, R.J., McCoy, A.J., Moriarty, N.W., Grosse-Kunstleve, R.W., Afonine, P.V., Zwart, P.H., and Hung, L.W. (2009). Decision-making in structure solution using Bayesian estimates of map quality: the PHENIX AutoSol wizard. Acta Crystallogr. D Biol. Crystallogr. *65*, 582–601.

Toledo, L.I., Murga, M., Gutierrez-Martinez, P., Soria, R., and Fernandez-Capetillo, O. (2008). ATR signaling can drive cells into senescence in the absence of DNA breaks. Genes Dev. *22*, 297–302.

Umezu, K., Sugawara, N., Chen, C., Haber, J.E., and Kolodner, R.D. (1998). Genetic analysis of yeast RPA1 reveals its multiple functions in DNA metabolism. Genetics *148*, 989–1005.

Unsal-Kaçmaz, K., and Sancar, A. (2004). Quaternary structure of ATR and effects of ATRIP and replication protein A on its DNA binding and kinase activities. Mol. Cell. Biol. *24*, 1292–1300.

Wakayama, T., Kondo, T., Ando, S., Matsumoto, K., and Sugimoto, K. (2001). Pie1, a protein interacting with Mec1, controls cell growth and checkpoint responses in Saccharomyces cerevisiae. Mol. Cell. Biol. *21*, 755–764.

Wang, F., Li, G., Altaf, M., Lu, C., Currie, M.A., Johnson, A., and Moazed, D. (2013). Heterochromatin protein Sir3 induces contacts between the amino terminus of histone H4 and nucleosomal DNA. Proc. Natl. Acad. Sci. USA *110*, 8495–8500.

Xu, X., Vaithiyalingam, S., Glick, G.G., Mordes, D.A., Chazin, W.J., and Cortez, D. (2008). The basic cleft of RPA70N binds multiple checkpoint proteins, including RAD9, to regulate ATR signaling. Mol. Cell. Biol. *28*, 7345–7353.

Yang, Z., Fang, J., Chittuluru, J., Asturias, F.J., and Penczek, P.A. (2012). Iterative stable alignment and clustering of 2D transmission electron microscope images. Structure *20*, 237–247.

Zhao, X., Muller, E.G., and Rothstein, R. (1998). A suppressor of two essential checkpoint genes identifies a novel protein that negatively affects dNTP pools. Mol. Cell *2*, 329–340.

Zhou, C., Pourmal, S., and Pavletich, N.P. (2015). Dna2 nuclease-helicase structure, mechanism and regulation by Rpa. eLife *4*, e09832.

Zou, L., and Elledge, S.J. (2003). Sensing DNA damage through ATRIP recognition of RPA-ssDNA complexes. Science *300*, 1542–1548.

STAR★METHODS

KEY RESOURCES TABLE

REAGENT or RESOURCE	SOURCE	IDENTIFIER
Antibodies		
Anti-Rad53	Santa Cruz	Cat#sc-6749; RRID: AB_668092
Anti-actin	Millipore	Cat#MAB1501; RRID: AB_2223041
Anti-GFP	Roche	Cat#11814460001; RRID: AB_390913
Anti-GFP	Santa Cruz	Cat#sc-8334; RRID: AB_641123
Anti-phospho-Ser122-Rfa2	Rockland	Cat#600-401-447; RRID: AB_217960
Anti-phospho-Ser129-H2A	Sigma-Aldrich	SG-2397 (custom made); N/A
Anti-Mec1	SDIX	Q5230 (custom made); N/A
Anti-Rfa1	Agrisera	Cat#AS07 214, RRID: AB_1031803
Anti-PK	Acris	Cat#SM1691; RRID: AB_1621125
Bacterial and Virus Strains		
E.coli BL21 (DE3)	NEB	Cat#C2527H
E.coli B834 (DE3)	Novagen	Cat#69041
DH10Bac	Thermo Scientific	Cat#10361012
Chemicals, Peptides, and Recombinant Proteins		
Hydroxyurea	USBiological	Cat#H9120
4-NQO	Sigma-Aldrich	Cat#N8141
Methyl methanesulfonate	Sigma-Aldrich	Cat#129925
Alpha-factor mating pheromone	Zymo Research	Cat#Y1001
Critical Commercial Assays		
SelenoMethionine Medium Complete	Molecular Dimensions	Cat#MD12-500
In-Fusion HD Cloning kit	Clontech	Cat#639650
Deposited Data		
$Ddc2^{N}$-$Rfa1^{N}$ crystal structure	This paper	PDB: 5OMB
$Ddc2^{N}$-$rfa1^{N}$-t11 crystal structure	This paper	PDB: 5OMC
Sc$Ddc2^{CCD}$ crystal structure	This paper	PDB: 5OMD
ssDNA-RPA crystal structure	Fan and Pavletich, 2012	PDB: 4GNX
Nucleosome crystal structure	Wang et al., 2013	PDB: 4JJN
Rfa2 winged helix crystal structure	Feldkamp et al., 2014	PDB: 4OU0
9-1-1 crystal structure	Dore et al., 2009	PDB: 3G65
$(Mec1\text{-}Ddc2)_2$ negative-stain EM	Sawicka et al., 2016	EMDB-4085
Raw fluorescence microscopy images	This paper	https://doi.org/10.17632/shzvjjbht8.1 https://doi.org/10.17632/83p9gjhggs.1 https://doi.org/10.17632/g5tzf37v28.1 https://doi.org/10.17632/jpkhhywwhx.1
Raw data for gels, blots and EM images	This paper	https://doi.org/10.17632/48xj5b2g86.1
Experimental Models: Cell Lines		
GIBCO *Sf*9 cells	Thermo Scientific	Cat#11496015
Experimental Models: Organisms/Strains		
S. cerevisiae: Strain background: W303	Hannah Klein Laboratory	HKY579-10A
Recombinant DNA		
pOPINF vector	Addgene	Cat#26042
pAC8 vector	Nicolas H. Thomae Laboratory	N/A

(*Continued on next page*)

Continued

REAGENT or RESOURCE	SOURCE	IDENTIFIER
Software and Algorithms		
XDS	Kabsch, 2010	http://xds.mpimf-heidelberg.mpg.de/
PHENIX AutoSol	Phenix software suite	https://www.phenix-online.org/
PHASER	Phenix software suite	https://www.phenix-online.org/
BUCCANEER	CCP4 software suite	http://www.ccp4.ac.uk/
COOT	Emsley et al., 2010	https://www2.mrc-lmb.cam.ac.uk/personal/pemsley/coot/
BUSTER	Bricogne, 2011	https://www.globalphasing.com/buster/
Molprobity	Chen et al., 2010	http://molprobity.biochem.duke.edu/
PyMOL	Open source	http://www.pymol.org/
ASTRA v6.1	Wyatt Technology	
NT.Analysis software v1.5.41	NanoTemper Technologies	
GraphPad Prism v6.01	GraphPad Software, Inc.	https://www.graphpad.com/scientific-software/prism/
VisiView	Visitron Systems	http://www.visitron.de/Products/Software/VisiView/visiview.html
EMAN2	Tang et al., 2007	http://blake.bcm.edu/emanwiki/EMAN2
SPARX	Hohn et al., 2007	http://sparx-em.org/sparxwiki/
UCSF Chimera	Pettersen et al., 2004	https://www.cgl.ucsf.edu/chimera/
Fiji ImageJ 1.51j	Open source	https://imagej.nih.gov/ij/

CONTACT FOR REAGENT AND RESOURCE SHARING

Further information and requests for resources and reagents should be directed to and will be fulfilled by the Lead Contact, Susan M. Gasser (susan.gasser@fmi.ch).

METHOD DETAILS

Protein engineering and purification from *E. coli*

*Kl*Ddc2^{N} (residues 1-109) from *K. lactis*; and *Sc*Ddc2^{N} (residues 1-136), *Sc*Ddc2^{CCD} (residues 73-136), Rfa1^{N} (residues 1-132), Rfa1^{N}-t11 (residues 1-132; K45E), Rfa1^{N} KREK (residues 1-132; K58A, R62A, E86A, K95A) from *S. cerevisiae* were separately cloned into pOPINF vectors using the In-Fusion system (Clontech) (Berrow et al., 2007) and individually expressed in *E. coli* BL21(DE3). Cells expressing appropriate target were pelleted, resuspended in lysis buffer (50 mM Tris-HCl, pH 7.5, 500 mM NaCl, 20 mM imidazole, 0.2% Tween-20) then rapidly frozen on dry-ice and stored at −80°C. The frozen cell suspension was thawed at room temperature and supplemented with complete EDTA-free Protease Inhibitor Cocktail (Roche) and Benzonase (Sigma) before sonication. The lysate was clarified by ultracentrifugation and then affinity purified via an N-terminal His6 tag using Ni-NTA Superflow resin (QIAGEN). His-tag was removed using His-tagged 3C protease and a second round of affinity purification. Lastly, target was purified using a Superdex 75 HiLoad 16/60 (GE Healthcare) column equilibrated in 20 mM Tris-HCl, pH 7.5, 150 mM NaCl, 1 mM TCEP, 0.02% NaN_3. Only in the case of Ddc2^{N}, anion exchange purification was done using a HiTrap Capto Q (GE Healthcare) column before size exclusion chromatography. Incorporation of seleno-methionine was performed with *E. coli* B834(DE3) as described by Molecular Dimensions' seleno-methionine media kit.

Protein engineering and purification from *Sf*9

Sir3wH-Ddc2 (*Kl*Ddc2 lacking residues 115-127 N-terminally fused to *Sc*Sir3 winged helix dimerization domain residues 840-978) and Mec1^{N} (*Kl*Mec1 residues 1-341 N-terminally tagged with Strep-II) were cloned into separate pAC-derived vectors (Abdulrahman et al., 2009). Recombinant baculoviruses were prepared using the *flash*BAC system. The Sir3wH-Ddc2-Mec1^{N} complex was expressed in *Sf*9 insect cells by co-infection of separate baculoviruses encoding Sir3wH-Ddc2 and Strep (II) tagged Mec1^{N}. Cells expressing appropriate target(s) were lysed in 50 mM Tris-HCl, pH 8.0, 150 mM NaCl, 2 mM $MgCl_2$, 2 mM TCEP, 0.2% Tween-20 freshly supplemented with complete EDTA-free Protease Inhibitor Cocktail (Roche) and Benzonase (Sigma). Following ultracentrifugation, target was extracted by Strep-Tactin Sepharose (IBA) affinity chromatography. The target was removed by overnight TEV protease treatment. The protein was then separated by a HiTrap Capto Q (GE Healthcare) anion-exchange column and lastly subjected to size exclusion chromatography on a Superdex 200 HiLoad 16/600 (GE Healthcare) column equilibrated in 20 mM Tris-HCl, pH 8.0, 150 mM NaCl and 1 mM TCEP.

Crystallization

Nanoliter crystallization experiments were performed with a Phoenix dispensing robot (Art Robbins) using the sitting-drop vapor diffusion method at 20°C. Ddc2^{N}-Rfa1^{N} co-crystals were obtained by mixing 1 mM *K*lDdc2^{N} and 1.2 mM seleno-methionine labeled *Sc*Rfa1^{N} at 4°C for 30 min and later at 20°C for 3 days in the presence of 0.2 M ammonium citrate tribasic pH 7.0 and 20% PEG 3350. Crystals were harvested and flash cooled in liquid nitrogen after cryoprotection with 20% ethylene glycol, 0.2 M ammonium citrate tribasic pH 7.0 and 20% PEG 3350. Ddc2^{N}-Rfa1^{N}-t11 co-crystals were obtained by mixing 1 mM *K*lDdc2^{N} and 1.2 mM *Sc*Rfa1^{N}-t11 at 4°C for 30 min and later at 20°C for 3 days in the presence of 0.2 M lithium sulfate monohydrate, 0.1 M Bis-Tris, pH 6.5 and 25% PEG 3350, were harvested and flash cooled in liquid nitrogen after cryoprotection with 18% ethylene glycol, 0.2 M lithium sulfate monohydrate, 0.1 M Bis-Tris, pH 6.5 and 25% PEG 3350. *Sc*Ddc2^{CCD} crystals, obtained in 5 days after mixing 0.5 mM *Sc*Ddc2^{CCD} with 0.1 M Tris-HCl, pH 8.5 and 24% PEG 400, were harvested and flash cooled in liquid nitrogen after cryoprotection with 25% ethylene glycol, 0.1 M Tris-HCl, pH 8.5 and 24% PEG 400.

Data collection and structure determination

Diffraction data were collected at the Swiss Light Source (Villigen, Switzerland) beamlines X06DA using a Pilatus 2M-F detector (Dectris) and X10SA using a Pilatus 6M detector. Ddc2^{N}-Rfa1^{N} and Ddc2^{N}-Rfa1^{N}-t11 co-crystals belonged to space group $P2_12_12_1$ (four chains per a.u. in both cases) and diffracted to 1.9 Å (λ_{peak} = 0.979 Å) and 2.4 Å (λ = 1.000 Å). *Sc*Ddc2^{CCD} crystallized in space group $P2\ 2\ 2_1$ (one chain per a.u.) and diffracted to 2.1 Å (λ = 1.000 Å). For all projects, diffraction data were integrated and scaled using the XDS program package (Kabsch, 2010). The structure of Ddc2^{N}-Rfa1^{N} was solved by single anomalous dispersion method using four seleno-methionine sites per molecule of Rfa1^{N} for phase calculation in PHENIX AutoSol (Terwilliger et al., 2009). Ddc2^{N}-Rfa1^{N}-t11 and *Sc*Ddc2^{CCD} structures were solved by the molecular replacement method with PHASER (McCoy et al., 2007) using Ddc2^{N}-Rfa1^{N} and PDB: 1A92 as search models, respectively. For all projects, phases were then used for automatic model building in PHENIX (Adams et al., 2011) and BUCCANEER (Cowtan, 2006) followed by manual completion of the model using COOT (Emsley et al., 2010). The structures were refined by the crystallographic simulated annealing routine followed by individual B-factor refinement in PHENIX and further rounds of manual rebuilding in COOT and refinement in BUSTER (Bricogne, 2011). The final structures were validated using Molprobity (Chen et al., 2010) and COOT. Structural images for figures were prepared with PyMOL (http://www.pymol.org/).

Molecular mass measurement by SEC-MALS

Purified *Sc*Ddc2^{N} and *Sc*Ddc2^{CCD} were concentrated up to 300 μM and 260 μM respectively, and filtered through a 0.1 μm Amicon filter before injection. 38 μL of each protein was separated on a Superdex 200 10/300 GL gel-filtration column (GE Healthcare) equilibrated in 20 mM Tris, pH 7.5, 200 mM NaCl, 1 mM TCEP, 0.02% NaN_3 at a flow rate of 0.65 mL/min. Light scattering was recorded on an in-line miniDAWN TREOS three-angle light scattering detector (Wyatt Technology) and protein concentration detected with an in-line Optilab Trex refractive index detector. The weight-averaged molecular mass of material contained in chromatographic peaks was determined using ASTRA 6 software (Wyatt Technology).

Microscale thermophoresis

Experiments were carried out in 20 mM Tris-HCl buffer, pH 8.0, containing 150 mM NaCl, 0.05% Tween-20 and 0.5 mg/ml BSA. Purified Rfa1^{N}, Rfa1^{N}-t11, Rfa1^{N} KREK and N-terminal Cy5-labeled peptides of *S. cerevisiae* Ddc2 (^{7}-GEFSSDDDDDILLELGTRPPR-^{27}) and Dna2 (^{355}-SSDEFSDDSLIELLNETQ-^{372}) (JPT Peptide Technologies, Berlin, Germany) were centrifuged at 13,200 *g* for 5 min at room temperature prior to the assays. A dilution series of Rfa1 proteins yielding different protein concentrations starting from 0.6 nM to 2000 μM was mixed separately with labeled Ddc2 or Dna2 peptide at a fixed concentration of 0.5 μM. After 15 min incubation at room temperature, followed by centrifugation at 5,000 *g* for 5 min, approximately 4 μL of each solution was filled into Monolith NT Premium Coated Capillaries (NanoTemper Technologies GmbH). Thermophoresis was measured using a Monolith NT.115 instrument (NanoTemper Technologies GmbH) at 23°C with 5 s/30 s/5 s laser off/on/off times, respectively. Instrument parameters were adjusted to 1%–20% LED power and 20% MST power. Data of three independently pipetted measurements were analyzed (NT.Analysis software version 1.5.41, NanoTemper Technologies GmbH) using the signal from thermophoresis and plotted using GraphPad Prism version 6.01 (La Jolla, CA, USA).

Immunoprecipitation and western blotting

Yeast strains are described in Table S1. If not stated otherwise, cells were cultured at 30°C in YPAD medium using standard procedures. For anti-GFP IP, 100 mL of log-phase culture was harvested by centrifugation, washed once with cold phosphate buffered saline, and snap-frozen in liquid nitrogen. The pellet was resuspended in IP buffer (50 mM HEPES pH 7.4, 150 mM NaCl, 2 mM EDTA, 0.5% NP-40) supplemented with Complete Protease Inhibitor and PhosSTOP tablets (Roche). In anti-GFP IP experiments to check RPA interaction, Benzonase nuclease was also added to the IP buffer. Cells were mechanically lysed by bead beating and the lysate was mixed with anti-GFP antibody (Roche Cat#11814460001) crosslinked to Dynabeads Protein G. Binding reaction was carried out at 4°C for 1.5 hr. After washing thrice with IP buffer, bound proteins were eluted with 0.2 M Glycine pH 1.9 and analyzed by western blotting. Anti-GFP antibody (Santa Cruz Cat#sc-8334) was used for western blots.

For western blot experiments, log-phase cultures were arrested in the G1 phase using alpha-factor mating pheromone for 80 min. Cultures were then mock treated or treated with DNA damaging agents. Cells were harvested at different time points and protein samples were prepared by NaOH/Trichloroacetic acid precipitation. Samples were resuspended in 50 μL of NuPAGE sample buffer supplemented with 50 mM DTT. Samples were boiled, electrophoresed by SDS-PAGE, and then transferred to PVDF membranes. The membranes were blocked with TBST (20 mM Tris-HCl, pH 7.5, 150 mM NaCl, 0.1% Tween 20) containing 5% BSA or 5% nonfat dried milk, and probed overnight with primary antibodies, followed by 1 hr incubation with secondary antibodies coupled to peroxidase. Blots were developed by using enhanced chemiluminescence.

Yeast drop assays

Overnight cultures of yeast cells were adjusted to OD_{600} of 0.1 and serially diluted 5-fold up to six dilutions. 2.5 μL of cells were dropped onto YPAD plates with or without DNA damaging agents and allowed to grow for two days at 30°C before taking photographs.

Fluorescence microscopy

Cells were grown in synthetic complete (SC) media (Formedium DSCK1000) complemented with all amino acids and with 4x additional adenine (72 mg/L) to prevent autofluorescence. In addition, cells were transformed with plasmid pRS402 #1388 conveying the ADE2 gene to reduce autofluorescence. To induce UV damage, 5 mL log phase culture was pelleted and resuspended in 200 μL of fresh SC media, spread on a YPAD plate and left for 5 min to dry. Cells were exposed to 100 J/m^2 UV using a Stratagene UV Stratalinker 2400. Following this, cells were washed off the YPAD plate and suspended in fresh SC media. Cells were fixed in fresh paraformaldehyde (PFA) 4% w/v for 5 min, washed six times in PBS and then attached to a 0.17 mm glass coverslip using Concanavalin A. Fixed cells were stained with DAPI by suspending the cells in a DAPI-PBS solution of 50 ng/mL DAPI for 30 min and then washed in PBS three times. Cells were imaged on a Nikon Eclipse Ti microscope, an EM-CCD Cascade II (Photometrics) camera, an ASI MS-2000 Z-piezo stage, and a PlanApo × 100, numerical aperture (NA) 1.45 total internal reflection fluorescence microscope oil objective and Visiview software. RFP was excited using a Coherent Sapphire 561 nm, 200 mW laser. GFP and DAPI were excited with Toptica iBEAM SMART 488 nm and 405 nm lasers, respectively. Brightfield images were acquired with a Lumencore Sola SM II LED light engine.

Negative-stain electron microscopy

0.02 mg/mL of Sir3wH-Ddc2-$Mec1^N$ in 20 mM Tris-HCl, pH 8.0, 150 mM NaCl, 1 mM TCEP was used for adsorption on glow-discharged Quantifoil grids (S7/2, Cu 400 mesh, Quantifoil Micro Tools GmbH, Grosslöbichau, Germany) coated with a continuous thin carbon film floated from mica. Samples (4 μL) were applied to the grids and, after blotting, negatively stained with 2% (w/v) uranyl acetate. Data were acquired with a Philips CM200FEG transmission electron microscope in low-dose mode operated at 200 keV. Images were recorded with a TVIPS F416 camera at a nominal magnification of × 50,000, resulting in a pixel size of 2.2 Å at the specimen level. Images were recorded by varying the defocus between −1.5 and −3.0 μm. 7,535 particles were picked using e2boxer.py (EMAN2) (Tang et al., 2007). Contrast transfer function parameters were calculated using sxcter.py (SPARX) (Hohn et al., 2007) and reference-free 2D class averages were generated using the Iterative Stable Alignment and Clustering (ISAC) method in SPARX (Yang et al., 2012).

Modeling structural assemblies

Composite structural models were assembled using crystal structures of the ssDNA-RPA complex (PDB: 4GNX), nucleosome core particle (PDB: 4JJN), Rfa2 winged helix (wH) domain (PDB: 4OU0), the 9-1-1 complex (PDB: 3G65), negative-stain EM map of $(Mec1\text{-}Ddc2)_2$ (EMDB-4085) and homology models of Dpb11 BRCT domains based on closest structural homologs of known structures identified in HHpred searches (PDB: 1L7B, 3L46, 3UEN, 4BMD). The $(Mec1\text{-}Ddc2)_2$ EM map was segmented along the 2-fold symmetry axis to highlight its homodimeric state using the Segger tool in UCSF Chimera (Pettersen et al., 2004). All composite structural models were assembled using PyMOL.

QUANTIFICATION AND STATISTICAL ANALYSES

MST binding assay

Data are represented as mean ± SEM of three independent experiments. Data were analyzed by NT.Analysis software version 1.5.41 (NanoTemper Technologies GmbH) and the dissociation constant (K_d) was calculated using GraphPad Prism version 6.01 (La Jolla, CA, USA). The details of the analysis are described in figure legends.

Immunoblots

Intensity calculation of immunoblots was done using Fiji image processing package. The band areas were boxed and backgrounds were subtracted. The bands of target protein were normalized to an appropriate loading control. Data are represented as mean ± SD from independent replicates. The details are described in figure legends.

Fluorescence microscopy

Fluorescence images were deconvolved using Huygens professional and the classic maximum likelihood estimate algorithm with a signal/noise ratio of 10, automatic background estimation and 40 iterations. For foci number quantification, Z stacks were obtained by taking 35 slices at 200 nm intervals. The EMCCD gain was set to 800 in all cases except to the brightfield were it was set to 1. Exposure times were: 30 ms DAPI, 100 ms GFP, 100 ms RFP, 10 ms brightfield. "Bright foci" were counted and defined as foci that have clear borders. Thresholding was applied in Fiji to help see foci over background nuclear signal. At least 100 cells were counted per replicate. Data are represented as mean ± SD from three independent replicates. The details of statistical analysis are described in figure legends.

DATA AND SOFTWARE AVAILABILITY

Accession Numbers

The accession numbers for the crystal structures reported in this paper are PDB: 5OMB ($Ddc2^{N}$-$Rfa1^{N}$), 5OMC ($Ddc2^{N}$-$Rfa1^{N}$-t11) and 5OMD (ScDdc2^{CCD}).

Original data used to generate any of the figure panels have been deposited at Mendeley:
https://doi.org/10.17632/shzvjjbht8.1
https://doi.org/10.17632/83p9gjhggs.1
https://doi.org/10.17632/g5tzf37v28.1
https://doi.org/10.17632/jpkhhywwhx.1
https://doi.org/10.17632/48xj5b2g86.1

Figure S1 (related to Figure 1)

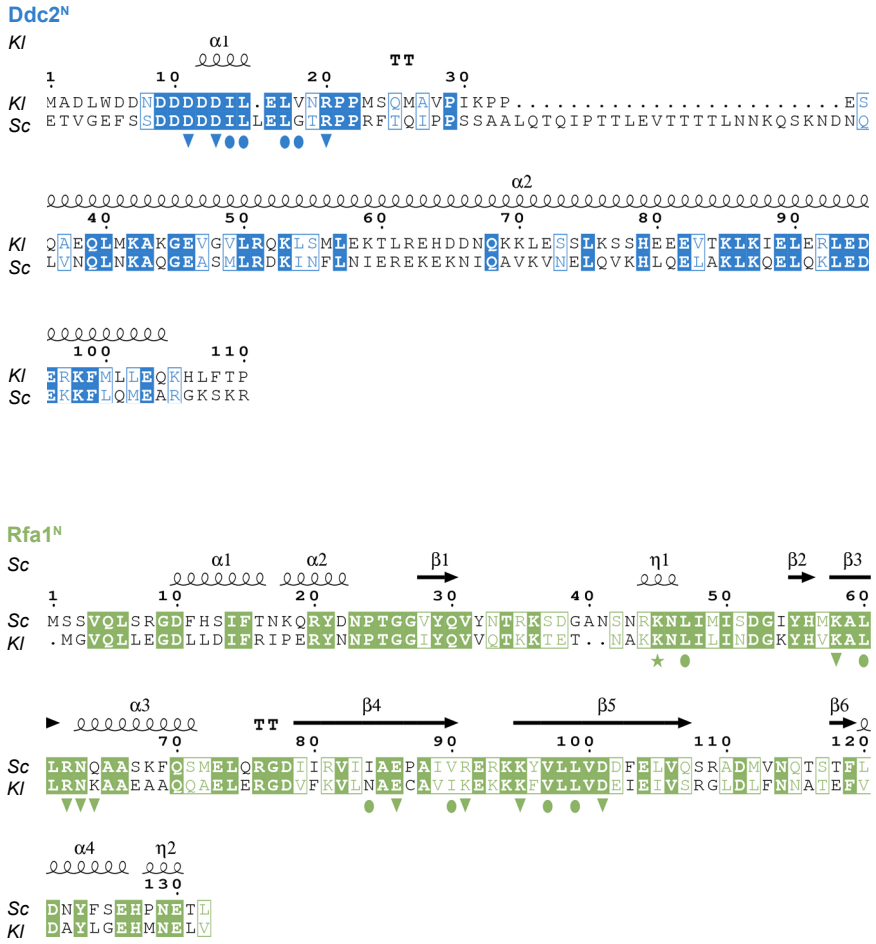

Figure S1: Pairwise sequence alignments of Ddc2^N and Rfa1^N (See also Figure 1)

Identical residues of Ddc2^N and Rfa1^N are colored in blue and green respectively. Highly conserved residues are bordered. Numbers on top of the alignment refer to the *K. lactis* protein sequence. Secondary structure elements present in the Ddc2^N-Rfa1^N crystal structure (see also Figure 1B) are indicated on top of the alignment (α, α-helix; β, β-strand; TT, turn; η, 3.10 helix). Polar (inverted triangles) and hydrophobic (oval) residues of the Ddc2^N-Rfa1^N interface are highlighted. K45, the residue mutated in *rfa1-t11*, is indicated by a star. *Sc*: *Saccharomyces cerevisiae*; *Kl*: *Kluyveromyces lactis*.

Figure S2 (related to Figure 2)

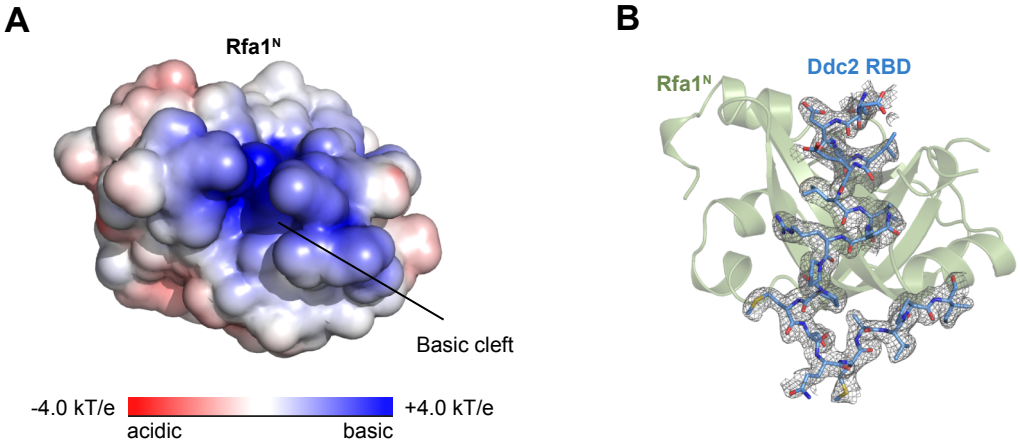

Figure S2: Ddc2^{N} binds the Rfa1^{N} basic-hydrophobic cleft (See also Figure 2)

A) Rfa1^{N} is displayed as a surface and colored according to the surface electrostatic potential, ranging from blue (basic) to red (acidic). Hydrophobic surface patches are shown in white. Surface electrostatic potential was computed using the APBS plug-in implemented in PyMOL (www.pymol.org).

B) Detailed view of the binding of Ddc2 RBD to Rfa1^{N} present in the Ddc2^{N}-Rfa1^{N} crystal structure (see also Figure 2B). Rfa1^{N} is displayed as a green cartoon model whereas Ddc2 RBD is shown as sticks (blue, atom colors). A composite simulated annealing $2mF_o$-DF_c omit electron density map contoured at 0.8 σ is displayed in gray.

Figure S3 (related to Figure 3)

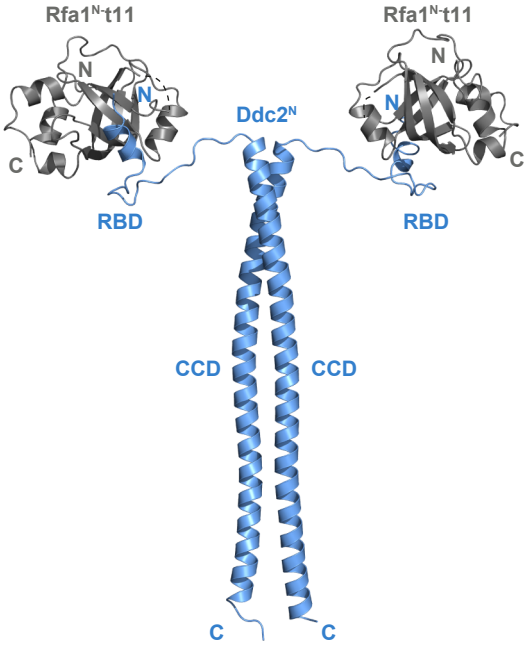

Figure S3: Crystal structure of Ddc2^{N}-Rfa1^{N}-t11 (See also Figure 3)

Crystal structure of the Ddc2^{N}-Rfa1^{N}-t11 complex in cartoon representation; Rfa1^{N}-t11 is colored in gray and Ddc2^{N} is colored in blue. Two loops lacking electron density due to flexibility are indicated by dashed lines. The RBD and the CCD are labeled.

Figure S4 (related to Figure 3)

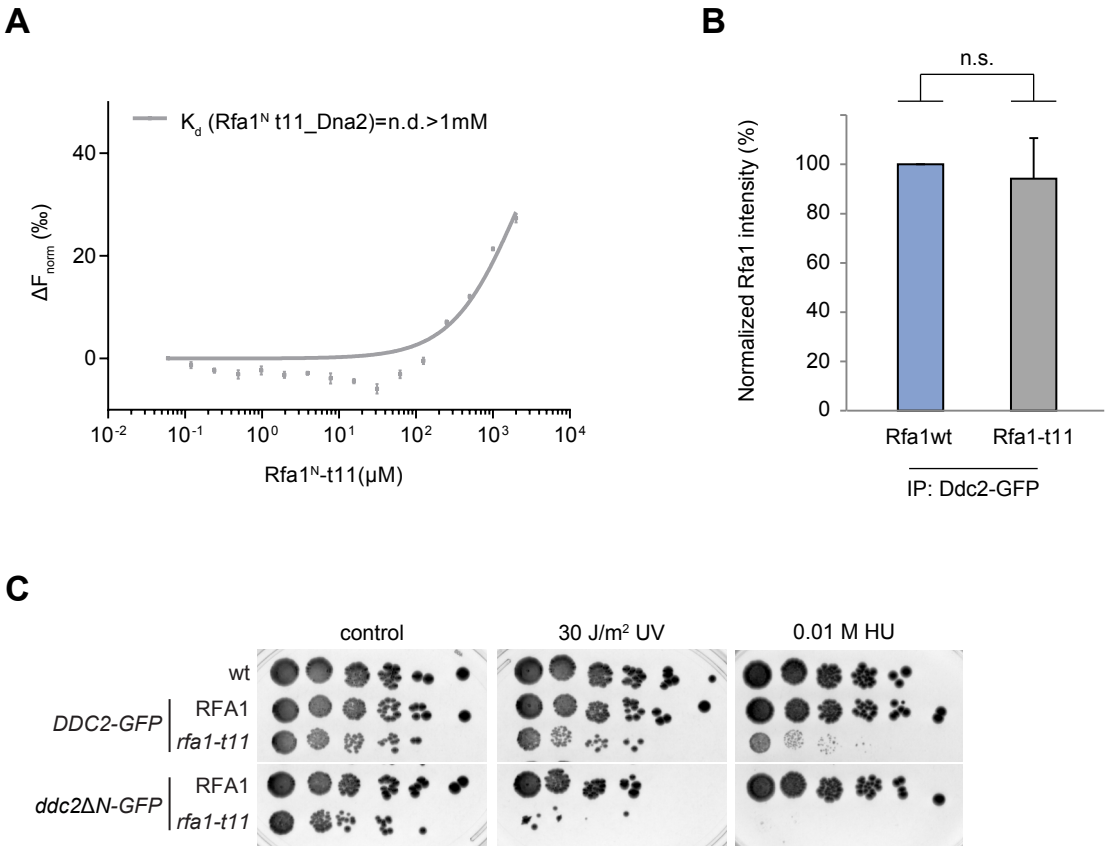

Figure S4: Ddc2 can bind the Rfa1-t11 mutant protein (See also Figure 3)

A) MST analysis of binding of Cy5-labeled *Sc*Dna2 RBD and *Sc*Rfa1^{N}-t11. K_d represents dissociation constant. ΔF_{norm} (‰) represents change in fluorescence during thermophoresis normalized to initial fluorescence. n.d. means not detectable (>1mM). Data are represented as mean ± SEM from three independent measurements.

B) Quantification of the intensities of Rfa1 wt and Rfa1-t11 bands normalized to the intensities of Ddc2-GFP bands after immunoprecipitation with Ddc2-GFP using an anti-GFP antibody. Data are represented as mean ± SD from three independent experiments. n.s. = not significant.

C) A 5-fold dilution series of isogenic strains GA-1981, 9827/8, 9835/6 (see also Table S1) on YPAD plates without or with 30 J/m^2 UV or 0.01 M HU. Plates were incubated at 30°C for two days.

Figure S5 (related to Figure 4)

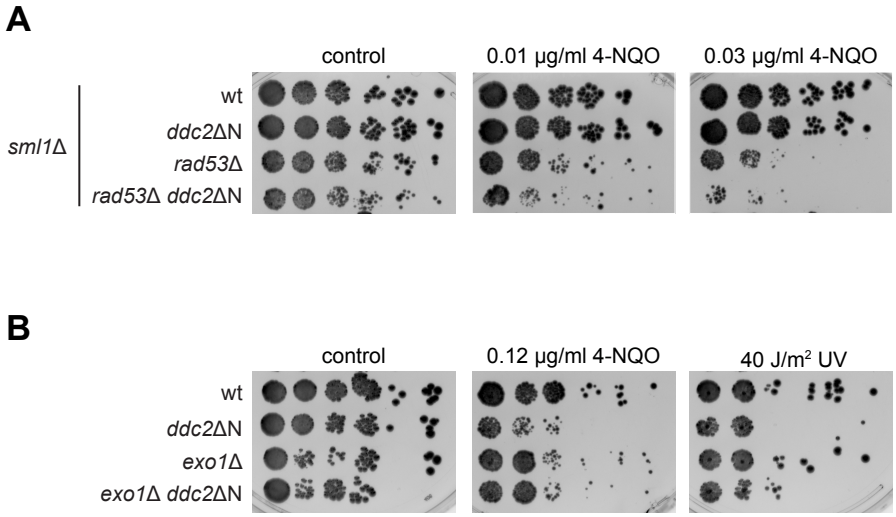

Figure S5: *ddc2*ΔN is additive with *rad53*Δ but epistatic with *exo1*Δ (See also Figure 4)

A) A 5-fold dilution series of isogenic strains GA-7371, 8891, 7373 and 10070 (see also Table S1) on YPAD plates without or with 0.01 µg/ml 4-NQO or 0.03 µg/ml 4-NQO. Plates were incubated at 30°C for two days.

B) A 5-fold dilution series of isogenic strains GA-1981, 6354, 9479 and 9970 (see also Table S1) on YPAD plates without or with 0.12 µg/ml 4-NQO or 40 J/m^2 UV. Plates were incubated at 30°C for two days.

Figure S6 (related to Figure 6)

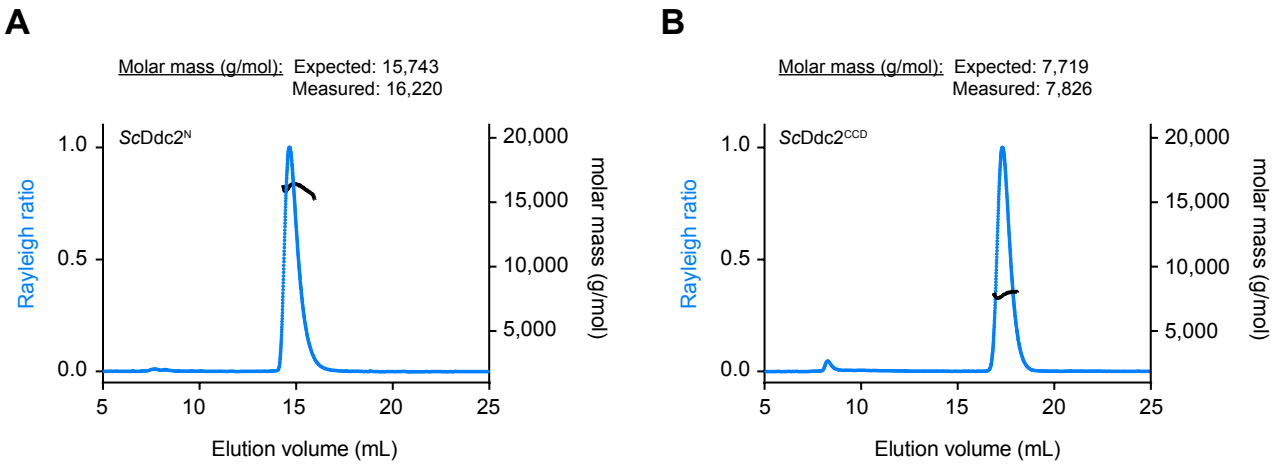

Figure S6: *Sc*Ddc2^{N} and *Sc*Ddc2^{CCD} are monomeric in solution (See also Figure 6)

Size-exclusion chromatography coupled with multi-angle light scattering (SEC-MALS) analysis of *Sc*Ddc2^{N} and *Sc*Ddc2^{CCD}. The Rayleigh ratio is indicated by the blue trace and the molar mass is shown by the black line. Experiments were performed in a buffer containing 150 to 200 mM NaCl.

A) The measured molar mass for monomeric *Sc*Ddc2^{N} (16.22 kDa) was calculated over peak fractions covering the elution volume 14.3 ml to 16 ml, which represent a monodisperse sample (polydispersity = 1.000).

B) The measured molar mass for monomeric *Sc*Ddc2^{CCD} (7.83 kDa) was calculated over peak fractions covering the elution volume 16.9 ml to 18.1 ml, which represent a monodisperse sample (polydispersity = 1.000).

Figure S7 (related to Figure 7)

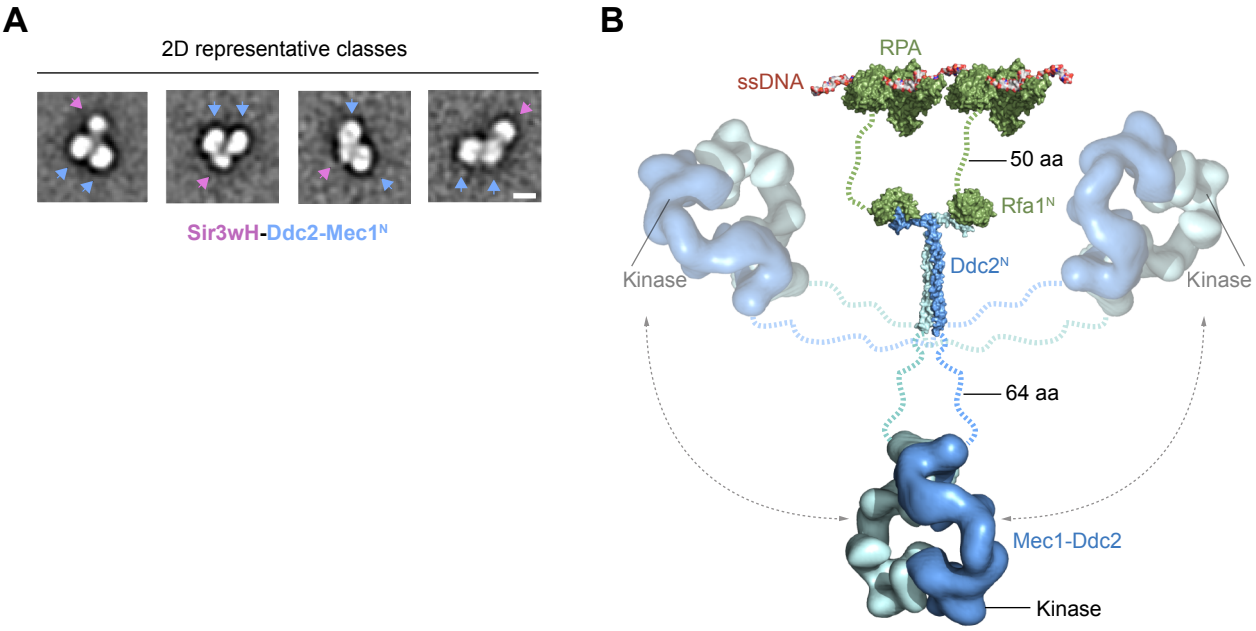

Figure S7: To-scale model of Mec1-Ddc2-RPA-ssDNA assembly (See also Figure 7)

A) Representative 2D class averages of Sir3wH-Ddc2-Mec1^N generated by SPARX. Pink arrows indicate Sir3wH homodimers linked to Ddc2; blue arrows indicate Ddc2-Mec1^N. Bar = 10 nm. Sir3wH-Ddc2-Mec1^N was purified from *Sf*9 cells and 0.02 mg/ml of pure protein was stained with 2% (w/v) uranyl acetate. 300 micrographs were collected and 7,535 particles were subjected to 2D classification.

B) Surface representation of the Mec1-Ddc2-RPA-ssDNA composite structural model assembled by combining the following structures: Crystal structure of an ssDNA-RPA complex lacking Rfa2wH and Rfa1^N - PDB ID: 4GNX; negative-stain EM map of $(Mec1\text{-}Ddc2)_2$ - EMD-4085; and crystal structure of the Ddc2^N-Rfa1^N complex - this study. RPA lacking Rfa2wH is shown as green surface. ssDNA is shown as red and white surface. The $(Mec1\text{-}Ddc2)_2$ EM map is segmented along the two-fold symmetry axis to highlight its homodimeric state. One Mec1-Ddc2 heterodimer is displayed in blue, while the other Mec1-Ddc2 heterodimer is displayed in cyan. Unstructured linkers are represented by dashed lines; aa represents amino acid residues. The putative conformational freedom of $(Mec1\text{-}Ddc2)_2$ owing to its flexible linkers is highlighted by two representatives of an ensemble which are displayed with transparent surfaces. The kinase domain is labeled.

Table S1: Yeast strains used in this study (Related to Figures 3, 4, 5, 6, S4C and S5)

strain	genotype	source
GA-1981	*MATa, ade2-1 ,trp1-1 ,his3-11 , -15, ura3-1, leu2-3, -112, can1-100* (W303), *RAD5*	H.L. Klein
GA-1982	*MATα, ade2-1 ,trp1-1 ,his3-11, -15, ura3-1, leu2-3, -112, can1-100* (W303), *RAD5*	H.L. Klein
GA-4968	*GA-1981 with rfa1-t11*	Seeber et al., 2016
GA-6354	*GA-1981 with exo1::Kan*	this study
GA-6905	*GA-1981 with rad26::NAT*	H.L. Klein
GA-6909	*GA-1981 with rad16::NAT*	H.L. Klein
GA-7371	*GA-1981 with sml1::Kan*	Hustedt et al. 2015
GA-7373	*GA-1981 with sml1::Kan, rad53::URA3*	Hustedt et al. 2015
GA-8163	*GA-1981 with tel1::HIS3*	this study
GA-8705	*GA-1981 with ddc2::DDC2-GFP-Kan, RFA1-RFP-HIS3*	Hustedt et al. 2015
GA-8891	*GA-1981 with sml1::Kan, ddc2::ddc2ΔN*	this study
GA-9149	*GA-1981 with ddc2::DDC2-GFP-HIS3, sml1::Kan*	this study
GA-9417	*GA-1981 with ddc2::ddc2ΔN, tel1::URA3*	this study
GA-9479	*GA-1981 with ddc2::ddc2ΔN*	this study
GA-9480	*GA-1981 with ddc2::ddc2ΔRBD*	this study
GA-9482	*GA-1981 with ddc2::ddc2ΔRBD, tel1::URA3*	this study
GA-9483	*GA-1981 with ddc2::ddc2ΔCCD*	this study
GA-9485	*GA-1981 with ddc2::ddc2ΔCCD, tel1::URA3*	this study
GA-9487	*GA-1981 with ddc2::ddc2ΔN, rad16::NAT*	this study
GA-9490	*GA-1981 with ddc2::ddc2ΔN, rad26::NAT*	this study
GA-9827	*GA-1981 with ddc2::DDC2-GFP-HIS3*	this study
GA-9828	*GA-1981 with ddc2::DDC2-GFP-HIS3, rfa1-t11*	this study
GA-9835	*GA-1981 with ddc2:: ddc2ΔN-GFP-HIS3*	this study
GA-9836	*GA-1981 with ddc2:: ddc2ΔN-GFP-HIS3, rfa1-t11*	this study
GA-9842	*MATa/MATα, DDC2-PKx9::TRP1/DDC2-GFP-HIS3, W303, RAD5*	this study
GA-9843	*MATa/MATα, ddc2::ddc2ΔN-PKx9::TRP1/ ddc2::ddc2ΔN -GFP-HIS3, W303, RAD5*	this study
GA-9844	*MATa/MATα, ddc2::ddc2ΔRBD-PKx9::TRP1/ ddc2::ddc2ΔRBD -GFP-HIS3, W303, RAD5*	this study
GA-9845	*MATa/MATα, ddc2::ddc2ΔCCD-PKx9::TRP1/ ddc2::ddc2ΔCCD -GFP-HIS3, W303, RAD5*	this study
GA-9846	*MATa/MATα, DDC2-PKx9::TRP1/DDC2, W303, RAD5*	this study
GA-9961	*GA-1981 with ddc2::ddc2ΔRBD-GFP-HIS3, RFA1-RFP-HIS3*	this study
GA-9963	*GA-1981 with ddc2::ddc2ΔCCD-GFP-HIS3, RFA1-RFP-HIS3*	this study
GA-9965	*GA-1981 with ddc2::ddc2ΔN-GFP-HIS3, RFA1-RFP-HIS3*	this study
GA-9970	*GA-1981 with ddc2::ddc2ΔN, exo1::Kan*	this study
GA-9972	*GA-1981 with ddc2::ddc2ΔRBD, exo1::Kan*	this study
GA-9974	*GA-1981 with ddc2::ddc2ΔCCD, exo1::Kan*	this study
GA-10070	*GA-1981 with sml1::Kan, rad53::URA3, ddc2::ddc2ΔN*	this study

Chapter 3:
ATRIP CCD dimerization depends on a predicted helix within the CCD

This chapter provides additional data, which is unpublished.

Summary

The coiled-coil domain (CCD) is a common oligomerization motif that is formed by approximately 10% of all amino acids in the proteome. CCDs consist of two to seven α-helices coiled around each other into a left-handed supercoil that features a heptad repeat of primarily hydrophobic residues. Some CCDs contain short sequences, so-called “trigger” sequences that promote the oligomerization of the entire CCD. The CCD oligomerization of the checkpoint protein ATRIP is not well studied. Using size-exclusion chromatography coupled with multi-angle light scattering (SEC-MALS), we report that the human ATRIP CCD is dimeric in solution, while the CCD of the *S. cerevisiae* ortholog Ddc2 is monomeric in solution. Secondary structure prediction suggests that both the orthologs contain a short N-terminal helix followed by a longer helix. Interestingly, we observed that the short N-terminal helix acts as a trigger sequence and is essential for CCD dimerization in human ATRIP but not yeast Ddc2.

Introduction

Coiled-coils were first described in the early 1950s by Francis Crick and Linus Pauling independently (Crick, 1952; Pauling and Corey, 1953). They noted that α-helices wrap around each other and their side chains pack in a knobs-into-holes manner. Since then, this ubiquitous repeat motif has been extensively studied. A typical coiled-coil consists of a heptad repeat, *abcdefg,* where *a* and *d* represent conserved hydrophobic amino acids, whereas *e* and *g* are solvent-exposed, polar residues (Figure 1). This amphipathic nature drives coiled-coil formation by burying the hydrophobic residues.

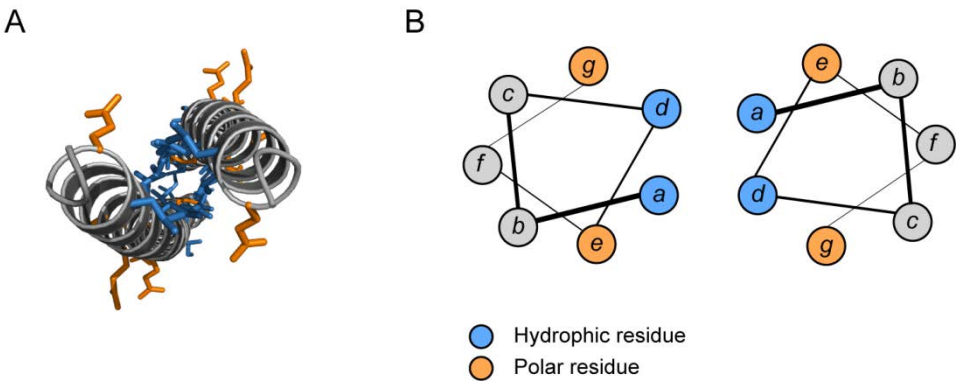

Figure 1: Coiled coil architecture. **(A)** Top view of the crystal structure of *S. cerevisiae* Ddc2 CCD (residues 73-136) (PDB ID: 5OMD, chapter 2) shown as gray cartoon. Hydrophobic residues are shown as blue sticks. Polar residues are shown as orange sticks. **(B)** Wheel diagram showing the heptad repeat in two parallel helices forming a coiled-coil (top view). Amino acid positions *a* and *d* (shown in blue) are occupied by hydrophobic residues and form the hydrophobic core, whereas amino acid positions *e* and *g* (shown in orange) are occupied by polar residues.

CCDs primarily function as oligomerization domains and have been proposed to act as molecular spacers or molecular rulers that either isolate functional domains or scaffold large protein complexes. Examples of such spacers are the 50 nm long outer membrane protein Omp-α CCD, the 110 nm long yeast spindle pole body protein Spc110 CCD, the 50 nm long cohesin CCD, and the 120 nm long DNA damage response protein Rad50 CCD (Engel et al., 1992; Hopfner et al., 2002; Kilmartin et al., 1993; Soh et al., 2015). An interesting feature of several CCDs is the presence of short sequences within the coiled-coil that are necessary for its oligomerization. The so-called “trigger” sequences are believed to form earlier in the folding process and probably act as a seeding event that promotes the oligomerization of the rest of the coiled-coil. Examples of such trigger sequences include the 13-residue autonomous helical folding unit within cortexillin I and GCN4; and a 7-residue sequence within the type I macrophage scavenger receptor (Frank et al., 2000; Kammerer et al., 1998; Steinmetz et al., 1998). Deleting such sequences was shown to prevent proper coiled-coil assembly.

Sequence analysis of the DNA damage response protein ATRIP predicts that residues 110-214 may fold into a CCD (see Results and discussion). Indeed, deletion of the predicted ATRIP CCD in human cells, disrupted ATRIP oligomerization, ATRIP interaction with its obligate partner ATR, and the recruitment of ATR-ATRIP to DNA damage sites (Ball and Cortez, 2005). However, this study did not reveal the degree of oligomerization of ATRIP. Recent structural and biochemical studies of the budding yeast Mec1-Ddc2 (Sawicka et al., 2016) and the Ddc2 N-terminus (see chapter 2) suggest that Ddc2 can exist as both monomer and dimer.

In this chapter, I describe the SEC-MALS analysis of human ATRIP and *S. cerevisiae* Ddc2 CCD. Our results suggest that the human ATRIP CCD contains a trigger sequence which is important for CCD dimerization.

Results and discussion

Sequence analysis using PCOILS (https://toolkit.tuebingen.mpg.de/#/tools/pcoils) of human ATRIP and *S. cerevisiae* Ddc2, hereafter referred to as HsATRIP and ScDdc2, respectively, predicted that residues 110-214 of HsATRIP, and residues 58-136 of ScDdc2, form a CCD (Figure 2A). Interestingly, secondary structure prediction by PSIPRED suggested that HsATRIP residues 110-138 may form a short α-helix, while residues 140-214 may form a longer α-helix (Figure 2B). Similarly, ScDdc2 residues 58-71 may form a short α-helix, while residues 73-136 may form a longer α-helix.

A

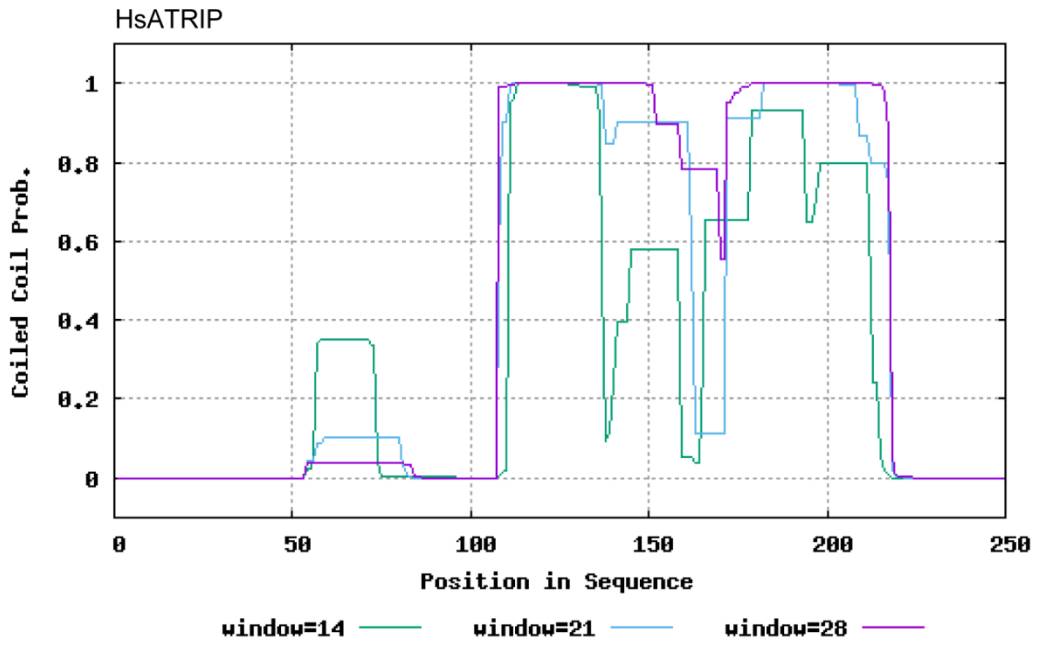

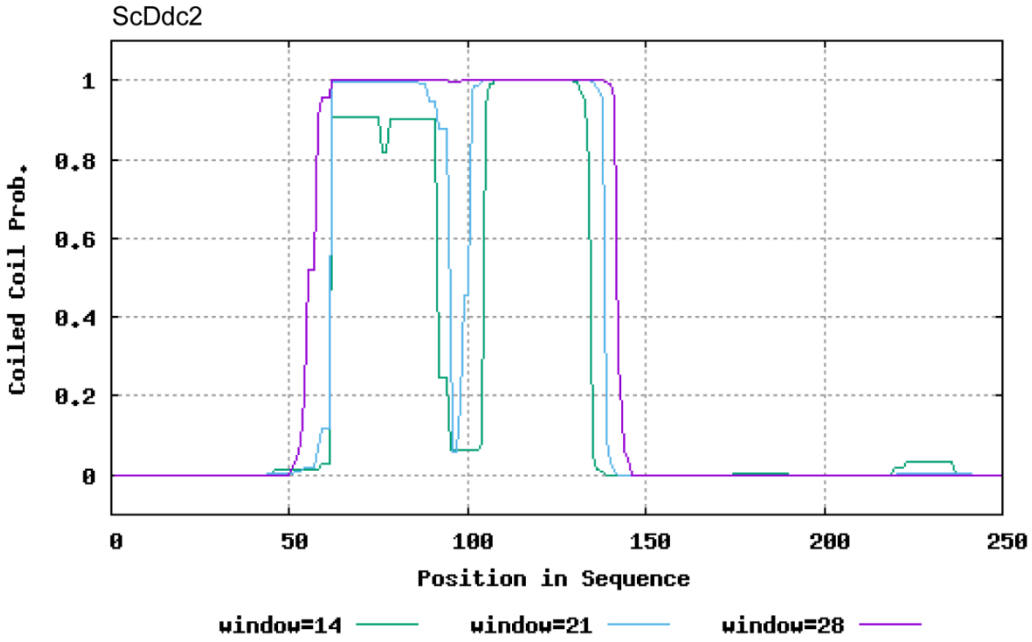
ScDdc2
Coiled Coil Prob.
1
0.8
0.6
0.4
0.2
0
0
50
100
150
200
250
Position in Sequence
window=14
window=21
window=28

B

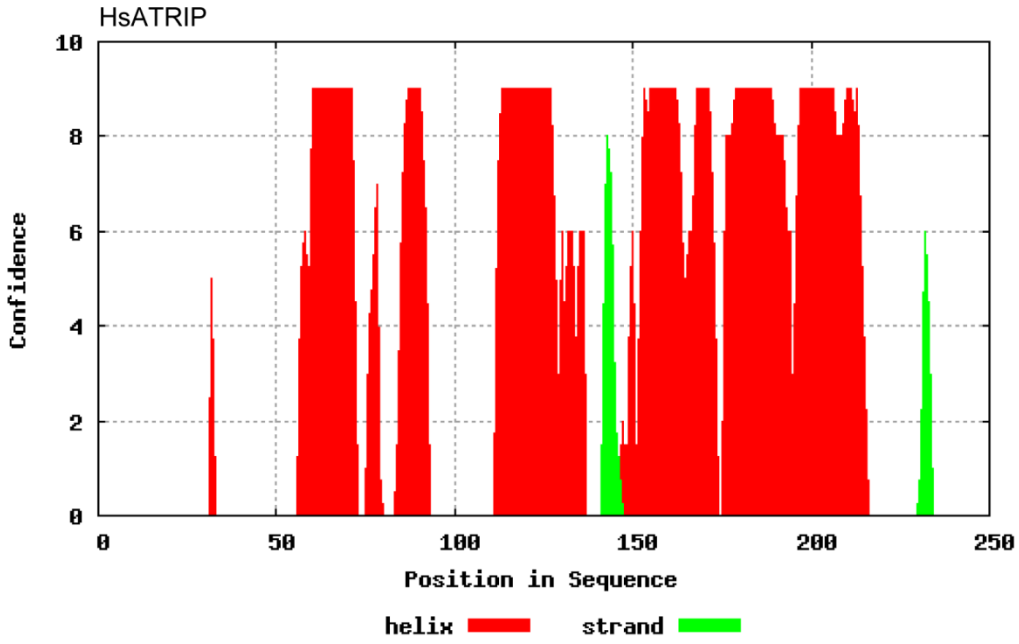
HsATRIP
Confidence
10
8
6
4
2
0
0
50
100
150
200
250
Position in Sequence
helix
strand

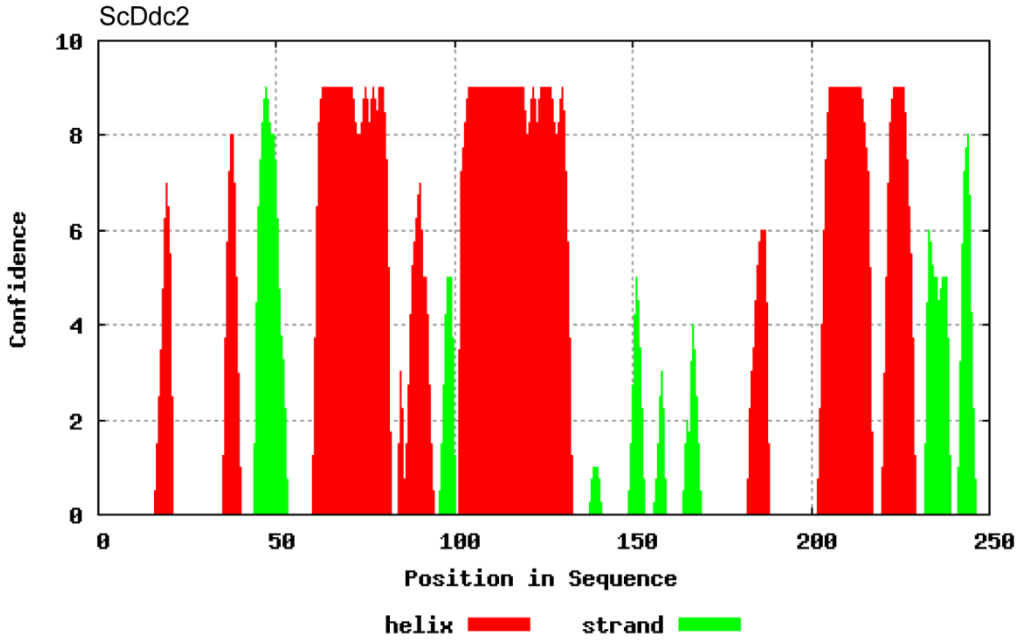

Figure 2: Coiled-coil and secondary structure prediction **(A)** Prediction of coiled-coil formation using PCOILS of HsATRIP and ScDdc2 aa residues 1-250. **(B)** Secondary structure prediction using PSIPRED of HsATRIP and ScDdc2 aa residues 1-250. α-helix formation predicted by PSIPRED is indicated in red, while β-strand formation is indicated in green.

Therefore, we expressed and purified the following four protein constructs: HsATRIP residues 110-214, HsATRIP residues 140-214, ScDdc2 residues 58-136 and ScDdc2 residues 73-136 (Figure 3). All the constructs could be easily purified to homogeneity.

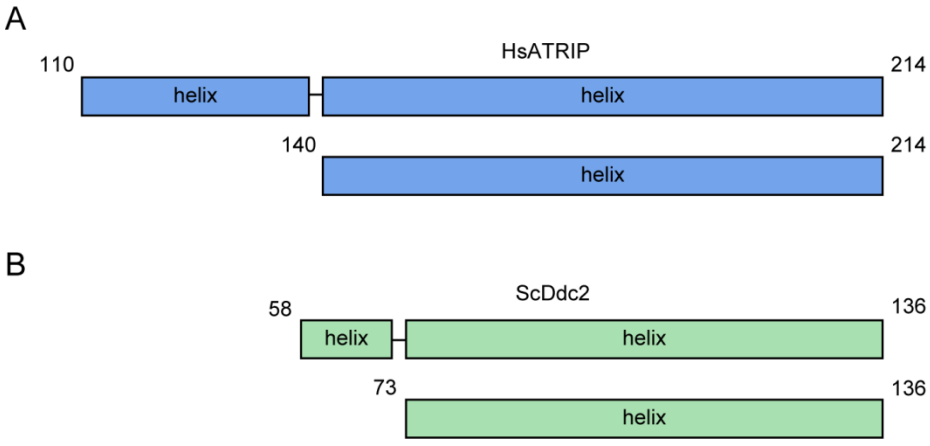

Figure 3: Schematic diagram of **(A)** HsATRIP (in blue) and **(B)** ScDdc2 (in green) constructs used for SEC-MALS. Helix formation predicted by PSIPRED is indicated. Amino acid boundaries are indicated.

Using SEC-MALS, we tested the oligomerization state of all the four CCD constructs. Surprisingly, HsATRIP 110-214 was dimeric, whereas, HsATRIP 140-214 was monomeric (Figure 4). This might suggest that residues 110-139 are necessary for coiled-coil dimerization. Since residues 110-138 are predicted to fold into a short α-helix, it is possible that residues 110-138 may act as a trigger sequence for ATRIP CCD dimerization. Unexpectedly, both ScDdc2 58-136 and 73-136 were monomeric even at the highest injected concentration of 1.7 mM in our SEC-MALS experiments (Figure 4). This suggests that the presence of a trigger helix, if at all, is not conserved in the yeast and human orthologs.

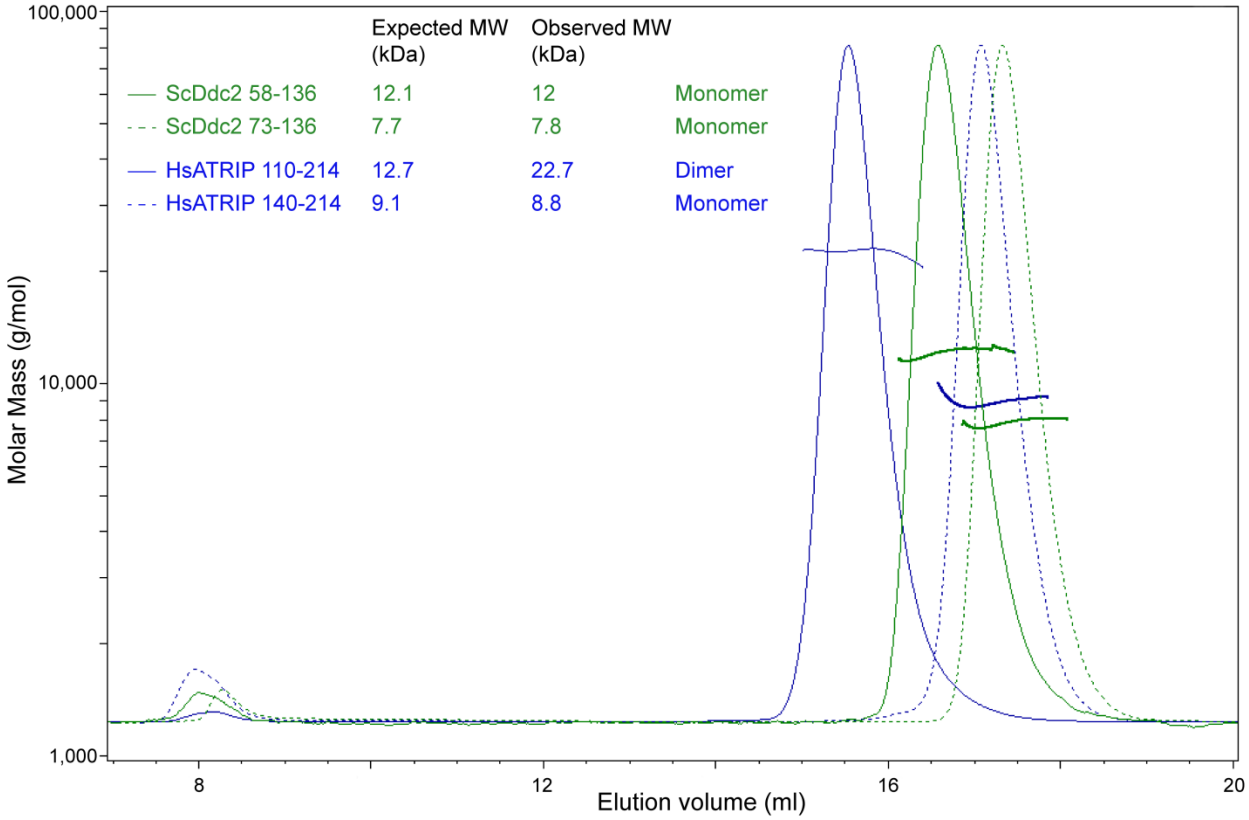

Figure 4: SEC-MALS analysis of HsATRIP and ScDdc2 constructs. The Rayleigh ratio is indicated by a solid blue line for HsATRIP 110-214, dashed blue line for HsATRIP 140-214, solid green line for ScDdc2 58-136 and dashed green line for ScDdc2 73-136. Molar mass calculated over peak fractions is indicated by a solid blue line for HsATRIP constructs and a solid green line for ScDdc2 constructs. MW: Molecular weight.

Interestingly, ScDdc2 73-136 formed a crystallographic dimer (chapter 2, Figure 1C). These results suggest that the Ddc2 CCD might not be a constitutive dimer and dimerization might be regulated to control the function of the Mec1-Ddc2 complex. Indeed, in human cells, replacing the CCD of ATRIP with a heterologous CCD from transcription factor GCN4, restored ATR-ATRIP oligomerization, stable ATR-

ATRIP interaction and recruitment to DNA damage sites (Ball and Cortez, 2005). It is imaginable that the homodimerization of the ATRIP CCD trigger helix is regulated by DNA damage, for example, DNA damage might promote trigger helix homodimerization and therefore ATR signaling, while repair of DNA damage might disrupt trigger helix homodimerization to attenuate ATR-mediated checkpoint pathway. In conclusion, we suggest that the ATRIP CCD dimerization might be regulated by a trigger helix at its N-terminus.

Methods

Protein engineering and purification from *E. coli*

HsATRIP residues 110-214, HsATRIP residues 140-214, ScDdc2 residues 58-136, ScDdc2 residues 73-136 and ScDdc2 residues 1-136 were separately cloned into pOPINF vectors using the In-Fusion system (Clontech) and individually expressed in *E. coli* BL21(DE3). Cells expressing appropriate target were pelleted, resuspended in lysis buffer (50 mM Tris-HCl, pH 7.5, 500 mM NaCl, 20 mM imidazole, 0.2% Tween-20), then rapidly frozen on dry-ice and stored at −80°C. For each target, the frozen cell suspension was thawed at room temperature and supplemented with complete EDTA-free Protease Inhibitor Cocktail (Roche) and Benzonase (Sigma) before sonication. The lysate was clarified by ultracentrifugation and then affinity purified via an N-terminal His6 tag using Ni-NTA Superflow resin (Qiagen). His-tag was removed using His-tagged 3C protease and a second round of affinity purification. Lastly, target was purified using a Superdex 75 HiLoad 16/60 (GE Healthcare) column equilibrated in 20 mM Tris-HCl, pH 7.5, 150 mM NaCl, 1 mM TCEP, 0.02% NaN_3.

Molecular mass measurement by SEC-MALS

SEC-MALS experiments were performed as in chapter 2. Purified proteins were concentrated up to 0.3 mM (1.7 mM for ScDdc2 58-136), and filtered through a 0.1 µm Amicon filter before injection. 38 µl of each protein was separated on a Superdex 200 10/300 GL gel-filtration column (GE Healthcare) equilibrated in 20 mM Tris, pH 7.5, 200 mM NaCl, 1 mM TCEP, 0.02% NaN_3 at a flow rate of 0.65 ml/min. Light scattering was recorded on an in-line miniDAWN TREOS three-angle light scattering detector (Wyatt Technology) and protein concentration detected with an in-line Optilab Trex refractive index detector. The weight-averaged molecular mass of material contained in chromatographic peaks was determined using ASTRA 6 software (Wyatt Technology).

References

Ball, H.L., and Cortez, D. (2005). ATRIP oligomerization is required for ATR-dependent checkpoint signaling. J Biol Chem *280*, 31390-31396.

Crick, F.H. (1952). Is alpha-keratin a coiled coil? Nature *170*, 882-883.

Engel, A.M., Cejka, Z., Lupas, A., Lottspeich, F., and Baumeister, W. (1992). Isolation and cloning of Omp alpha, a coiled-coil protein spanning the periplasmic space of the ancestral eubacterium Thermotoga maritima. EMBO J *11*, 4369-4378.

Frank, S., Lustig, A., Schulthess, T., Engel, J., and Kammerer, R.A. (2000). A distinct seven-residue trigger sequence is indispensable for proper coiled-coil formation of the human macrophage scavenger receptor oligomerization domain. J Biol Chem *275*, 11672-11677.

Hopfner, K.P., Craig, L., Moncalian, G., Zinkel, R.A., Usui, T., Owen, B.A., Karcher, A., Henderson, B., Bodmer, J.L., McMurray, C.T.*, et al.* (2002). The Rad50 zinc-hook is a structure joining Mre11 complexes in DNA recombination and repair. Nature *418*, 562-566.

Kammerer, R.A., Schulthess, T., Landwehr, R., Lustig, A., Engel, J., Aebi, U., and Steinmetz, M.O. (1998). An autonomous folding unit mediates the assembly of two-stranded coiled coils. Proc Natl Acad Sci U S A *95*, 13419-13424.

Kilmartin, J.V., Dyos, S.L., Kershaw, D., and Finch, J.T. (1993). A spacer protein in the Saccharomyces cerevisiae spindle poly body whose transcript is cell cycle-regulated. J Cell Biol *123*, 1175-1184.

Pauling, L., and Corey, R.B. (1953). Compound helical configurations of polypeptide chains: structure of proteins of the alpha-keratin type. Nature *171*, 59-61.

Sawicka, M., Wanrooij, P.H., Darbari, V.C., Tannous, E., Hailemariam, S., Bose, D., Makarova, A.V., Burgers, P.M., and Zhang, X. (2016). The Dimeric Architecture of Checkpoint Kinases Mec1ATR and Tel1ATM Reveal a Common Structural Organization. J Biol Chem *291*, 13436-13447.

Soh, Y.M., Burmann, F., Shin, H.C., Oda, T., Jin, K.S., Toseland, C.P., Kim, C., Lee, H., Kim, S.J., Kong, M.S.*, et al.* (2015). Molecular basis for SMC rod formation and its dissolution upon DNA binding. Mol Cell *57*, 290-303.

Steinmetz, M.O., Stock, A., Schulthess, T., Landwehr, R., Lustig, A., Faix, J., Gerisch, G., Aebi, U., and Kammerer, R.A. (1998). A distinct 14 residue site triggers coiled-coil formation in cortexillin I. EMBO J *17*, 1883-1891.

Chapter 4:

RPA mediates recruitment of MRX to forks and double-strand breaks to hold sister chromatids together

Andrew Seeber[1], Anna Maria Hegnauer[2], Nicole Hustedt[2], Ishan Deshpande[1], Jerome Poli[2], Jan Eglinger[2], Philippe Pasero[3], Heinz Gut[2], Miki Shinohara[4], Karl Peter Hopfner[5], Kenji Shimada[2], Susan M. Gasser[1]

[1]Friedrich Miescher Institute for Biomedical Research (FMI), Maulbeerstrasse 66, 4058 Basel, Switzerland
[2]University of Basel, Faculty of Natural Sciences, Klingelbergstrasse 50, CH-4056 Basel, Switzerland
[3]Institute of Human Genetics, CNRS UPR 1142, 34090 Montpellier, France
[4]Institute for Protein Research, Osaka University, Suita, Osaka 565-0871, Japan
[5]Gene Center LMU Munich, Feodor-Lynen Strasse 25, 81377 Munich, Germany

Published in *Mol Cell*, 2016, 64(5):951-966.

Summary

The Mre11-Rad50-Xrs2 (MRX) complex is related to SMC complexes that form rings capable of holding two distinct DNA strands together. MRX functions at stalled replication forks and double-strand breaks (DSBs). A mutation in the N-terminal OB fold of the 70 kDa subunit of yeast replication protein A, *rfa1-t11*, abrogates MRX recruitment to both types of DNA damage. The rfa1 mutation is functionally epistatic with loss of any of the MRX subunits for survival of replication fork stress or DSB recovery, although it does not compromise end-resection. High-resolution imaging shows that either the *rfa1-t11* or the *rad50*Δ mutation lets stalled replication forks collapse and allows the separation not only of opposing ends but of sister chromatids at breaks. Given that cohesin loss does not provoke visible sister separation as long as the RPA-MRX contacts are intact, we conclude that MRX also serves as a structural linchpin holding sister chromatids together at breaks.

Molecular Cell
Article

RPA Mediates Recruitment of MRX to Forks and Double-Strand Breaks to Hold Sister Chromatids Together

Andrew Seeber,[1,2] Anna Maria Hegnauer,[1] Nicole Hustedt,[1,6] Ishan Deshpande,[1,2] Jérôme Poli,[1] Jan Eglinger,[1] Philippe Pasero,[3] Heinz Gut,[1] Miki Shinohara,[4] Karl-Peter Hopfner,[5] Kenji Shimada,[1] and Susan M. Gasser[1,2,7,*]
[1]Friedrich Miescher Institute for Biomedical Research, Maulbeerstrasse 66, 4058 Basel, Switzerland
[2]University of Basel, Faculty of Natural Sciences, Klingelbergstrasse 50, 4056 Basel, Switzerland
[3]Institute of Human Genetics, CNRS UPR 1142, 34090 Montpellier, France
[4]Institute for Protein Research, Osaka University, Suita, Osaka 565-0871, Japan
[5]Gene Center LMU Munich, Feodor-Lynen Strasse 25, 81377 Munich, Germany
[6]Present address: The Lunenfeld-Tanenbaum Research Institute, Mount Sinai Hospital, 600 University Avenue, Toronto, ON M5G 1X5, Canada
[7]Lead Contact
*Correspondence: susan.gasser@fmi.ch
http://dx.doi.org/10.1016/j.molcel.2016.10.032

SUMMARY

The Mre11-Rad50-Xrs2 (MRX) complex is related to SMC complexes that form rings capable of holding two distinct DNA strands together. MRX functions at stalled replication forks and double-strand breaks (DSBs). A mutation in the N-terminal OB fold of the 70 kDa subunit of yeast replication protein A, *rfa1-t11*, abrogates MRX recruitment to both types of DNA damage. The *rfa1* mutation is functionally epistatic with loss of any of the MRX subunits for survival of replication fork stress or DSB recovery, although it does not compromise end-resection. High-resolution imaging shows that either the *rfa1-t11* or the *rad50Δ* mutation lets stalled replication forks collapse and allows the separation not only of opposing ends but of sister chromatids at breaks. Given that cohesin loss does not provoke visible sister separation as long as the RPA-MRX contacts are intact, we conclude that MRX also serves as a structural linchpin holding sister chromatids together at breaks.

INTRODUCTION

The DNA damage and intra-S phase checkpoints are important response mechanisms that allow cells to deal with damage from exogenous or endogenous sources both by arresting the cell cycle when necessary and by activating the appropriate repair machinery (Ciccia and Elledge, 2010; Harrison and Haber, 2006; Hustedt et al., 2013). Central to the checkpoint response are the conserved checkpoint kinases Mec1-Ddc2 (ATR-ATRIP) and Tel1 (ATM). Importantly, the trimeric complex that binds single-strand DNA (ssDNA), replication protein A (RPA), acts as a recruitment platform for checkpoint and repair proteins, including but not limited to Mec1-Ddc2 and 9-1-1, the DNA damage clamp, both at stalled forks and at DNA double-strand breaks (DSBs) (Paciotti et al., 2000; Rouse and Jackson, 2002; Xu et al., 2008; Zou and Elledge, 2003; Kanoh et al., 2006; Majka et al., 2006). The failure of RPA to coat ssDNA results in replication catastrophe and also compromises homologous recombination (HR), underscoring the crucial role of this complex (Hustedt et al., 2013; Toledo et al., 2013). Although checkpoint activation coordinates cell cycle events, the maintenance of the physical structure of a stalled fork or a DSB is also crucial for repair, especially repair that is based on recombination with a sister chromatid (Bjergbaek et al., 2005; Petermann and Helleday, 2010; San Filippo et al., 2008; Wang et al., 2004).

Structural maintenance of chromosomes (SMC) complexes are central to long-range chromatin organization and are required for the proper meiotic segregation of replicated DNA, chromosome condensation, and homology-based DNA repair (Uhlmann, 2016). SMC proteins are characterized by a distinct coiled-coil domain that contains a hinge, allowing the coil to fold back on itself, bringing the N- and C-terminal globular domains together (Hirano, 2006). The best characterized SMC protein complex is cohesin, which comprises two SMC proteins, Smc1/3, and two non-SMC proteins, Scc1 (Mcd1) and Scc3. The latter serve as a clasp to bridge the head domains of Smc1/3. This complex keeps sister chromatids paired, particularly in G2 and prometaphase (Uhlmann et al., 1999). Cohesin is also recruited to DSBs and stalled replication forks, where it contributes to repair (Heidinger-Pauli et al., 2008; Ström et al., 2007; Ström and Sjögren, 2007; Unal et al., 2004, 2007) and replication fork recovery (Tittel-Elmer et al., 2012).

The Mre11/Rad50/Xrs2 (MRX) complex is structurally similar to cohesin and is often characterized as the first responder to a DSB (Lisby et al., 2004). MRX promotes the initiation of end-resection with the co-factor Sae2 (CtIP) (Garcia et al., 2011; Lengsfeld et al., 2007; Mimitou and Symington, 2008; Williams et al., 2009). Although abundant data implicate MRX in

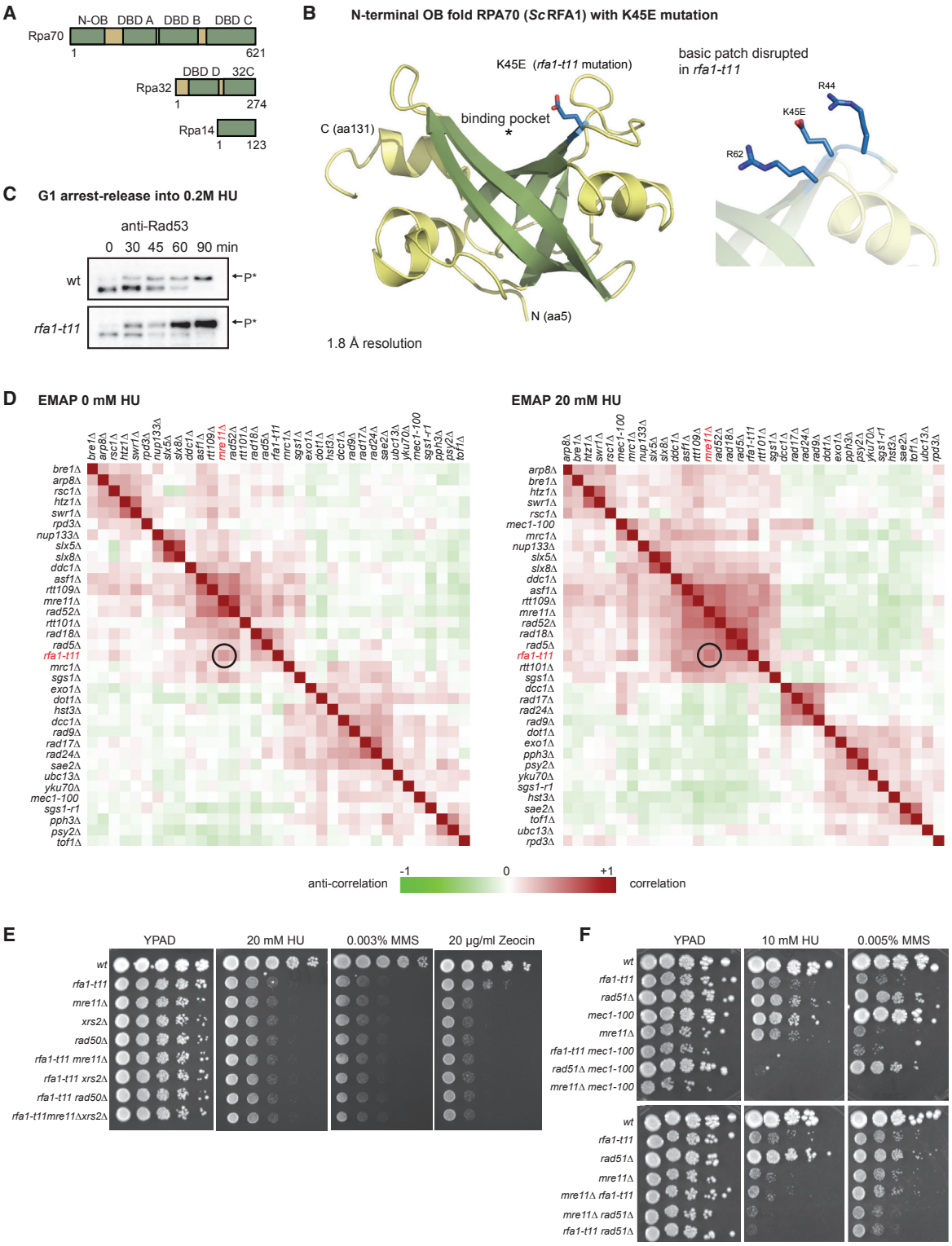

Figure 1. *rfa1-t11* Is Checkpoint Proficient and Is Epistatic with Loss of MRX on HU

(A) Diagram of the three subunits of RPA. Rfa1 (*Sc*RPA70) contains four OB domains. Unlike the others, the N-OB binds DNA poorly but binds proteins.

(B) Crystal structure of budding yeast Rfa1-t11$_{1–132}$ in cartoon with the five-stranded β-barrel forming the OB fold colored in dark green. Residues 1–4 are not shown. The E45 side chain is indicated in blue atom colors, while helices and coiled elements are in pale yellow. *Putative MRX-binding site. Right: E45 in the Rfa1-t11$_{1–132}$ structure with residues R44, K45E, and R62 displayed as sticks and blue atom colors. K45E disrupts this basic patch.

(legend continued on next page)

checkpoint activation, telomere elongation, and initiation of resection (reviewed in Stracker and Petrini, 2011; Lafrance-Vanasse et al., 2015), only a few studies have asked whether it plays a structural role at damage. Supporting this, it was shown that the two sides of a DSB separate from each other in ~12%–15% of cells lacking MRX (Kaye et al., 2004; Lobachev et al., 2004). MRX is thought to form a dimer complex with two Rad50 subunits, which, like Smc1 and Smc3 in cohesin, have long coiled-coil arms that can stretch up to ~600 Å (de Jager et al., 2001a; Hopfner et al., 2002; Moreno-Herrero et al., 2005). These coiled-coil arms can dimerize at their tips through a zinc hook domain, allowing the formation of ring-like structures or higher order oligomers that could hold two DNA molecules together (de Jager et al., 2001b; Hopfner et al., 2002). Functional studies showing that the hook domain is essential for MRX function in DNA repair, telomere maintenance, and meiotic DSB formation (Hohl et al., 2011; Wiltzius et al., 2005) are consistent with this hypothesis but do not prove it. Genetic data also implicate MRX in the repair of DSBs by sister chromatid exchange (González-Barrera et al., 2003; Hartsuiker et al., 2001).

Our study starts from the discovery of an epistatic relationship between a point mutation in the large subunit of RPA, *rfa1-t11*, and null alleles of *MRE11*, *RAD50*, or *XRS2*, under conditions of replication stress in *S. cerevisiae*. The *rfa1-t11* allele bears a single point mutation (K45E) in the N-oligonucleotide binding (OB) fold of Rfa1, which renders the strain deficient for both mitotic and meiotic recombination, although end-resection occurs normally (Dubrana et al., 2007; Umezu et al., 1998). We show here that *rfa1-t11* fails to stabilize stalled replication forks, leading to fork collapse. Rather than impairing activation of the S phase checkpoint, *rfa1-t11* reduces the recruitment of MRX to both stalled replication forks and DSBs in vivo, resulting in an inability to restart stalled forks and end separation at DSBs. We show that Rfa1 and MRX interact in an *rfa1-t11*-sensitive manner in vitro. Finally, we find that MRX holds sisters and break ends together in an RPA-dependent manner at DSBs in vivo, even when cohesin is inactivated. This provides direct evidence that MRX plays a structural role at stalled replication forks and breaks.

RESULTS

The *rfa1-t11 K45E* Mutation Disrupts a Basic Patch in Rfa1's N-OB Binding Pocket

The ssDNA-binding protein RPA is composed of three subunits, all of which are essential for cell viability in budding yeast (Figure 1A). The largest subunit (ScRpa70 or Rfa1) contains 4 OB fold domains, three of which are implicated in ssDNA binding, while the N-terminal OB-fold serves as a recruitment platform for other proteins involved in replication stress and DSB repair, including Ddc2/ATRIP and Sgs1 in budding yeast, and Rad9 and p53 in mammalian cells (Ball et al., 2007; Bochkareva et al., 2005; Dutta et al., 1993; Flynn and Zou, 2010; Hegnauer et al., 2012; Xu et al., 2008).

In earlier studies, RPA was mutagenized for non-lethal mutations, in order to identify crucial binding partners and domain-specific functions (Binz and Wold, 2008; Umezu et al., 1998; Zou et al., 2006). A previously characterized mutation, *rfa1-t11* (K45E), was reported to be specifically defective in HR, while supporting normal DNA replication (Kanoh et al., 2006; Wang and Haber, 2004). The lysine-to-glutamate charge reversal maps to the binding pocket of the N-terminal OB fold. Intriguingly, it confers recessive sensitivity to hydroxyurea (HU), which induces replication stress by inhibiting dNTP synthesis (Figure S1A), although without HU there was no delay in S phase entry: replication forks fire and progress without pausing or forming aberrant recombination intermediates (Figures S1B and S1C).

To understand the structural changes provoked by the K45E substitution, we expressed, purified, and crystallized the mutant N-terminal OB fold of yeast Rfa1 (aa 1–132) and solved its structure at 1.8 Å (Figure 1B; Table 1) using the single-wavelength anomalous diffraction method (Supplemental Experimental Procedures). Indeed, the *rfa1-t11* mutation disrupts a basic patch in the binding pocket of the N-terminal OB fold, as the mutant residue protrudes into the binding cleft. Given that the ligands of this domain are acidic, we predicted that this K45E mutation might interfere with protein-protein interactions that are important at stalled forks.

The N-terminal OB domain is responsible for the recruitment of ATRIP/Ddc2 to ssDNA and activation of the ATR kinase (Rouse and Jackson, 2002; Zou and Elledge, 2003). Mec1-Ddc2 is responsible for the vast majority of Rad53 phosphorylation induced by replication stress (Hustedt et al., 2013). Therefore, we tested for defects in checkpoint activation on a synchronized population of *rfa1-t11* cells, after releasing from G1 arrest into 0.2 M HU for 90 min. Rad53, however, was efficiently activated in the *rfa1-t11* mutant and showed a pronounced shift in electrophoretic migration (Figure 1C). A similar assay in a strain bearing *rfa1-t11* combined with *tel1Δ* showed the same shift, arguing that Rad53 activation on HU is primarily mediated by Mec1 (Figure S1D). Importantly, impaired Mec1 kinase activation is not responsible for the *rfa1-t11* mutant's sensitivity to HU.

MRX and rfa1-t11 Show Similar Epistatic Miniarray Profile Patterns in Response to Replication Stress

To identify *rfa1-t11*'s pathway of action, we performed an epistatic miniarray profile (EMAP) to compare the growth of *rfa1-t11* and 34 other query strains crossed to 1,311 deletion strains or decreased abundance by mRNA perturbation (DAmP) alleles, grown in 0, 20, or 100 mM HU (Hustedt et al., 2015). This resulted in a gene network of 45,885 interactions that had either synergistic or suppressive effects or failed to grow altogether on HU (Figures 1A, S2A, and S2B). One can correlate the patterns of sensitivity to identify genetic pathways affected similarly by specific mutants, because mutants that share phenotypic correlations often share functionality (Morrison

(C) Western blot showing Rad53 phosphorylation upshift (*) after release from α-factor into 0.2 M HU in WT and *rfa1-t11* strains.
(D) Heatmaps of Pearson correlation coefficients showing patterns of synergism between 1,311 nuclear proteins in 0 and 20 mM HU. Red indicates a correlation, while green indicates an anti-correlation. Black ring highlights the strong correlation between *rfa1-t11* and *mre11Δ*.
(E) A 10-fold dilution series showing epistasis of MRX components with *rfa1-t11* on genotoxic drugs.
(F) Additivity with *mec1-100* and *rad51Δ*. All strains are W303 *RAD5+* isogenic strains (Table S1).

Table 1. Crystallographic Data Collection and Refinement Statistics

	Rfa1-t11$_{1-132}$ Se-Met Peak[a]
Data Collection	
Space group	P 2_1
Unit cell dimensions	
a, *b*, *c* (Å)	29.62, 115.35, 69.03
α, β, γ (°)	90.0, 90.7, 90.0
Resolution range (Å)[b]	50.0–1.8 (1.85–1.80)
Wavelength (Å)	0.97941
Completeness (%)[b]	95.4 (86.2)
Redundancy[b]	2.4 (2.3)
R_{sym}[b]	0.079 (0.527)
$I/\sigma(I)$[b]	8.0 (1.7)
CC (1/2) (%)[b]	99.5 (67.9)
Unique reflections	80,762
Refinement	
R_{work}	0.164
R_{free}	0.214
Resolution range (Å)	44.3–1.8
Reflections (all)	41,721
Reflections (test set)	2,086 (5%)
Number of atoms	4,246
Figure of merit	0.415
B Factors (Å^2)	
Overall	31.7
Protein	31.0
Solvent	39.4
RMSD	
Bond lengths (Å)	0.01
Bond angles (°)	1.05
Ramachandran Plot	
Allowed (%)	100.0
Outliers (%)	0.0

RMS, root mean square.
[a]Data collection statistics are reported for unmerged Friedel pairs.
[b]Values in parentheses refer to the highest-resolution shell.

et al., 2007). For example, the histone variant *HTZ1* pattern correlates best with the nucleosome remodeler *SWR1*, which incorporates Htz1 into nucleosomes (Figures 1D and S2B).

To our surprise we found that *rfa1-t11* correlated most strongly with *mre11Δ* in both the absence and presence of 20 mM HU (Figure 1D). On 100 mM HU (Figure S2B), the EMAP pattern of *rfa1-t11* correlated additionally with *mec1-100*, an S phase defective allele of Mec1 kinase that is particularly sensitive to HU (Paciotti et al., 2001). Consistently, at 100 mM HU the *rfa1-t11* and *mre11Δ* EMAPs were similar to the template switch pathway, whereas at 20 mM the patterns of sensitivity scored for *mre11Δ* and *rfa1-t11* resemble a null allele of replication fork component *mrc1*Δ. This led to a deeper examination of the genetic relationship of *rfa1-t11*, *mec1-100*, and the MRX complex.

We created double mutants of *rfa1-t11* with deletions of *MRE11*, *RAD50*, or *XRS2* and tested them for epistasis on a range of DNA-damaging agents. Confirming the EMAP, we found that the sensitivity of *rfa1-t11* for growth on HU is completely epistatic with *mre11Δ*, *rad50Δ*, or *xrs2Δ*. That is, single and double mutants had nearly identical survival rates on HU (Figure 1E). The same is true for the triple mutant, *rfa1-t11 mre11Δ xrs2Δ*, on either HU or methyl methanesulfonate (MMS), an alkylating agent that also delays replication fork progression. On Zeocin, which induces single- and double-strand breaks, the two complexes again appeared to act on a common survival pathway, as the double mutants lacked additivity, although MRX loss of function alleles were significantly more sensitive than *rfa1-t11*. Nonetheless, these data confirmed that *rfa1-t11* likely acts through MRX and not on a parallel repair pathway at stalled forks and DSBs.

We next tested whether the *rfa1-t11* allele is epistatic or additive with mutations in Mec1, the checkpoint kinase, or the recombination protein Rad51. If *rfa1-t11*'s main defect were an inability to load or modulate Rad51 on HU (Kantake et al., 2003), one would expect these two mutants to be epistatic. However, neither *rad51Δ* nor *mec1-100* was epistatic with the *rfa1-t11* allele (Figure 1F), each showing a synthetic lethality with *rfa1-t11* on HU. Similarly, *ddc1Δ*, which compromises the 9-1-1 complex, showed synthetic lethality in combination with *rfa1-t11* on HU (data not shown). Our data suggest that RPA works with MRX to maintain replication fork integrity on HU, defining a pathway that acts in parallel to checkpoint activation and to Rad51 (Figure 1F). Consistently, *rad51Δ* was synergistically sensitive with *mre11Δ* and *mec1-100* on HU or MMS (Figure 1F).

The Replication Fork Is Unable to Resume after HU-Induced Arrest in the rfa1-t11 Mutant

To examine how *rfa1-t11* affects replication fork integrity, we scored the resumption of replication after release from an acute fork arrest in 0.2 M HU. After 6 hr on HU, the recovery rate for *mec1-100* cells is <10% of wild-type (wt) levels, while both the *mre11Δ* and *rfa1-t11* strains reduce recovery to about 20% of WT levels. Strikingly, the *rfa1-t11* mutant is again completely epistatic with the loss of Mre11 and is synergistically lethal with *mec1-100* (Figure 2A). This places the *rfa1-t11* defect on the pathway through which MRX ensures fork restart on HU (Figures 1D, 1E, and S2).

To see if this reflects the loss of DNA polymerase α (polα) at forks arrested by 0.2 M HU, we scored the presence of polα at forks that were arrested synchronously near early firing origins, using chromatin immunoprecipitation (ChIP) (Cobb et al., 2003). In contrast to results in an isogenic WT background, we scored a striking loss of DNA polα at *ARS607* in the *rfa1-t11* mutant (Figure 2B). This does not reflect an impaired checkpoint response, as there is no polα at the late firing origin *ARS501* (Figure 2B). In contrast, in *mec1-100* cells, impaired Rad53 activation allows late origin firing (Cobb et al., 2005).

To see if the resumption of DNA synthesis after HU arrest is compromised by *rfa1-t11*, we performed a DNA combing assay that measures fork progression by incorporation of BrdU, a thymidine analog, after a transient exposure to 0.2 M HU and release into HU-free media. Whereas WT forks resume

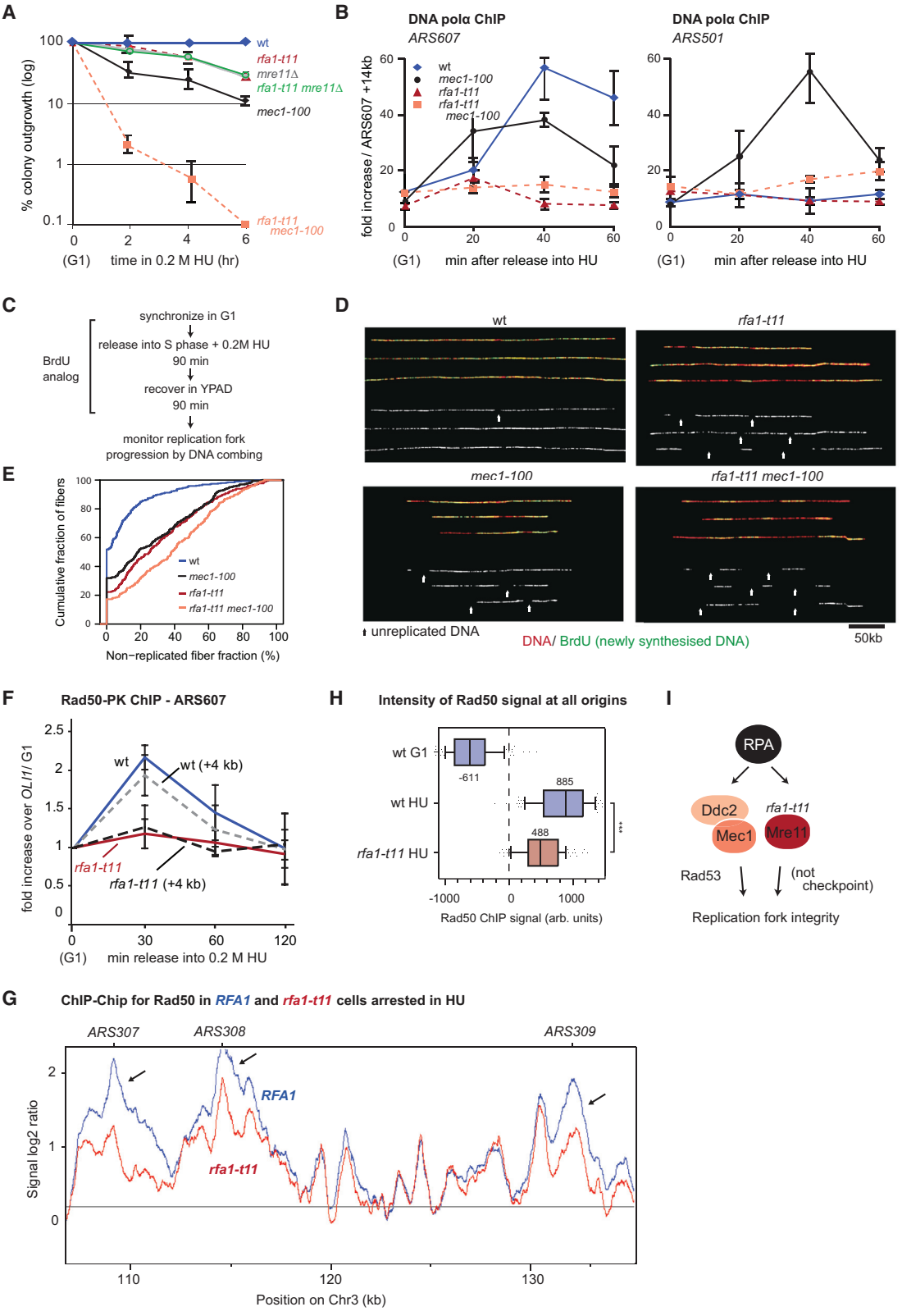

(legend on next page)

elongation, the *rfa1-t11* mutant is strongly impaired in the resumption of DNA synthesis (Figures 2D and 2E, white arrows). Again, we note that the *rfa1-t11* defect is additive with *mec1-100*. Similar phenotypes have been observed in MRX deletion alleles, although not for nuclease-deficient Mre11 mutants (Tittel-Elmer et al., 2009).

rfa1-t11 Interferes with Recruitment of MRX to Stalled Replication Forks

Given the epistasis of *mre11Δ* with *rfa1-t11*, we examined whether the K45E mutation in RPA compromises the recruitment of MRX to stalled replication forks. We performed PK-tagged Rad50 ChIP after treatment with 0.2 M HU in WT and mutant strains. Indeed, by quantitative ChIP for Rad50-PK, we found that Rad50 recruitment to stalled forks at *ARS607* was compromised by the *rfa1-t11* mutation (Figure 2F). To make sure that this was a general phenomenon and not unique to one site, we performed genome-wide ChIP of HA-tagged Rad50 on cells synchronously released from α-factor into 0.2 M HU. Figure 2G shows the pattern of Rad50 binding across a typical domain on Chr3, which includes several origins and non-origin binding sites. Whereas Rad50 binding at non-origin sites was not impaired in the *rfa1-t11* strain, its signal was strongly reduced at origins. We integrated this over all origins of the yeast genome (Figure 2H) and found ≥50% reduction in MRX (Rad50) at origins on HU. Combining our data with observations of Tittel-Elmer et al. (2012), we propose that Rfa1 recruits MRX to stalled replication forks, the failure of which allows replication fork collapse on HU soon after origin firing. This pathway of fork maintenance is independent of Rad53 activation (Figure 2I).

MRX Interacts with RPA through the N-OB Fold of Rfa1

The epistasis and recruitment data on HU suggested that RPA might directly bind MRX. To detect this interaction and monitor its response to the *rfa1-t11* mutation, we co-immunoprecipitated Rad50-PK from extracts of WT and *rfa1-t11* strains, probing for Rfa1 with an antibody that reacts equally with mutant and WT Rfa1 (Figure 3A). We find that Rad50 can indeed co-precipitate Rfa1, while it binds rfa1-t11 less efficiently (Figure 3B). The converse precipitation (i.e., by anti-Rfa1) confirmed that the MRX interaction was sensitive to the *rfa1-t11* mutation. The binding did not depend on DNA or RNA, since recovery was unchanged after treatment with Benzonase, which degrades nucleic acids (Figures 3B and S3A). Pull-downs from cell extracts using antibody specific for Xrs2 recovered Rad50 and Rfa1 but failed to recover rfa1-t11 (Figure 3B).

To determine the component of MRX that binds Rfa1, we repeated the Rad50-PK pull-down from extracts of *mre11Δ* or *xrs2Δ* strains. Rad50-PK precipitates a lower amount of Rfa1 in the absence of either Mre11 or Xrs2, suggesting either the existence of multiple contacts between Rfa1 and MRX or a need for MRX complex integrity for the interaction (Figure 3C). A double point mutation in Xrs2 (*xrs2-AA*) that disrupts Mre11 binding and/or the truncation (*xrs2-664*) of the Xrs2 C terminus (Shima et al., 2005) compromised Rfa1 recovery to the same extent as *rfa1-t11* in *XRS2*$^{+}$ cells (Figure S3B), suggesting a role for MRX conformation or complex integrity in Rfa1 interaction.

Finally, we examined the specificity of binding by comparing yeast two-hybrid (Y2H) interactions of Rfa1 with rfa1-t11. Intriguingly, both Mre11 and Xrs2 bound Rfa1 by Y2H, but only Xrs2 binding was *rfa1-t11* sensitive (Figures S3C and S3D). Y2H with Rad50 was not possible because the cloned fusions were lethal. Unfortunately, Y2H does not exclude that the endogenous MRX subunits form tertiary complexes with the bait during the assay, and thus from the Y2H and pull-down results we concluded only that multiple contact sites exist between MRX and RPA, with a subset being sensitive to the *rfa1-t11* mutation.

To map the interactions more precisely, we used a scanning peptide microarray that consisted of 206 18-aa-long peptides (overlapping by 9 aa), covering all of MRX, except the coiled-coiled arms of Rad50. The peptides were spotted onto glass slides in triplicate and were incubated with purified recombinant Rfa1 or *rfa1-t11* N-OB domains (Figure 3D). Bound proteins were visualized through anti-Rfa1 staining and a secondary Alexa647-tagged antibody, whose fluorescence was quantified on a protein array analyzer (ImageJ plugin; see Supplemental Experimental Procedures). The efficiency of binding of either Rfa1 or rfa1-t11 is plotted in Figure 3E, and the full list of peptides and their associated intensities are listed in Table S2.

We scored several clusters of Rfa1-binding peptides that were sensitive to the *rfa1-t11* mutation: namely, in the nuclease domain of Mre11, in the ATPase domain of Rad50, and two defined regions in Xrs2, one each in the N-terminal FHA domain and the C-terminal Mre11-binding domain (Figure 3E). When mapped onto the 3D structure of Mre11-Rad50 (Seifert et al., 2015), the peptides cluster in two surface areas: the double-stranded DNA (dsDNA) binding cleft of the Rad50 dimer, and a surface patch on the lateral side of the Mre11 phosphodiesterase domain (Figure 3F). Although peptides from Xrs2 also showed differential interaction, two of these map to binding sites for other proteins, and they do not cluster as do those in Mre11 or

Figure 2. Resumption of Replication after HU-Induced Stalling Fails in the *rfa1-t11* Mutant

(A) Recovery assay after G1 arrest with α-factor and release into 0.2 M HU of indicated mutants (*rfa1-t11*, *mre11Δ*, and *mec1-100*; n = 3).

(B) ChIP of DNA polα at either the early-firing ARS607 or late-firing ARS501 (Cobb et al., 2003) after release from G1 arrest into in 0.2 M HU (n = 3).

(C) Experimental scheme of DNA combing: synchronized cells are released into 0.2 M HU with a BrdU analogue for 90 min, after which the HU is washed out and the cells are allowed to recover again with analogue. DNA was combed and new synthesis was visualized by antibodies against BrdU and DNA.

(D) Example images of DNA combing with gaps (white arrows) and shorter lengths of newly synthesized DNA in mutant backgrounds.

(E) Cumulative frequency graph showing the non-replicated fiber fraction in WT and mutant strains.

(F) Rad50-PK ChIP to ARS607 after release from α-factor into 0.2 M HU (n = 3).

(G) Example plots of genome-wide Rad50-HA ChIP-chip showing loss of Rad50 at origins 307–309 in *rfa1-t11*.

(H) Boxplots of Rad50 ChIP-chip signals at all origins after release in to 0.2 M HU for 60 min at 25°C, in indicated strains. Error bars represent the SEM.

(I) Model placing *rfa1-t11* on a pathway with MRX, parallel to Mec1 activation, to confer replication fork integrity.

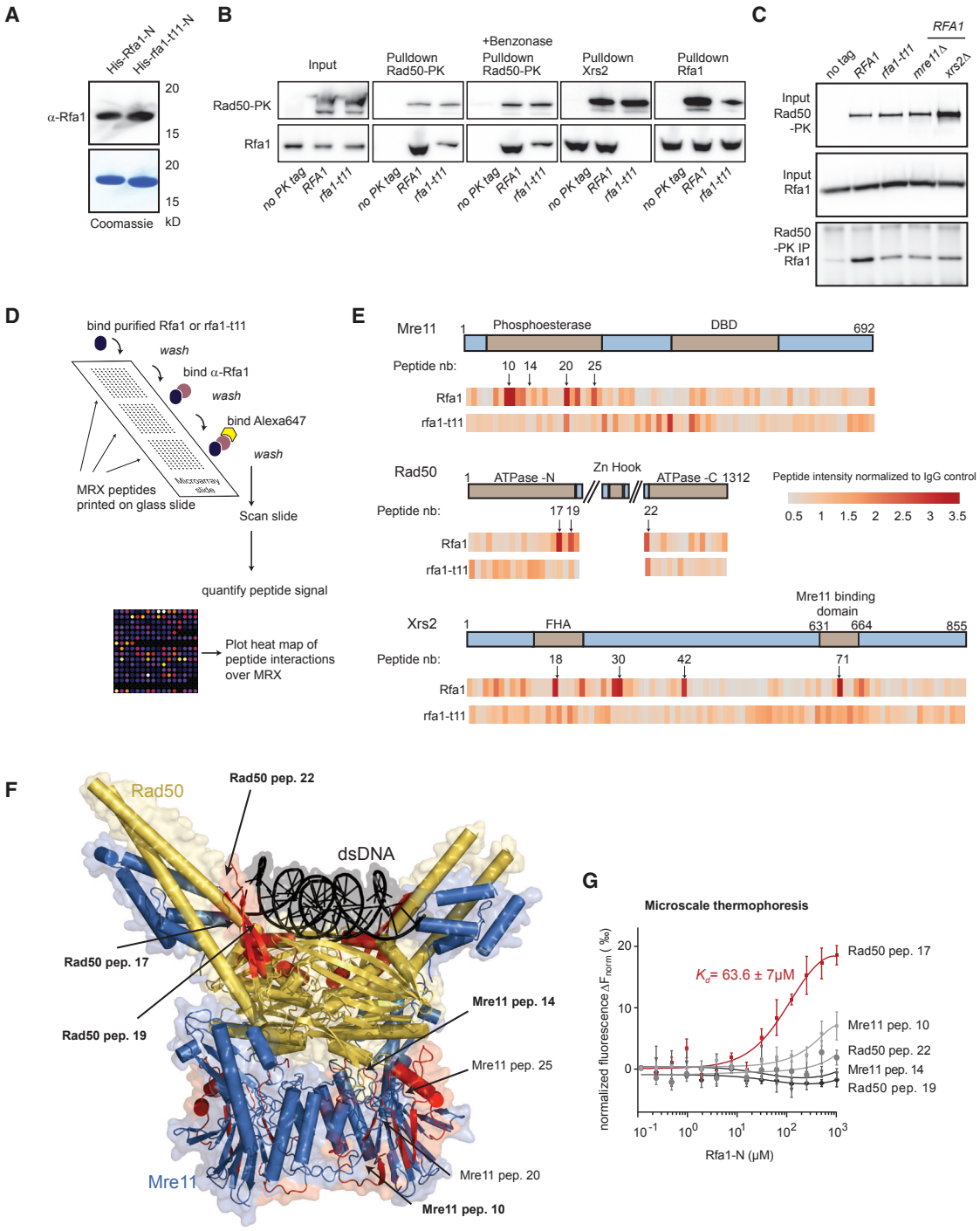

Figure 3. The Interaction between MRX and Rfa1 Is Disrupted in *rfa1-t11*

(A) Western blot showing that the Rfa1 antibody recognizes the N-OB of both Rfa1 and rfa1-t11 equally.

(B) Co-immunoprecipitation from yeast extracts in WT RFA1 and *rfa1-t11* using either antibodies against the PK tag, Xrs2, or Rfa1. Samples were Benzonase treated (Figure S3A).

(C) Rad50-PK co-immunoprecipitation as in (A) using the indicated mutants.

(D) Scheme of MRX scanning peptide microarray probed with N-OB of either Rfa1 or rfa1-t11. Two hundred six peptides (18 aa each) were spotted onto a glass slide for binding to Rfa1 or rfa1-t11 N-OB from (A). Supplemental Experimental Procedures describe signal detection and quantitation.

(E) Interaction heatmaps for either Rfa1 or rfa1-t11 across MRX. Arrows indicate regions of strong (red) binding sensitive to the *rfa1-t11* mutation (n = 3).

(legend continued on next page)

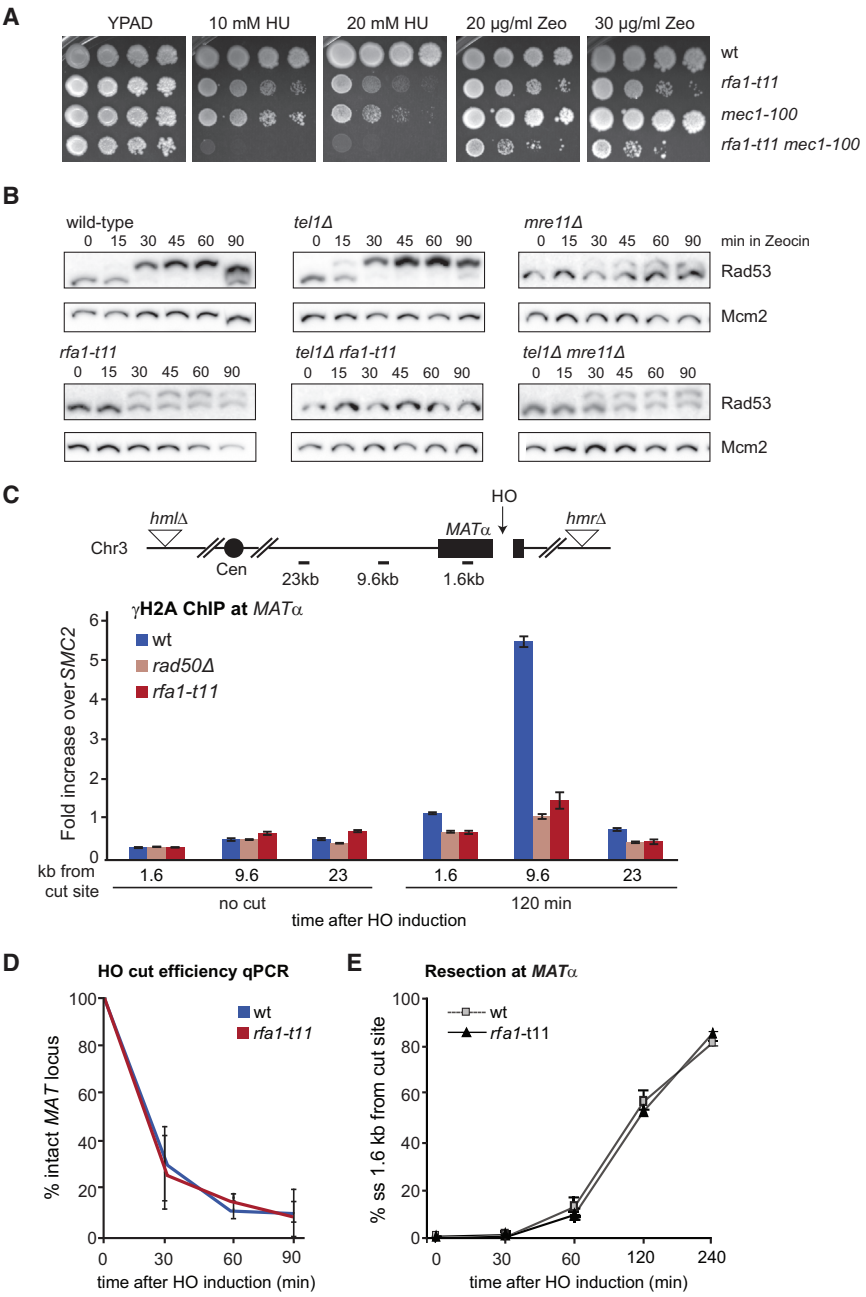

Figure 4. *rfa1-t11* Has a Diminished Checkpoint Response to DSBs, but Resection Is Intact

(A) A 10× dilution series on YPAD ± HU and Zeocin of isogenic strains with the indicated genotypes.

(B) Western blot showing Rad53 phosphorylation upshift after release from α-factor into 250 μg/ml Zeocin. No Rad53 phosphorylation was detectable in *tel1Δ rfa1-t11*. Mcm2 is the loading control.

(C) γH2A ChIP to a HO-induced DSB at *MATα* (van Attikum et al., 2007) at 120 min after cut induction (n = 4).

(D) Cut efficiency time course from Figure 5A showing that WT and *rfa1-t11* have similar cut efficiencies. After replication, both sisters are likely to be cut at once.

(E) QAOS assay showing equal accumulation of ssDNA at 1.6kb from the DSB at *MATα* in WT and *rfa1-t11*, reproduced from Dubrana et al. (2007). Error bars represent SEM.

rfa1-t11 Impairs Mec1-Dependent Checkpoint Activation at DSBs

Because *rfa1-t11* had previously been shown to be important to recruit Ddc2 (ATRIP) and Mec1 (ATR) to a DSB (Dubrana et al., 2007; Zou and Elledge, 2003), we next interrogated its genetic relationship with *mec1-100* on Zeocin, which induces both single- and double-strand breaks. Although *rfa1-t11* is sensitive to Zeocin, *mec1-100* has a mild slow-growth phenotype (Figure 4A). In contrast to growth on HU, where the combination of *rfa1-t11* and *mec1-100* was synthetically lethal, the combination of *rfa1-t11* and *mec1-100* was only slightly additive on Zeocin. MRX both helps recruit the DNA damage checkpoint kinase Tel1 (ATM) to DSBs (Nakada et al., 2003a, 2003b) and promotes resection to allow Ddc2-Mec1 activation, explaining their epistasis.

To check the epistatic relationship of Rfa1 and Mre11 on Zeocin, we scored the effects of *rfa1-t11*, *mre11Δ*, *tel1Δ*, and their pairwise combinations on Rad53 phosphorylation. We found that *rfa1-t11* and *mre11Δ* mutations compromised checkpoint activation by Zeocin to a similar degree (Figure 4B), yet in the case of *rfa1-t11*, the impaired checkpoint response was strongly additive with *tel1Δ*; that is, the *tel1Δ rfa1-t11* completely failed to activate the DNA damage checkpoint

Rad50. Microscale thermophoresis (MST) showed that the Rad50 peptide 17 had the highest affinity for Rfa1-N (Figure 3G). The other peptides tested showed weaker binding. This does not rule out that they contribute to a binding site but suggests that the ATPase-domain of Rad50 contains a key interaction site, which is indeed sensitive to the K45E mutation.

(F) Crystal structure of *Chaetomium thermophilum* Mre11-Rad50 dimer with dsDNA (Seifert et al., 2015). Peptides scored in the microarray as strongly interacting with RFA1 OB fold domain are highlighted in red.

(G) Purified Rfa1-N (dilution series from 0.12 to 1,000 μM) was incubated with 25 μM Cy5-labeled Rad50 and Mre11 peptides for 15 min at rt. Dissociation constant K_d of 63.6 ± 7 μM is for Rad50 peptide 17 and Rfa1-N (n = 3), error bars represent SEM, and ΔF_{norm} (‰) represents change in fluorescence during thermophoresis normalized to initial fluorescence. A detailed list of peptides is provided in Table S2.

(Figure 4B). This suggests that the *rfa1-t11* defect in checkpoint at DSBs arises from the loss of Mec1 (ATR) activity. Indeed, by ChIP *rfa1-t11* and *rad50Δ* were shown to reduce the accumulation of phosphorylated H2A (γH2A, a Mec1 target), at an HO-induced DSB (Figure 4C). We conclude that *rfa1-t11* compromises the Mec1 checkpoint response at DNA breaks (i.e., on Zeocin) but does not impair Mec1 activation at stalled forks. This difference likely stems from the redundancy of co-activators and mediators at stalled forks, namely, 9-1-1, Dbp11, Dna2, Mrc1, Sgs1, and RPA (Hustedt et al., 2013). We note that although DSB activation of checkpoint kinases was compromised by *rfa1-t11*, both the efficiency of HO endonuclease cleavage and resection rates were at WT levels (Figure 4DE).

rfa1-t11 Reduces Recruitment of MRX to DSBs and Reduces Repair Efficiency

To see whether RPA is implicated in the recruitment or stabilization of MRX at DSBs, possibly by binding either a short overhang or an internal ssDNA stretch, we measured the recruitment Rad50-PK to a HO endonuclease-induced DSB at *MAT* by ChIP. Consistent with previously published results, MRX binding is strongest at early time points and close to the cut site (compare 0.6 versus 1.6 kb probes). This interaction is reduced (although not entirely eliminated) in the *rfa1-t11* mutant (Figure 5A). Consistently, Mre11-YFP focus formation was reduced by roughly 50% in response to Zeocin in the *rfa1-t11* mutant (Figure 5B). One further function attributed to MRX at DSBs is the recruitment of cohesin (Unal et al., 2004, 2007). We therefore tested whether *rfa1-t11*, like *rad50*Δ, fails to recruit cohesin to an HO-induced DSB. ChIP for cohesin subunit Scc1-HA (Mcd1) at a DSB confirmed that both mutants reduce cohesin recruitment similarly after HO induction (Figure 5C).

In contrast to the observation that *rfa1-t11* decreases MRX levels at DSBs, it was recently reported that the loss of Sae2 leads to more MRX at DSBs (Chen et al., 2015; Gobbini et al., 2015). We therefore tested whether *sae2*Δ would compensate for the reduced RPA-MRX binding in the *rfa1-t11* mutant. Indeed, growth defects of *rfa1-t11* on Zeocin, HU, MMS and the topoisomerase I inhibitor camptothecin, were partially rescued by the elimination of Sae2 (Figure S3E). Again, this supports the model that *rfa1-t11* confers sensitivity to DNA damage because of impaired MRX recruitment.

To see if *rfa1-t11* affects DSB repair by a pathway other than HR, we tested the impact of the mutation on repair by end-joining of two incompatible DSBs that flank a *URA3* reporter gene (Ma et al., 2003; Matsuzaki et al., 2012). After cleavage and repair, the survivors are either URA^- (indicating repair by microhomology-mediated repair of non-complementary DSB ends following resection) or URA^+ (precise end-ligation). Like mutations in the MRX complex, *rfa1-t11* reduced the recovery of both URA^- and URA^+ colonies (Figure 5D). Importantly, the *xrs2Δ* mutation is epistatic with *rfa1-t11* in this assay (Iwasaki et al., 2016), consistent with drop assays on Zeocin that place MRX and Rfa1 on the same repair pathway. Given that *rfa1-t11* does not block resection, we suggest that RPA acts by recruiting or stabilizing MRX at breaks, allowing it to hold the two break ends together for either precise or imprecise end-joining.

RFA1 OB Fold Integrity Is Necessary to Allow MRX to Hold the Ends of a DSB Together

We next tested whether *rfa1-t11* directly interferes with the end-tethering activity of MRX by scoring the separation of ends by tagged with different fluorescent protein fusions on either side of an inducible DSB (Kaye et al., 2004; Lobachev et al., 2004). As expected, following cleavage by a galactose-inducible I-SceI endonuclease, the loss of MRX integrity provoked a significant increase in DSB end separation in cells arrested at G2/M by the DNA damage checkpoint (Figure 6A; see also Kaye et al., 2004; Lobachev et al., 2004). Importantly, the level of end separation scored for *mre11Δ* and *rad50Δ* mutants was the same for *rfa1-t11* (Figure 6A).

The fact that *rfa1-t11* compromised cohesin loading (Figure 5C) led us to test whether this mutation interferes with the tight association of sister chromatids, which we could score in a strain bearing a *lacO* array adjacent to the HO-induced break at *MATα* (Figure 6B). Sister cohesion at DSBs is commonly ascribed to cohesin, but on the basis of its architecture and dimensions, MRX should also be able to hold sister chromatids together (Hopfner et al., 2002). To test a potential role for MRX in sister-sister pairing at breaks, we used multiple DSB imaging approaches. First, super-resolution structured illumination microscopy (SIM) was used to analyze small changes in the area occupied by the paired *lacO* arrays adjacent to a break, in late S/G2 phase cells. Second, we performed high-speed time-lapse imaging of the arrays to measure the kinetics of separation following break induction, in unarrested S phase cells. Finally, we examined the maintenance of sister-sister juxtaposition after efficient DSB induction in cells that are arrested by microtubule depolymerization and fixed, comparing *rfa1-t11* with mutants in cohesin and MRX.

We first confirmed that we can resolve two sister chromatids with 3D SIM imaging of the cleaved *MATα* locus (Figure 6BC). Following projection of the 3D image stack to a 2D plane for a large number of late S phase cells, we found that the volume and shape of the fluorescent *lacO* signal are significantly larger in the *rfa1*-t11 mutant, even though the sisters only fully separated in <1% of cells (Figure 6CD). We next confirmed the validity of this spot-size assay by using a strain in which the essential cohesin subunit Scc1 (Mcd1) was cleaved by a galactose-induced TEV protease (Figure 6D). The efficiency of Scc1 cleavage was documented by western blot (Figures S4A and S4B). In S phase cells, we scored a robust increase in the area occupied by the cut-proximal *lacO* focus after Scc1 cleavage, presumably reflecting compromised pairing of sister chromatids (Figures 6D, red arrow and S4C). We applied the same analysis to the strain bearing a HO-mediated DSB at the *MATα* locus adjacent to a *lacO* array (Figure 6B). In WT cells there is a slight increase in array area as cells progress from G1 to S phase; at 120 min after HO induction, there is again a slight increase in locus size (Figure 6D). In the *rfa1-t11* or *rad50Δ* strains, however, the size of the *lacO* signal stemming from the two sisters, increased more significantly than was detected upon Scc1 cleavage (Figure 6D; 0.9 versus 0.6 μm^2).

Given that chromatin loci show continual movement in living cells, and that fixation can introduce artifacts, we examined the behavior of the *lacO* arrays on the two tagged sisters using

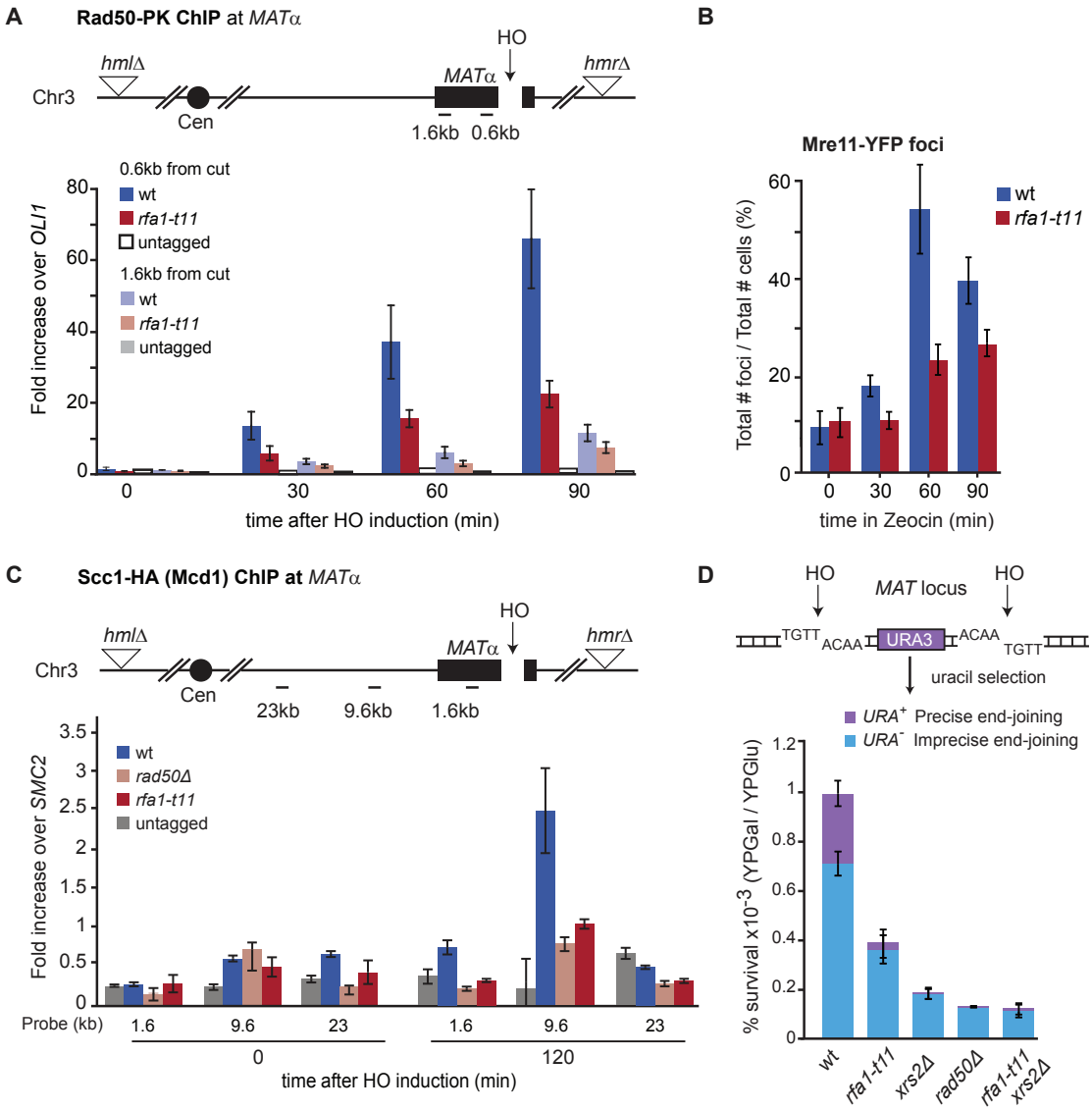

Figure 5. *rfa1-t11* Reduces the Recruitment of MRX to DSBs

(A) Rad50-PK ChIP at an HO-induced DSB at *MATα* on Chr3 in asynchronous cells (n = 5) (for probes, see van Attikum et al., 2007). HO cut efficiencies for each experiment are in Table S3. We assume that both sisters are cut, given the high rate of cleavage scored for individual loci.

(B) Mre11-YFP foci accumulation after 250 μg/ml Zeocin (n ≥ 65). Details are provided in Table S4.

(C) Scc1-HA ChIP to an HO-induced DSB at 120 min after induction (n = 4) as in (A).

(D) Scheme of the NHEJ repair pathways that yield either *URA*− (imprecise end-joining) or *URA*+ (precise end-joining) phenotypes (Matsuzaki et al., 2012). Graph shows the percentage *URA*− and *URA*+ survivors in various genotypes (n = 3).

Error bars represent SEM except for (B), in which they represent the SD.

a high-speed, high-resolution imaging assay with and without cut induction (Figure 7). In the strains used in Figure 6B, we acquired z stacks on a spinning-disk confocal microscope (8× 0.2 nm z stacks, 10 ms exposure) continuously over 1 min, yielding 750 stacks per movie at a 3D spatial resolution of ~256 nm. The movies were projected stack by stack on to a 2D plane for analysis by the ImageJ (Fiji) plugin Trackmate (Supplemental Experimental Procedures), and we quantified the percentage of frames in which two spots can be resolved. Again we used the TEV-cleavable Scc1 strain to confirm that we can monitor a loss of sister chromatid cohesion at a tagged *ARS607* (Figures S4D and S4E). Spot separation was very low in a normal WT S phase (~2% of frames separated), while after 1 hr TEV induction, separation increased to ~11% (Figure S4E).

Next we induced HO-mediated cleavage at *MATα* (Figure 7A) and monitored sister chromatid dynamics in WT, *rad50Δ*, or *rfa1-t11* cells. After 2 hr of HO induction in WT S phase cells, 8% of the frames showed resolution of the two sisters into two

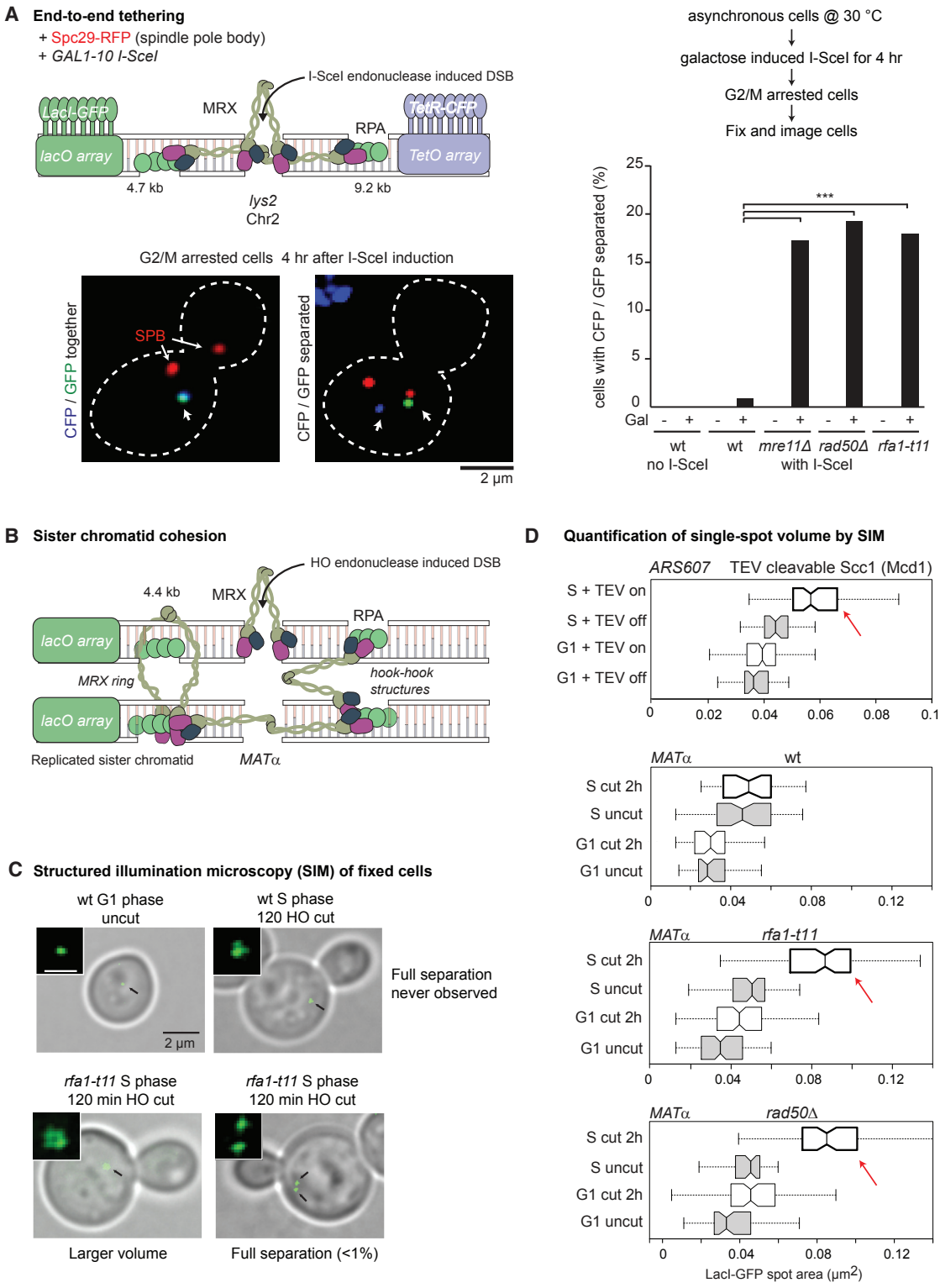

Figure 6. RFA1-Mediated Recruitment of MRX to DSBs Is Necessary for Tethering Ends and Sister Chromatids

(A) Scheme of strain used for tracking both sides of a galactose inducible I-SceI DSB on Chr2. LacO/LacI-GFP tags one side and TetO/TetR-CFP the other (Lobachev et al., 2004). MRX can tether ends through Rad50's hook domain by directly binding to the DSB end or by interaction with RPA. Examples of separation of GFP/CFP signals after I-SceI cut induction. Graph shows the percentage separated GFP/CFP in large budded cells ($n \geq 107$). For details and statistics, see Table S4. Cells scored were late G2/M (large bud and SPBs <0.6 µm apart). For uncleaved controls, mid-S and G2/M cells were scored.

(legend continued on next page)

spots, while in either *rad50Δ* or *rfa1-t11* strains, 16% to 19% of the frames had separated sisters (Figure 7B). We ruled out that this is an artifact of galactose addition by expressing HO in a strain that is resistant to cleavage, *mata*^{inc}. In conclusion, sister chromatid juxtaposition at a DSB is compromised by loss of MRX or its recruitment through RPA.

To see if this reflects compromised bridging through MRX itself or a failure to recruit and load cohesin at the DSB (Figure 5C; Unal et al., 2007), we tested the effects of destabilizing Scc1 (Mcd1) at the base of the cohesin ring (Figure 7A). Specifically, we scored sister *lacO* foci pairing at the induced cut at *MATα* in a temperature sensitive allele of Scc1 called *mcd1-1* (Heidinger-Pauli et al., 2008). Previous studies showed that a 1 hr incubation at the non-permissive temperature (37°C) was sufficient to inactivate cohesin. Our time-lapse imaging showed that without DSB induction, S phase *mcd1-1* cells have separated *lacO* foci in ~25% of frames at 37°C (Figure 7C). Remarkably, after DSB induction following cohesin inactivation (1 hr at 37°C), spot separation was actually reduced to 5%, suggesting that the induction of the break stabilizes sister-sister pairing. Importantly, this effect was lost by combining the *mcd1-1* mutant with *rfa1-t11* (Figure 7C). The simplest interpretation of this is that MRX holds sister chromatids together at a DSB, even in the absence of functional cohesin. We note that this result is in contrast to a previous report in which a DSB was not sufficient to keep sisters together (Unal et al., 2007), although in that case, the experimental setup involved a 2 hr induction of two adjacent DSBs after 4 hr of Nocodazole arrest. Under that condition, cohesin seemed to contribute to sister cohesion.

To rule out kinetic limitations of our time-lapse assay, which scores unfixed cells immediately after cleavage, we tested an experimental setup much like that used by Unal et al. (2007). The cells were grown to log phase, and nocodazole was added at the same time as either glucose (no HO cut) or galactose (induction of HO). After 1 hr, cells were shifted to 37°C to inactivate cohesin, and cells were fixed and imaged. G2/M cells were scored for LacI-GFP spot separation (Figure 7D). Remarkably we found that whereas loss of the cohesin ring (*mcd1-1* at 37°C) allowed sisters to separate at an uncut locus, sister pairing was restored in a manner dependent on Rad50 (MRX) and a functional Rfa1 N-terminal OB fold after cut induction (Figures 7D–7F). This argues that upon DSB induction, the recruitment of MRX by Rfa1 is necessary and sufficient to hold both DSB ends and two broken sister chromatids together, as this can be achieved in the absence of intact cohesin (Figure 7F).

DISCUSSION

Since their discovery and description, a role of SMC-family protein complexes in the tethering of broken DNA ends or in the maintenance of sister chromatid pairing has been debated (Huang and Kolodner, 2005; Nasmyth and Haering, 2005; Uhlmann, 2016). MRX is closely related to cohesin, condensin, and the SMC5/6 complex, and we document here an "SMC-like" function for the MRX complex at DSBs, where it appears to both hold ends together and contribute to the pairing of broken sisters. In this function, MRX recruitment is compromised by a mutation in the N-terminal domain of Rfa1. This helps answer the long-standing question of how MRX is targeted to sites of damage.

rfa1-t11 and MRX Mutations Work Epistatically to Compromise Fork Integrity under Stress

By EMAP analysis against a panel of 1,311 knockout alleles, we found that the sensitivity of *rfa1-t11* to HU parallels that of *mre11Δ* (Figure 1). Although the MRX interaction with RPA is not entirely compromised by the *rfa1-t11* mutation, in all fork-stalling and recovery assays performed *rfa1-t11* acted epistatically with MRX mutations. Consistently, MRX recruitment to HU-stalled forks is compromised by the *rfa1-t11* mutation, yet *rfa1-t11* does not impair activation of the replication checkpoint on HU. Rad53 is efficiently phosphorylated in both the *mre11Δ* and *rfa1-t11* strains on HU (Kanoh et al., 2006). As expected, *rfa1-t11* defects are additive with *mec1-100*, an S phase-specific allele of the ATR kinase, Mec1, which fails to activate Rad53 in response to replication stress (Cobb et al., 2005; Hustedt et al., 2015). At stalled forks, MRX is thought both to process fold-back structures, preventing ligation or over-resection, and to tether replicated sisters together, prior to the loading of cohesin (Tittel-Elmer et al., 2012).

The MRX Complex Has a Structural Role at DSBs

We also document a clear but unanticipated role for Rfa1 in the recruitment and stability of MRX at DSBs (Figures 5, 6, and 7). MRX tethering by RPA at breaks in late S phase contributes both to end-to-end tethering and the juxtaposition of broken sisters (late S/G2). On Zeocin, the *rfa1-t11* mutation compromises Mec1-dependent Rad53 activation (Figure 4), which likely reflects a role for the Rfa1 N-terminal OB fold in the recruitment of Mec1-Ddc2 at DSB (Zou and Elledge, 2003; Dubrana et al., 2007). Again, we have tested the effects of *rfa1-t11* in a range of yeast backgrounds, generating the mutant allele by de novo mutagenesis. In all cases, *rfa1-t11* was epistatic to *mre11Δ*.

A previous study documented a role for MRX in the recruitment of cohesin at breaks (Unal et al., 2007). We confirmed this, but we found that it is MRX, not cohesin, that holds sisters together at breaks at early time points. Our experiments differ from theirs in two significant ways: first, they induced two sets of DSBs near each other, while we induced only one. Second, Unal

(B) Construct used to measure sister chromatid pairing at an HO-induced DSB. Cut efficiencies are scored for each experiment (Table S3). MRX can hold sister chromatids together at DSBs through Rad50 hook-hook interactions or its ring structure.
(C) Examples of bright-field/GFP merged SIM images of WT and *rfa1-t11* fixed cells bearing the construct at time indicated after cleavage induction (B). Insets show enlarged LacI-GFP foci (scale bar represents 0.5 μm). The focus area is quantified by Fiji (Table S4). Fully separated foci were never observed in WT S phase cells and rarely in *rfa1-t11* cells. Foci were nonuniform in *rfa1-t11* and *rad50Δ*.
(D) Boxplots of LacI-GFP spot areas before and after 1 hr TEV induction (upper plot) or 2 hr after HO cut (lower three plots) ($n \geq 35$). Full statistics are provided in Table S4.

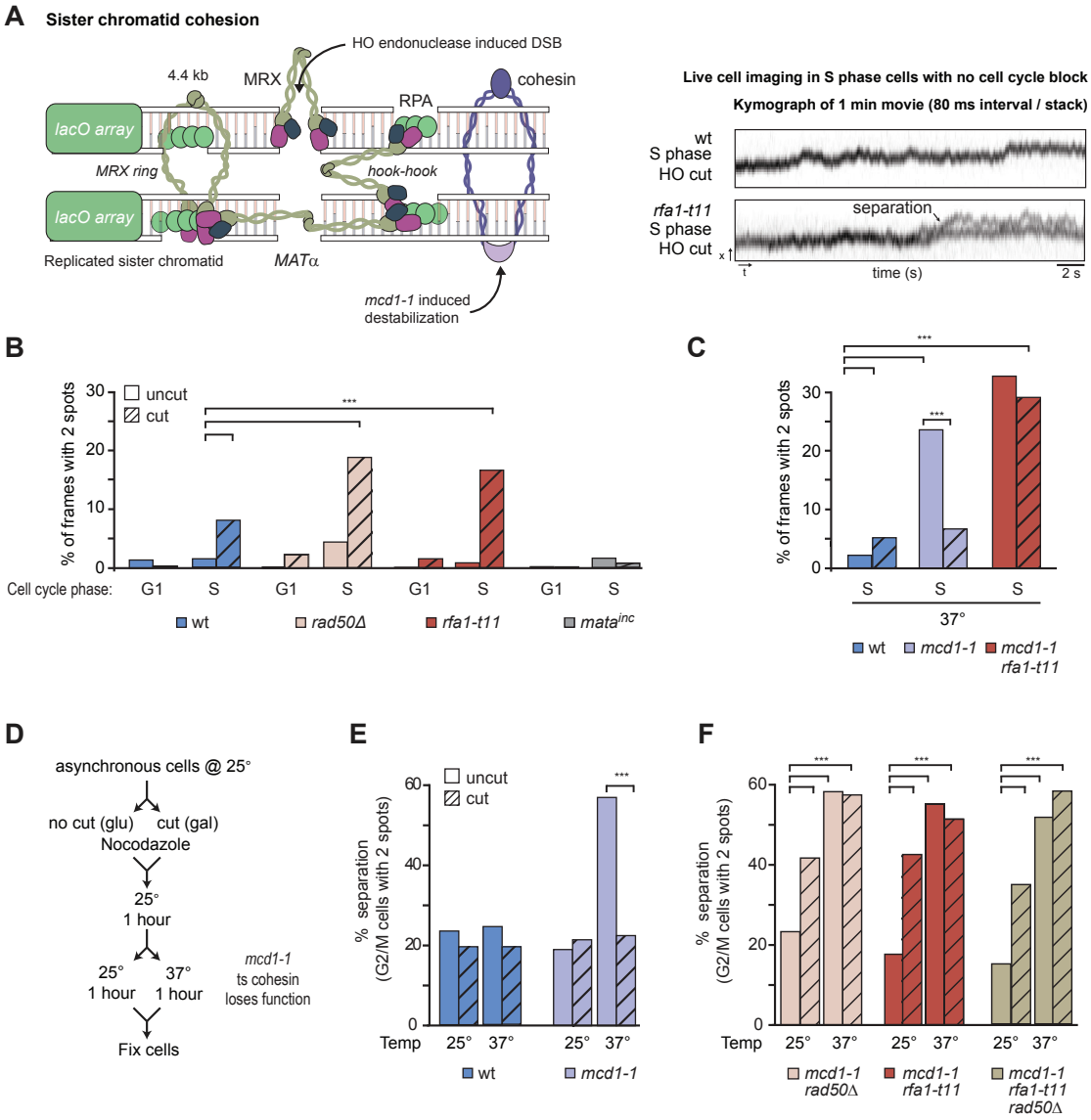

Figure 7. MRX Is Sufficient and Necessary to Hold Sister Chromatids Together at DSBs

(A) Construct used to measure changes in sister chromatid pairing at a HO induced DSB at *MATα*. Cohesin binding is later and more distant from the cut site. Right: an example kymograph of live cell imaging of a LacI-GFP spot projected through the x axis over time in WT versus *rfa1-t11* after 120 min galactose induction of HO. Black arrows indicate separation events. Uncut conditions are on glucose.

(B and C) Quantitation of the number of frames containing two LacI-GFP spots at either 25°C (B) or 37°C (C) ($n \geq 5$). All details and statistics are provided in Table S4, and example movies are available in the Supplemental Information.

(D) Experimental layout for the sister chromatid cohesion assay using the construct in (A). Asynchronous cultures of indicated mutants were grown at 25°C until log phase, 15 μg/ml nocodazole and either glucose (no cut) or galactose (cut) were added. Growth for 1 hr preceded a shift to 37°C and fixation.

(E) Quantitation of the number of G2/M cells with separated sister chromatids (two spots) in the indicated isogenic strains carrying the construct in (A).

(F) Quantitation as in (E) for the indicated mutants ($n \geq 201$) (see Table S4 for statistics). *$p < 0.005$. HO cut efficiencies are provided in Table S3.

et al. (2007) first treated cells with the microtubule-depolymerizing drug nocodazole for 4 hr before inducing the DSB for a further 2 hr. This extended arrest in G2/M may alter the behavior of the break.

It is unclear how MRX contributes to cohesin loading, as the two proteins do not interact (Tittel-Elmer et al., 2012). It may simply be that MRX holds sisters together to allow cohesin loading. In any case, it appears that through its interaction with Rfa1, MRX serves an additional role at DSBs by stabilizing both end-to-end and sister-sister contacts.

A recent study examined the role of the Rad50 zinc hook in DSB repair by monitoring sister chromatid exchange in mitosis. Those investigators found that strains with mutations in the zinc hook domain that partially impair hook dimerization without

blocking complex assembly have milder effects on sister chromatin exchange than full *RAD50* deletions (Hohl et al., 2015). We propose that these hook mutations reduce, but do not ablate, Rad50 dimerization. At a DSB multiple MRX molecules bind and even with a weakened Rad50 hook, their combined effect may be sufficient to hold both ends and sisters together (Figures 6 and 7). Cohesin may provide further structural support later in repair.

Rfa1 Interaction Sites on MRX Are Relevant to Biological Function and Human Disease

The validated interaction sites between Rfa1 and MRX cluster in two major sites. One is located in the DNA-binding cleft of the Rad50 dimer. In the presence of ATP, Rad50 primarily binds dsDNA and duplexes with extended 3′ overhangs (Seifert et al., 2015). Thus, the location of the interacting peptides would be consistent with a side-by-side binding of Rad50 and RPA at ssDNA/dsDNA junctions. The second cluster of interacting peptides maps to a surface on the N-terminal phosphodiesterase domain of Mre11 (peptides 9–12; Table S3), which was recently shown to be mutated in Mre11 hypomorphic alleles that suppress the damage sensitivity of *sae2Δ* (Seifert et al., 2015). This mutation allows easier MRX removal from ssDNA during the later stages of HR (Chen et al., 2015).

In addition, the Mre11 peptide 25 (aa 217–234), which binds Rfa1 in an *rfa1-t11*-sensitive manner in vitro, contains a site that is mutated in patients suffering from ataxia-telangiectasia-like disease (ATLD; Mre11 mutations W210C and W243R) (Fernet et al., 2005; Regal et al., 2013; Schiller et al., 2012). Very close to this interaction site is the *mre11-58* mutation (H213Y), which confers a rad50-S-like phenotype (Usui et al., 1998), affecting Mre11's nuclease activity and/or its interaction to Nbs1/Xrs2 (Schiller et al., 2012). The fact that this domain interacts with Rfa1 in an *rfa1-t11*-sensitive manner suggests that a loss of Rfa1 binding may also contribute to the ATLD phenotypes. We note that some interactions sites may require switching between open and closed conformational states of MRX (Lim et al., 2011; Möckel et al., 2012) and that some of Rfa1-MRX interactions are insensitive to the *rfa1-t11* mutation. In the case of Mre11 peptides 37–39, interaction was enhanced with the mutant Rfa1 domain. Intriguingly, this conserved Mre11 region is deleted in some ATLD patients (Δ340–366) who are predisposed to pulmonary adenocarcinoma (Regal et al., 2013).

High-Speed and Super-Resolution Imaging Allows New Insights into Chromatin Biology

We have been able to analyze sister chromatid pairing with super-resolution microscopy of short fluorescent tags either on the two sisters or both sides of a DSB. Although the resolution achieved here (250 nm and 80 ms 3D stack imaging) is sufficient to document sister separation, the imaging method can be improved to provide even more information about the forces that hold sisters together. Extending these experiments to include other SMC proteins such as condensin or the SMC5/6 complex will surely provide a fuller understanding of long-range chromatin interactions in living cells.

EXPERIMENTAL PROCEDURES

Yeast Growth Conditions, Plasmids, Repair Assays and ChIP

All strains used were derived from W303-1A or JKM179 (see Table S1). EMAP, drop assays, and DNA-combing methods are described in Supplemental Experimental Procedures. Cohesin experiments used nocodazole at 15 μg/ml with the yeast culture adjusted to 1% DMSO before nocodazole addition. Imprecise and precise NHEJ assays were as in Matsuzaki et al. (2012). ChIP experiments were performed as described in Cobb et al. (2003). For ChIP-chip and associated bioinformatics analysis, see Tittel-Elmer et al. (2012).

Protein Purification, Structure Studies, Peptide Arrays, and Microscale Thermophoresis

Details are presented in Supplemental Experimental Procedures. The scanning peptide array covered all of MRX except the coiled-coil domains of Rad50, with 18-aa-long peptides with 9 aa overlap spotted onto a glass slide by JPT Peptide Technologies.

Microscopy and Error Calculation

Details for live and fixed fluorescent imaging and quantitative analysis including spot volume and spot separation in time lapse movies are described in Supplemental Experimental Procedures. Structured illumination imaging used a Zeiss Elyra S.1 microscope with an Andor iXon 885 EMCCD camera.

Error bars on graphs represent the SEM unless otherwise stated. Categorical data such as the one- versus two-spot cohesin assay was tested for significance using a two-tailed Fisher's exact test (GraphPad), computing exact p values using the method of summing small p values. The large spot separation movie data set was tested for significance using a chi-square with Yates correction test (GraphPad) against the relevant strain genotype uncut. Continuous data such as LacI-GFP spot size was shown to be normally distributed and then tested for differences using a two-tailed Student's t test (GraphPad). Significance cutoff was $p < 0.05$. All p values are listed in Table S4.

ACCESSION NUMBERS

The accession numbers for the rfa1-t11 N-OB crystal structure and the Rad50 ChIP-chip data reported in this paper are PDB: 5M1X and GEO: GSE88816, respectively.

SUPPLEMENTAL INFORMATION

Supplemental Information includes Supplemental Experimental Procedures, four figures, four tables, and one movie and can be found with this article online at http://dx.doi.org/10.1016/j.molcel.2016.10.032.

AUTHOR CONTRIBUTIONS

A.S., K.S., and S.M.G. planned experiments, analyzed data, and wrote the manuscript. A.S. and A.M.H. performed most experiments. N.H. carried out the EMAP. J.P. performed Rad50 ChIP-chip. I.D. performed MST, purified Rfa1, and determined rfa1-t11 structure, guided by H.G. M.S. performed the NHEJ assay. J.E. wrote scripts for image analysis. A.S., A.M.H., N.H., and K.S. created strains. K.-P.H. modeled the Rad50-Mre11 structure and peptide position. P.P. and J.P. supervised DNA combing.

ACKNOWLEDGMENTS

We thank J. Bianco and the Pasero lab for assistance, M. Stadler for statistical analysis, L. Gelman and S. Bourke for imaging help, C. Soustelle and A. Nicolas for the *rfa1-t11* plasmid, M. Kawai for technical assistance, J. Cobb for advice, K. Lobachev, K. Bloom, D. Koshland, and M. Resnick for strains, and J. Petrini for the Mre11 antibody. We thank V. Dion, U. Rass, and S.M.G. lab members for proofreading. The S.M.G. laboratory thanks the Swiss National Science Foundation (310030B_156936), Human Frontier Science Program (RGP0016), European Molecular Biology Organization, and Novartis

Research Foundation for support. K.-P.H acknowledges funding by the ERC (advanced grant ATMMACHINE 322869).

Received: August 3, 2016
Revised: September 29, 2016
Accepted: October 21, 2016
Published: November 23, 2016

REFERENCES

Ball, H.L., Ehrhardt, M.R., Mordes, D.A., Glick, G.G., Chazin, W.J., and Cortez, D. (2007). Function of a conserved checkpoint recruitment domain in ATRIP proteins. Mol. Cell. Biol. *27*, 3367–3377.

Binz, S.K., and Wold, M.S. (2008). Regulatory functions of the N-terminal domain of the 70-kDa subunit of replication protein A (RPA). J. Biol. Chem. *283*, 21559–21570.

Bjergbaek, L., Cobb, J.A., Tsai-Pflugfelder, M., and Gasser, S.M. (2005). Mechanistically distinct roles for Sgs1p in checkpoint activation and replication fork maintenance. EMBO J. *24*, 405–417.

Bochkareva, E., Kaustov, L., Ayed, A., Yi, G.S., Lu, Y., Pineda-Lucena, A., Liao, J.C., Okorokov, A.L., Milner, J., Arrowsmith, C.H., and Bochkarev, A. (2005). Single-stranded DNA mimicry in the p53 transactivation domain interaction with replication protein A. Proc. Natl. Acad. Sci. U S A *102*, 15412–15417.

Chen, H., Donnianni, R.A., Handa, N., Deng, S.K., Oh, J., Timashev, L.A., Kowalczykowski, S.C., and Symington, L.S. (2015). Sae2 promotes DNA damage resistance by removing the Mre11-Rad50-Xrs2 complex from DNA and attenuating Rad53 signaling. Proc. Natl. Acad. Sci. U S A *112*, E1880–E1887.

Ciccia, A., and Elledge, S.J. (2010). The DNA damage response: making it safe to play with knives. Mol. Cell *40*, 179–204.

Cobb, J.A., Bjergbaek, L., Shimada, K., Frei, C., and Gasser, S.M. (2003). DNA polymerase stabilization at stalled replication forks requires Mec1 and the RecQ helicase Sgs1. EMBO J. *22*, 4325–4336.

Cobb, J.A., Schleker, T., Rojas, V., Bjergbaek, L., Tercero, J.A., and Gasser, S.M. (2005). Replisome instability, fork collapse, and gross chromosomal rearrangements arise synergistically from Mec1 kinase and RecQ helicase mutations. Genes Dev. *19*, 3055–3069.

de Jager, M., Dronkert, M.L., Modesti, M., Beerens, C.E., Kanaar, R., and van Gent, D.C. (2001a). DNA-binding and strand-annealing activities of human Mre11: implications for its roles in DNA double-strand break repair pathways. Nucleic Acids Res. *29*, 1317–1325.

de Jager, M., van Noort, J., van Gent, D.C., Dekker, C., Kanaar, R., and Wyman, C. (2001b). Human Rad50/Mre11 is a flexible complex that can tether DNA ends. Mol. Cell *8*, 1129–1135.

Dubrana, K., van Attikum, H., Hediger, F., and Gasser, S.M. (2007). The processing of double-strand breaks and binding of single-strand-binding proteins RPA and Rad51 modulate the formation of ATR-kinase foci in yeast. J. Cell Sci. *120*, 4209–4220.

Dutta, A., Ruppert, J.M., Aster, J.C., and Winchester, E. (1993). Inhibition of DNA replication factor RPA by p53. Nature *365*, 79–82.

Fernet, M., Gribaa, M., Salih, M.A., Seidahmed, M.Z., Hall, J., and Koenig, M. (2005). Identification and functional consequences of a novel MRE11 mutation affecting 10 Saudi Arabian patients with the ataxia telangiectasia-like disorder. Hum. Mol. Genet. *14*, 307–318.

Flynn, R.L., and Zou, L. (2010). Oligonucleotide/oligosaccharide-binding fold proteins: a growing family of genome guardians. Crit. Rev. Biochem. Mol. Biol. *45*, 266–275.

Garcia, V., Phelps, S.E., Gray, S., and Neale, M.J. (2011). Bidirectional resection of DNA double-strand breaks by Mre11 and Exo1. Nature *479*, 241–244.

Gobbini, E., Villa, M., Gnugnoli, M., Menin, L., Clerici, M., and Longhese, M.P. (2015). Sae2 function at DNA double-strand breaks is bypassed by dampening Tel1 or Rad53 activity. PLoS Genet. *11*, e1005685.

González-Barrera, S., Cortés-Ledesma, F., Wellinger, R.E., and Aguilera, A. (2003). Equal sister chromatid exchange is a major mechanism of double-strand break repair in yeast. Mol. Cell *11*, 1661–1671.

Harrison, J.C., and Haber, J.E. (2006). Surviving the breakup: the DNA damage checkpoint. Annu. Rev. Genet. *40*, 209–235.

Hartsuiker, E., Vaessen, E., Carr, A.M., and Kohli, J. (2001). Fission yeast Rad50 stimulates sister chromatid recombination and links cohesion with repair. EMBO J. *20*, 6660–6671.

Hegnauer, A.M., Hustedt, N., Shimada, K., Pike, B.L., Vogel, M., Amsler, P., Rubin, S.M., van Leeuwen, F., Guénolé, A., van Attikum, H., et al. (2012). An N-terminal acidic region of Sgs1 interacts with Rpa70 and recruits Rad53 kinase to stalled forks. EMBO J. *31*, 3768–3783.

Heidinger-Pauli, J.M., Unal, E., Guacci, V., and Koshland, D. (2008). The kleisin subunit of cohesin dictates damage-induced cohesion. Mol. Cell *31*, 47–56.

Hirano, T. (2006). At the heart of the chromosome: SMC proteins in action. Nat. Rev. Mol. Cell Biol. *7*, 311–322.

Hohl, M., Kwon, Y., Galván, S.M., Xue, X., Tous, C., Aguilera, A., Sung, P., and Petrini, J.H. (2011). The Rad50 coiled-coil domain is indispensable for Mre11 complex functions. Nat. Struct. Mol. Biol. *18*, 1124–1131.

Hohl, M., Kochańczyk, T., Tous, C., Aguilera, A., Krężel, A., and Petrini, J.H. (2015). Interdependence of the rad50 hook and globular domain functions. Mol. Cell *57*, 479–491.

Hopfner, K.P., Craig, L., Moncalian, G., Zinkel, R.A., Usui, T., Owen, B.A., Karcher, A., Henderson, B., Bodmer, J.L., McMurray, C.T., et al. (2002). The Rad50 zinc-hook is a structure joining Mre11 complexes in DNA recombination and repair. Nature *418*, 562–566.

Huang, M.E., and Kolodner, R.D. (2005). A biological network in Saccharomyces cerevisiae prevents the deleterious effects of endogenous oxidative DNA damage. Mol. Cell *17*, 709–720.

Hustedt, N., Gasser, S.M., and Shimada, K. (2013). Replication checkpoint: tuning and coordination of replication forks in S phase. Genes (Basel) *4*, 388–434.

Hustedt, N., Seeber, A., Sack, R., Tsai-Pflugfelder, M., Bhullar, B., Vlaming, H., van Leeuwen, F., Guénolé, A., van Attikum, H., Srivas, R., et al. (2015). Yeast PP4 interacts with ATR homolog Ddc2-Mec1 and regulates checkpoint signaling. Mol. Cell *57*, 273–289.

Iwasaki, D., Hayashihara, K., Shima, H., Higashide, M., Terasawa, M., Gasser, S.M., and Shinohara, M. (2016). The MRX complex ensures NHEJ fidelity through multiple pathways including Xrs2-FHA-dependent Tel1 activation. PLoS Genet. *12*, e1005942.

Kanoh, Y., Tamai, K., and Shirahige, K. (2006). Different requirements for the association of ATR-ATRIP and 9-1-1 to the stalled replication forks. Gene *377*, 88–95.

Kantake, N., Sugiyama, T., Kolodner, R.D., and Kowalczykowski, S.C. (2003). The recombination-deficient mutant RPA (rfa1-t11) is displaced slowly from single-stranded DNA by Rad51 protein. J. Biol. Chem. *278*, 23410–23417.

Kaye, J.A., Melo, J.A., Cheung, S.K., Vaze, M.B., Haber, J.E., and Toczyski, D.P. (2004). DNA breaks promote genomic instability by impeding proper chromosome segregation. Curr. Biol. *14*, 2096–2106.

Lafrance-Vanasse, J., Williams, G.J., and Tainer, J.A. (2015). Envisioning the dynamics and flexibility of Mre11-Rad50-Nbs1 complex to decipher its roles in DNA replication and repair. Prog. Biophys. Mol. Biol. *117*, 182–193.

Lengsfeld, B.M., Rattray, A.J., Bhaskara, V., Ghirlando, R., and Paull, T.T. (2007). Sae2 is an endonuclease that processes hairpin DNA cooperatively with the Mre11/Rad50/Xrs2 complex. Mol. Cell *28*, 638–651.

Lim, H.S., Kim, J.S., Park, Y.B., Gwon, G.H., and Cho, Y. (2011). Crystal structure of the Mre11-Rad50-ATPγS complex: understanding the interplay between Mre11 and Rad50. Genes Dev. *25*, 1091–1104.

Lisby, M., Barlow, J.H., Burgess, R.C., and Rothstein, R. (2004). Choreography of the DNA damage response: spatiotemporal relationships among checkpoint and repair proteins. Cell *118*, 699–713.

Lobachev, K., Vitriol, E., Stemple, J., Resnick, M.A., and Bloom, K. (2004). Chromosome fragmentation after induction of a double-strand break is an active process prevented by the RMX repair complex. Curr. Biol. *14*, 2107–2112.

Ma, J.L., Kim, E.M., Haber, J.E., and Lee, S.E. (2003). Yeast Mre11 and Rad1 proteins define a Ku-independent mechanism to repair double-strand breaks lacking overlapping end sequences. Mol. Cell. Biol. *23*, 8820–8828.

Majka, J., Binz, S.K., Wold, M.S., and Burgers, P.M. (2006). Replication protein A directs loading of the DNA damage checkpoint clamp to 5′-DNA junctions. J. Biol. Chem. *281*, 27855–27861.

Matsuzaki, K., Terasawa, M., Iwasaki, D., Higashide, M., and Shinohara, M. (2012). Cyclin-dependent kinase-dependent phosphorylation of Lif1 and Sae2 controls imprecise nonhomologous end joining accompanied by double-strand break resection. Genes Cells *17*, 473–493.

Mimitou, E.P., and Symington, L.S. (2008). Sae2, Exo1 and Sgs1 collaborate in DNA double-strand break processing. Nature *455*, 770–774.

Möckel, C., Lammens, K., Schele, A., and Hopfner, K.P. (2012). ATP driven structural changes of the bacterial Mre11:Rad50 catalytic head complex. Nucleic Acids Res. *40*, 914–927.

Moreno-Herrero, F., de Jager, M., Dekker, N.H., Kanaar, R., Wyman, C., and Dekker, C. (2005). Mesoscale conformational changes in the DNA-repair complex Rad50/Mre11/Nbs1 upon binding DNA. Nature *437*, 440–443.

Morrison, A.J., Kim, J.A., Person, M.D., Highland, J., Xiao, J., Wehr, T.S., Hensley, S., Bao, Y., Shen, J., Collins, S.R., et al. (2007). Mec1/Tel1 phosphorylation of the INO80 chromatin remodeling complex influences DNA damage checkpoint responses. Cell *130*, 499–511.

Nakada, D., Matsumoto, K., and Sugimoto, K. (2003a). ATM-related Tel1 associates with double-strand breaks through an Xrs2-dependent mechanism. Genes Dev. *17*, 1957–1962.

Nakada, D., Shimomura, T., Matsumoto, K., and Sugimoto, K. (2003b). The ATM-related Tel1 protein of Saccharomyces cerevisiae controls a checkpoint response following phleomycin treatment. Nucleic Acids Res. *31*, 1715–1724.

Nasmyth, K., and Haering, C.H. (2005). The structure and function of SMC and kleisin complexes. Annu. Rev. Biochem. *74*, 595–648.

Paciotti, V., Clerici, M., Lucchini, G., and Longhese, M.P. (2000). The checkpoint protein Ddc2, functionally related to S. pombe Rad26, interacts with Mec1 and is regulated by Mec1-dependent phosphorylation in budding yeast. Genes Dev. *14*, 2046–2059.

Paciotti, V., Clerici, M., Scotti, M., Lucchini, G., and Longhese, M.P. (2001). Characterization of mec1 kinase-deficient mutants and of new hypomorphic mec1 alleles impairing subsets of the DNA damage response pathway. Mol. Cell. Biol. *21*, 3913–3925.

Petermann, E., and Helleday, T. (2010). Pathways of mammalian replication fork restart. Nat. Rev. Mol. Cell Biol. *11*, 683–687.

Regal, J.A., Festerling, T.A., Buis, J.M., and Ferguson, D.O. (2013). Disease-associated MRE11 mutants impact ATM/ATR DNA damage signaling by distinct mechanisms. Hum. Mol. Genet. *22*, 5146–5159.

Rouse, J., and Jackson, S.P. (2002). Lcd1p recruits Mec1p to DNA lesions in vitro and in vivo. Mol. Cell *9*, 857–869.

San Filippo, J., Sung, P., and Klein, H. (2008). Mechanism of eukaryotic homologous recombination. Annu. Rev. Biochem. *77*, 229–257.

Schiller, C.B., Lammens, K., Guerini, I., Coordes, B., Feldmann, H., Schlauderer, F., Möckel, C., Schele, A., Strässer, K., Jackson, S.P., and Hopfner, K.P. (2012). Structure of Mre11-Nbs1 complex yields insights into ataxia-telangiectasia-like disease mutations and DNA damage signaling. Nat. Struct. Mol. Biol. *19*, 693–700.

Seifert, F.U., Lammens, K., and Hopfner, K.P. (2015). Structure of the catalytic domain of Mre11 from *Chaetomium thermophilum*. Acta Crystallogr. F Struct. Biol. Commun. *71*, 752–757.

Shima, H., Suzuki, M., and Shinohara, M. (2005). Isolation and characterization of novel xrs2 mutations in Saccharomyces cerevisiae. Genetics *170*, 71–85.

Stracker, T.H., and Petrini, J.H. (2011). The MRE11 complex: starting from the ends. Nat. Rev. Mol. Cell Biol. *12*, 90–103.

Ström, L., and Sjögren, C. (2007). Chromosome segregation and double-strand break repair - a complex connection. Curr. Opin. Cell Biol. *19*, 344–349.

Ström, L., Karlsson, C., Lindroos, H.B., Wedahl, S., Katou, Y., Shirahige, K., and Sjögren, C. (2007). Postreplicative formation of cohesion is required for repair and induced by a single DNA break. Science *317*, 242–245.

Tittel-Elmer, M., Alabert, C., Pasero, P., and Cobb, J.A. (2009). The MRX complex stabilizes the replisome independently of the S phase checkpoint during replication stress. EMBO J. *28*, 1142–1156.

Tittel-Elmer, M., Lengronne, A., Davidson, M.B., Bacal, J., François, P., Hohl, M., Petrini, J.H., Pasero, P., and Cobb, J.A. (2012). Cohesin association to replication sites depends on rad50 and promotes fork restart. Mol. Cell *48*, 98–108.

Toledo, L.I., Altmeyer, M., Rask, M.B., Lukas, C., Larsen, D.H., Povlsen, L.K., Bekker-Jensen, S., Mailand, N., Bartek, J., and Lukas, J. (2013). ATR prohibits replication catastrophe by preventing global exhaustion of RPA. Cell *155*, 1088–1103.

Uhlmann, F. (2016). SMC complexes: from DNA to chromosomes. Nat. Rev. Mol. Cell Biol. *17*, 399–412.

Uhlmann, F., Lottspeich, F., and Nasmyth, K. (1999). Sister-chromatid separation at anaphase onset is promoted by cleavage of the cohesin subunit Scc1. Nature *400*, 37–42.

Umezu, K., Sugawara, N., Chen, C., Haber, J.E., and Kolodner, R.D. (1998). Genetic analysis of yeast RPA1 reveals its multiple functions in DNA metabolism. Genetics *148*, 989–1005.

Unal, E., Arbel-Eden, A., Sattler, U., Shroff, R., Lichten, M., Haber, J.E., and Koshland, D. (2004). DNA damage response pathway uses histone modification to assemble a double-strand break-specific cohesin domain. Mol. Cell *16*, 991–1002.

Unal, E., Heidinger-Pauli, J.M., and Koshland, D. (2007). DNA double-strand breaks trigger genome-wide sister-chromatid cohesion through Eco1 (Ctf7). Science *317*, 245–248.

Usui, T., Ohta, T., Oshiumi, H., Tomizawa, J., Ogawa, H., and Ogawa, T. (1998). Complex formation and functional versatility of Mre11 of budding yeast in recombination. Cell *95*, 705–716.

van Attikum, H., Fritsch, O., and Gasser, S.M. (2007). Distinct roles for SWR1 and INO80 chromatin remodeling complexes at chromosomal double-strand breaks. EMBO J. *26*, 4113–4125.

Wang, X., and Haber, J.E. (2004). Role of *Saccharomyces* single-stranded DNA-binding protein RPA in the strand invasion step of double-strand break repair. PLoS Biol. *2*, E21.

Wang, X., Ira, G., Tercero, J.A., Holmes, A.M., Diffley, J.F., and Haber, J.E. (2004). Role of DNA replication proteins in DSB-induced recombination in *S. cerevisiae*. Mol. Cell. Biol. *24*, 6891–6899.

Williams, R.S., Dodson, G.E., Limbo, O., Yamada, Y., Williams, J.S., Guenther, G., Classen, S., Glover, J.N., Iwasaki, H., Russell, P., and Tainer, J.A. (2009). Nbs1 flexibly tethers Ctp1 and Mre11-Rad50 to coordinate DNA double-strand break processing and repair. Cell *139*, 87–99.

Wiltzius, J.J., Hohl, M., Fleming, J.C., and Petrini, J.H. (2005). The Rad50 hook domain is a critical determinant of Mre11 complex functions. Nat. Struct. Mol. Biol. *12*, 403–407.

Xu, X., Vaithiyalingam, S., Glick, G.G., Mordes, D.A., Chazin, W.J., and Cortez, D. (2008). The basic cleft of RPA70N binds multiple checkpoint proteins, including RAD9, to regulate ATR signaling. Mol. Cell. Biol. *28*, 7345–7353.

Zou, L., and Elledge, S.J. (2003). Sensing DNA damage through ATRIP recognition of RPA-ssDNA complexes. Science *300*, 1542–1548.

Zou, Y., Liu, Y., Wu, X., and Shell, S.M. (2006). Functions of human replication protein A (RPA): from DNA replication to DNA damage and stress responses. J. Cell. Physiol. *208*, 267–273.

Chapter 5:
Concluding remarks and future prospects

This thesis contributes to our understanding of the initial steps in the DNA damage response.

Specifically, in chapter 2, I reveal a mode of assembly of the DNA damage checkpoint kinase Mec1 at DNA damage sites through the interaction of Mec1 regulatory subunit Ddc2 and the ssDNA binding protein RPA. Four major conclusions based on structural, biochemical and *in vivo* data are discussed below.

1. Ddc2 N-terminus homodimerizes and binds the N-terminus of the largest RPA subunit Rfa1

We determined the crystal structure of the Ddc2 N-terminus bound to the Rfa1 N-terminal OB-fold domain (Rfa1 N-OB). The crystal structure showed that the Ddc2 N-terminus includes an Rfa1-binding domain (RBD) and a coiled-coil domain (CCD) connected by a linker. We showed that the acidic-hydrophobic Ddc2 RBD binds the basic-hydrophobic cleft of the Rfa1 N-OB, both *in vitro* as well as *in vivo*, to recruit Mec1-Ddc2 to DNA damage sites. We observed that the Ddc2 CCD is a 103 Å long helix that homodimerizes in a parallel fashion, creating an A_2B_2 stoichiometry of Ddc2-Rfa1 in the crystallographic asymmetric unit. We also determined the crystal structure of the Ddc2 CCD alone. In immunoprecipitation experiments, the Ddc2 CCD was essential for Mec1-Ddc2 homodimerization *in vivo*.

2. Ddc2 binds Rfa1-t11

The Rfa1 N-OB cleft binds multiple DNA damage response proteins including Ddc2, MRX, Sgs1, p53 and Dna2 (Ball et al., 2007; Hegnauer et al., 2012; Lin et al., 1996; Seeber et al., 2016; Zhou et al., 2015). It was previously shown that the Rfa1-t11 (K45E) mutant protein is defective for recruiting Ddc2 to DNA double-strand breaks, but not to stalled replication forks (Dubrana et al., 2007; Kanoh et al., 2006; Zou and Elledge, 2003). To investigate Ddc2 binding to Rfa1-t11, we performed the following structural, biochemical and *in vivo* experiments. Using microscale thermophoresis (MST), we showed that Ddc2 binds Rfa1 and Rfa1-t11 with comparable dissociation constants of 0.4 µM and 2.6 µM, respectively. We next determined the co-crystal structure of the Ddc2 N-terminus bound to the Rfa1-t11 N-OB domain and found that the mechanism of binding is identical to that of Ddc2 and wild-type Rfa1. Importantly, Ddc2 still bound Rfa1-t11 *in vivo* in microscopy and immunoprecipitation experiments.

3. Ddc2 N-terminus is important for survival after damage by UV/4-NQO

We observed that the Ddc2 N-terminus is important for cell survival when budding yeast *Saccharomyces cerevisiae* is exposed to UV-light or UV-mimetic drug 4-NQO. Notably, both the RBD and the CCD contributed to survival. We also observed that checkpoint pathway induction, monitored by the phosphorylation of Rad53, a major Mec1 target, is dependent on the Ddc2 N-terminus after damage by 4-NQO, but not after replication stress. Expectedly, we observed that without the Ddc2 N-terminus, Mec1-Ddc2 is not recruited to RPA foci at DNA damage sites and cannot homodimerize. Moreover, the

Ddc2 CCD seems to play a role in substrate selectivity e.g. phosphorylation of histone H2A at S129 (γH2A).

4. Homodimeric Mec1-Ddc2 assembles on two adjacent ssDNA-RPA molecules

An important implication of this study was that our Ddc2-Rfa1 crystal structure (PDB ID: 5OMB) was able to link the RPA-ssDNA crystal structure (PDB ID: 4GNX) and the negative stain EM map of Mec1-Ddc2 (EMD-4085) to build a composite structural model showing the assembly of homodimers of Mec1-Ddc2 on two adjacent ssDNA-RPA molecules. The model reinforces our finding that the Ddc2 N-terminus acts not only as a recruitment domain, but also as a structural spacer to allow the Mec1 kinase to phosphorylate several targets while remaining bound to DNA damage sites. The model also supports the notion that Ddc2 recruitment to RPA and Ddc2 CCD homodimerization are linked, probably to ensure timely and local Mec1 activity.

Chapter 3 focuses on the oligomerization of the CCDs of human ATRIP and yeast Ddc2.

An N-terminal trigger helix in the ATRIP CCD is important for CCD homodimerization

Some coiled-coils contain a trigger sequence which initiates coiled-coil assembly and drives oligomerization (Frank et al., 2000; Kammerer et al., 1998; Steinmetz et al., 1998). Whether HsATRIP or ScDdc2 CCD contains such a trigger sequence was unclear. SEC-MALS analysis of HsATRIP and ScDdc2 CCDs with and without the N-terminal predicted helix showed that the N-terminal predicted helix is required for dimerization of HsATRIP but not ScDdc2.

Chapter 4 focuses on how MRX is recruited to stalled replication forks and DNA double-strand breaks by interacting with a domain in RPA that also binds Ddc2. Below, I will discuss the conclusion of my contribution to this study.

MRX does not bind Rfa1-t11

The *rfa1-t11* allele renders cells defective in recombination and DNA repair, but proficient in replication (Dubrana et al., 2007; Soustelle et al., 2002; Umezu et al., 1998). This K45E mutation lies in a loop connecting two β-strands of the five-stranded N-OB cleft that binds several proteins in the DNA damage response pathway (see conclusion 2 of chapter 2). How this mutation would affect the binding of Rfa1 to its ligands was unclear. To understand the structural changes provoked by the K45E substitution, we determined the structure of the mutant by X-ray crystallography and observed that the mutation disrupts a basic patch in the binding pocket of the N-OB fold. Next, using MST, we showed that a peptide present in the ATPase domain of Rad50 binds to the Rfa1 N-OB domain with a dissociation constant of 63 μM. Interestingly, the MRX-Rfa1 interaction was sensitive to the *rfa1-t11* mutation as observed in a scanning

peptide microarray assay. Therefore, chapter 2 and chapter 4 suggest that the *rfa1-t11* mutation affects binding of Rfa1 to some ligands such as MRX and Dna2, but not others such as Ddc2.

Future directions

A key question that remains unanswered is: What is the structure of full length Mec1-Ddc2 complexes bound to the ssDNA-RPA platform? This question has been the focus of several researchers for more than a decade. Given the recent advancement in the field of cryo-EM and the resulting structure determinations of other PIKK complexes, one might expect to see the full length Mec1-Ddc2-RPA structure in the near future. Ddc2 and RPA have long flexible linkers that may result in multiple conformations. This problem could be solved by using a co-activator of Mec1, such as Dpb11. However, Dpb11 itself includes a long and flexible C-terminal tail. Instead, the 9-1-1 checkpoint clamp may be used to stimulate and potentially stabilize Mec1. Moreover, 9-1-1 binds the ds-ssDNA junction and would therefore remain adjacent to the ssDNA that binds RPA. The implications from such a structure might be far-reaching and would possibly help answer other key questions in the field such as: How do the two conserved aromatic amino acid residues in Mec1 co-activators stimulate the Mec1 kinase? What are the homodimerization and heterodimerization motifs in Mec1-Ddc2? Moreover, structural studies on human complexes could be useful for drug design experiments.

A question this thesis raises is: Why is the Ddc2 N-terminus so important for cell survival after DNA damage by UV-light compared to other DNA-damaging agents? One possibility is that the different lesions might activate Mec1 in a different manner and a co-activator of Mec1 that is specific for UV-damage depends on the Ddc2 N-terminus. Another possibility is that the Ddc2 N-terminus interacts with a component of the NER machinery for efficient recruitment, especially to the initial 24-30 nt gap generated during NER. These hypotheses could be tested by analyzing the interactome of the Ddc2 N-terminus using mass spectrometry.

The second question raised by this thesis is: Does the Ddc2 CCD act as a structural spacer to allow Mec1 to phosphorylate several targets while remaining bound to ssDNA? Although, I have partly answered this question by monitoring the phosphorylation of Rad53, Rfa2 and histone H2A in a *ddc2* mutant lacking the CCD, a large scale mass spectrometry-based phosphoproteomics experiment might provide a more complete understanding.

The third question raised by this thesis is: Does the Ddc2 CCD homodimerize only upon recruitment to ssDNA-RPA stretches? Data from chapter 2 suggests that the Ddc2 CCD is not a constitutive dimer and the recruitment domain is important for Ddc2 dimerization in DNA damaging conditions. It is tempting to hypothesize that Ddc2 recruitment to damage sites increases its local concentration and promotes Ddc2 CCD dimerization. Ddc2 CCD dimerization might be a necessary event for Mec1 activation, thus ensuring that Mec1 is activated only at DNA damage sites. This could be tested by performing fluorescence

resonance energy transfer assays. For example, fluorescence of a mixture of donor-tagged Ddc2 N-terminus and acceptor-tagged Ddc2 N-terminus could be measured in the absence or presence of reconstituted ssDNA-RPA.

In conclusion, this thesis describes the assembly of the checkpoint kinase Mec1-Ddc2 on ssDNA-RPA at sites of DNA damage. It focuses on the Ddc2 N-terminus which includes a homodimerization coiled-coil domain and an N-terminal recruitment domain that binds RPA. These two domains function together and promote cell survival after DNA damage by UV-light.

References

Ball, H.L., Ehrhardt, M.R., Mordes, D.A., Glick, G.G., Chazin, W.J., and Cortez, D. (2007). Function of a conserved checkpoint recruitment domain in ATRIP proteins. Mol Cell Biol *27*, 3367-3377.

Dubrana, K., van Attikum, H., Hediger, F., and Gasser, S.M. (2007). The processing of double-strand breaks and binding of single-strand-binding proteins RPA and Rad51 modulate the formation of ATR-kinase foci in yeast. J Cell Sci *120*, 4209-4220.

Frank, S., Lustig, A., Schulthess, T., Engel, J., and Kammerer, R.A. (2000). A distinct seven-residue trigger sequence is indispensable for proper coiled-coil formation of the human macrophage scavenger receptor oligomerization domain. J Biol Chem *275*, 11672-11677.

Hegnauer, A.M., Hustedt, N., Shimada, K., Pike, B.L., Vogel, M., Amsler, P., Rubin, S.M., van Leeuwen, F., Guenole, A., van Attikum, H*., et al.* (2012). An N-terminal acidic region of Sgs1 interacts with Rpa70 and recruits Rad53 kinase to stalled forks. EMBO J *31*, 3768-3783.

Kammerer, R.A., Schulthess, T., Landwehr, R., Lustig, A., Engel, J., Aebi, U., and Steinmetz, M.O. (1998). An autonomous folding unit mediates the assembly of two-stranded coiled coils. Proc Natl Acad Sci U S A *95*, 13419-13424.

Kanoh, Y., Tamai, K., and Shirahige, K. (2006). Different requirements for the association of ATR-ATRIP and 9-1-1 to the stalled replication forks. Gene *377*, 88-95.

Lin, Y.L., Chen, C., Keshav, K.F., Winchester, E., and Dutta, A. (1996). Dissection of functional domains of the human DNA replication protein complex replication protein A. J Biol Chem *271*, 17190-17198.

Seeber, A., Hegnauer, A.M., Hustedt, N., Deshpande, I., Poli, J., Eglinger, J., Pasero, P., Gut, H., Shinohara, M., Hopfner, K.P*., et al.* (2016). RPA Mediates Recruitment of MRX to Forks and Double-Strand Breaks to Hold Sister Chromatids Together. Mol Cell *64*, 951-966.

Soustelle, C., Vedel, M., Kolodner, R., and Nicolas, A. (2002). Replication protein A is required for meiotic recombination in Saccharomyces cerevisiae. Genetics *161*, 535-547.

Steinmetz, M.O., Stock, A., Schulthess, T., Landwehr, R., Lustig, A., Faix, J., Gerisch, G., Aebi, U., and Kammerer, R.A. (1998). A distinct 14 residue site triggers coiled-coil formation in cortexillin I. EMBO J *17*, 1883-1891.

Umezu, K., Sugawara, N., Chen, C., Haber, J.E., and Kolodner, R.D. (1998). Genetic analysis of yeast RPA1 reveals its multiple functions in DNA metabolism. Genetics *148*, 989-1005.

Zhou, C., Pourmal, S., and Pavletich, N.P. (2015). Dna2 nuclease-helicase structure, mechanism and regulation by Rpa. Elife *4*.

Zou, L., and Elledge, S.J. (2003). Sensing DNA damage through ATRIP recognition of RPA-ssDNA complexes. Science *300*, 1542-1548.

List of abbreviations

4-NQO	4-nitroquinoline 1-oxide
BER	Base excision repair
CCD	Coiled-coil domain
CDK	Cyclin-dependent kinase
$Ddc2^{CCD}$	Coiled-coil domain of Ddc2
$Ddc2^{N}$	Ddc2 N-terminus
DDR	DNA damage response
DNA	Deoxyribonucleic acid
dNTP	Deoxyribonucleotide triphosphate
DSB	Double-strand break
EM	Electron microscopy
GFP	Green fluorescent protein
HR	Homologous recombination
HU	Hydroxyurea
IR	Ionizing radiation
K_d	Dissociation constant
Kl	*Kluyveromyces lactis*
MMR	Mismatch repair
MMS	Methyl methanesulfonate
MRX	Mre11-Rad50-Xrs2
MST	Microscale thermophoresis
NER	Nucleotide excision repair
NHEJ	Nonhomologous end-joining
NMR	Nuclear magnetic resonance
N-OB	N-terminal oligosaccharide/oligonucleotide binding
PAGE	Polyacrylamide gel electrophoresis
PDB	Protein data bank
PIKK	Phosphoinositide 3-kinase related protein kinase
RBD	Rfa1-binding domain
$Rfa1^{N}$	Rfa1 N-terminus
RFP	Red fluorescent protein
RMSD	Root mean-squared deviation
RPA	Replication protein A
SAD	Single-wavelength anomalous diffraction
SAXS	Small-angle X-ray scattering
Sc	*Saccharomyces cerevisiae*
SDS	Sodium dodecyl sulfate
SEC-MALS	Size-exclusion chromatography coupled with multi-angle light scattering
SSB	Single-strand break
ssDNA	Single-stranded DNA
UV	Ultraviolet
WH	Winged helix
wt	Wild-type

Acknowledgments

I am grateful to my mentors, Prof. Susan Gasser and Dr. Heinz Gut, for their constant motivation, invaluable guidance and expert advice during all the phases of my thesis. I am also grateful to Prof. Laurence Pearl, for being a part of my thesis committee, and participating in insightful discussions that were instrumental for my research. I would like to specially thank Dr. Jeremy Keusch, a fantastic colleague, for teaching me how to express and purify proteins, for helpful discussions, and for organizing the lab. I also thank Dr. Kenji Shimada for being a wonderful teacher and helping me with yeast methods.

I thank members of the Protein Structure Facility and the Gasser laboratory for maintaining the team spirit and a healthy working atmosphere which allowed me to focus on my work. The constant discussions and brain-storming sessions were a hallmark of my thesis and I am thankful to my colleagues for that. Dr. Monika Tsai, Veronique Kalck and Razel Arpagaus maintain the Gasser lab in a clean and organized way and I am thankful to them.

Research at the FMI is very collaborative and greatly supported by numerous technical platforms. Among them, I would like to thank Dr. Daniel Hess from the Protein Analysis Facility for mass spectrometry analysis, and Dr. Alexandra Graff Meyer from the Electron Microscopy facility for helping with negative-stain EM experiments. I would also like to thank Dr. Simone Cavadini for crucial help with EM analysis and Dr. Andrew Seeber for two fruitful collaborations.

Finally, this thesis would not have been possible without the extraordinary support of my family and friends. Their contribution to the thesis is priceless and beyond the scope of this page.